ADVANCES IN WAVE PROPAGATION
IN HETEROGENEOUS EARTH,
R.-S. Wu, V. Maupin, eds.

Advances in Geophysics, **Vol. 48**, 421-516
DOI10.1016/S0065-2687(06)48008-0
R. Dmowska, ed.,
Elsevier - Academic Press, 2007

The Finite-Difference Time-Domain Method for Modeling of Seismic Wave Propagation

by

Peter Moczo [1], Johan O. A. Robertsson [2], and Leo Eisner [3]

[1] Faculty of Mathematics, Physics and Informatics, Comenius University, Bratislava, Slovak Republic; moczo@fmph.uniba.sk

[2] WesternGeco Oslo Technology Center, Schlumberger House, Asker, Norway; JRobertsson@oslo.westerngeco.slb.com

[3] Schlumberger Cambridge Research Ltd., Cambridge, United Kingdom; leisner@cambridge.oilfield.slb.com

Contents

Abstract

We present a review of the recent development in finite-difference time-domain modeling of seismic wave propagation and earthquake motion. The finite-difference method is a robust numerical method applicable to structurally complex media. Due to its relative accuracy and computational efficiency it is the dominant method in modeling earthquake motion and it also is becoming increasingly more important in the seismic industry and for structural modeling. We first introduce basic formulations and properties of the finite-difference schemes including promising recent advances. Then we address important topics as material discontinuities, realistic attenuation, anisotropy, the planar free surface boundary condition, free-surface topography, wavefield excitation (including earthquake source dynamics), nonreflecting boundaries, and memory optimization and parallelization.

Key words: anisotropy, attenuation, earthquake motion, earthquake source dynamics, finite-difference method, free surface, nonreflecting boundaries, numerical modeling, optimally accurate operators, seismic waves

Introduction

Faithfully synthesizing observed seismic data requires simulation of seismic wave propagation in realistic computational models which can include anisotropic media, nonplanar interfaces between layers and blocks, velocity/density/quality-factor gradients inside layers, and often with free-surface topography. In particular, the rheology of the medium should allow for realistic attenuation. Anisotropy increasingly becomes more important particularly in structural studies and is essential in many applications in seismic exploration. The modeling of large earthquakes requires at least kinematic modeling of the rupture propagation but the dynamic modeling is likely to provide more realistic simulations in the near future. Since analytical methods do not provide solutions for realistic (structurally complex) models, approximate methods are necessary. Among them, the finite-difference (FD) method is still the dominant method in modeling earthquake motion and it also is becoming increasingly more important in the seismic industry and structural modeling. This is because the FD method can handle relatively complex models, provides the „complete“ solution as waves interact with the model, can be relatively accurate, and, at the same time, relatively computationally efficient. In addition to this, the FD method can be relatively easily parallelized. It is important to stress the word relatively - this chapter should explain why.

In the FD method, a computational domain is covered by a space-time grid, that is, by a set of discrete grid positions in space and time. The functions describing a wavefield as well as those describing material properties of the medium are represented by their values at the grid positions. In principle, the space-time grid may be arbitrary and usually no assumption is made about the function values in-between the grid points. Spatial and time derivatives of a function at a given grid position are approximated by the so-called FD formulae, the derivative being expressed using the function values at a specified set of the grid positions in a neighborhood of the given position. The original differential equation is thus replaced by a system of algebraic (FD) equations. The system of FD equations and their numerical solution have three basic properties – consistency of the FD equations with the original differential equations, stability and convergence of the numerical solution. These properties have to be analyzed prior to the numerical calculation.

In principle, the FD method can be applied either in the time or frequency domain. While for the forward modeling the time-domain formulation requires less calculations (at least for simple simulations), the frequency-domain formulation may be more efficient in inverse problems when simulations for multiple source locations are required, at least in 2D (Pratt, 1990; Pratt et al., 1998). As most of the FD applications to date focus on the forward modeling, this chapter only addresses the FD time-domain (FDTD) formulation.

The FD method belongs to the domain methods together with, for example, the finite-element, spectral element or the pseudospectral method (Chaljub et al. 2006). Therefore, in general, it is less accurate than boundary methods but much more efficient when applied to complex models (for comparison see, e.g., Takenaka et al., 1998).

Because, formally, the FD method almost always can provide some numerical results, those who are not familiar with the properties of the FD method and particularly with its inherent limitations, sometimes overestimate the capability and accuracy of the FD method, and especially some simple, user-friendly looking FD schemes and codes. An improper application of the FD method can give very inaccurate results. On the other hand, when properly treated, the FD method shows accuracy similar to that of

other full waveform techniques, and can be a strong modeling tool applicable to many important problems of recent seismology and seismic prospecting.

In this chapter we try to provide a limited review of the recent progress in FDTD modeling of seismic wave propagation and earthquake motion as well as partial tutorial describing in detail specific FDTD techniques that can be used to solve real practical problems. Because explicit, heterogeneous, staggered-grid FD schemes clearly have dominated in the recent FDTD modeling we focus on them.

In the following subsections we briefly introduce basic concepts and properties of the FD method, some of them directly in relation to solving the elastodynamic equation. A more detailed introduction to the FD method would require considerably large space. Basics of the FD method can be found in applied mathematical textbooks such as, for example, Forsythe and Wasow (1960), Isaacson and Keller (1966), Richtmyer and Morton (1967), Marchuk (1982), Anderson et al. (1984), Mitchell and Griffiths (1994), Morton and Mayers (1994), Durran (1999), Cohen (2002). Detailed introductory texts on the application of the FD method to seismic wave propagation and seismic motion modeling can be found in Boore (1972), Levander (1989), Moczo (1998), Carcione et al. (2002), and Moczo et al. (2004b). Though focused on the computational electrodynamics, the extensive book of Taflove and Hagness (2005) is a good reference to the application of the FDTD method to partial differential equations in physics.

The Grid

Consider a Cartesian coordinate system (x, y, z) and a computational domain in the four-dimensional space of variables (x, y, z, t) with t meaning time. Consider a set of discrete points (x_I, y_J, z_K, t_m) given by $x_I = x_0 + I\Delta x$, $y_J = y_0 + J\Delta y$, $z_K = z_0 + K\Delta z$, $t_m = t_0 + m\Delta t$; $I, J, K, m = 0, 1, 2, \ldots$. The spatial increments Δx, Δy and Δz are usually referred to grid spacings, while Δt is the time step. The set of points (positions) defines a space-time grid. In many applications, the regular (uniform) rectangular grid with the grid spacings $\Delta x = \Delta y = \Delta z = h$ is a natural and reasonable choice. The value of a function u at a grid position (x_I, y_J, z_K, t_m), that is $u(I, J, K, m)$ or $u^m_{I,J,K}$, is approximated by a grid function $U^m_{I,J,K} = U(x_I, y_J, z_K, t_m)$.

Depending on the particular problem, other than Cartesian coordinate systems can be used to define a grid. For instance, spherical coordinates can be used for the whole Earth's models, and cylindrical for modeling boreholes. The choice of the grid determines the structure and properties of the FD approximations to derivatives and consequently the properties of the FD equations. Here we focus on FD schemes constructed for grids corresponding to the Cartesian coordinate systems.

In some problems it may be advantageous to define a non-uniform grid. Examples are grids with irregularly varying size of the grid spacing or discontinuous (combined) grids with a sudden change in size of the grid spacing. Such grids can better accommodate geometry of the model or reduce the total number of grid points covering the computational space. These grids belong to the structured grids: at a grid point the neighbor grid points are always known (for example, they are defined using some mathematical rule). On the other hand, at a grid point of the unstructured grid some additional information is needed about the neighbor grid points. Most FD techniques use structured grids because the algorithms are faster than those on the unstructured grids.

Another and perhaps more important aspect is whether all functions are approximated at the same grid position or not. In a conventional grid, all functions are approximated at the same grid positions. In a partly-staggered grid, displacement or particle-velocity components are located at one grid position whereas the stress-tensor components are located at another grid position. In a staggered grid, each displacement and/or particle-velocity component and each shear stress-tensor component has its own grid position. The normal stress-tensor components share another grid position. The staggered distribution of quantities in space is related (through the equation of motion) to the staggered distribution of quantities in time. In all types of grids, an effective density is assigned to a grid position of each displacement or particle-velocity component while an effective elastic modulus is assigned to each grid position of the stress-tensor components. The so-called grid cells of the conventional, partly-staggered and staggered grids are illustrated in Fig. 1.

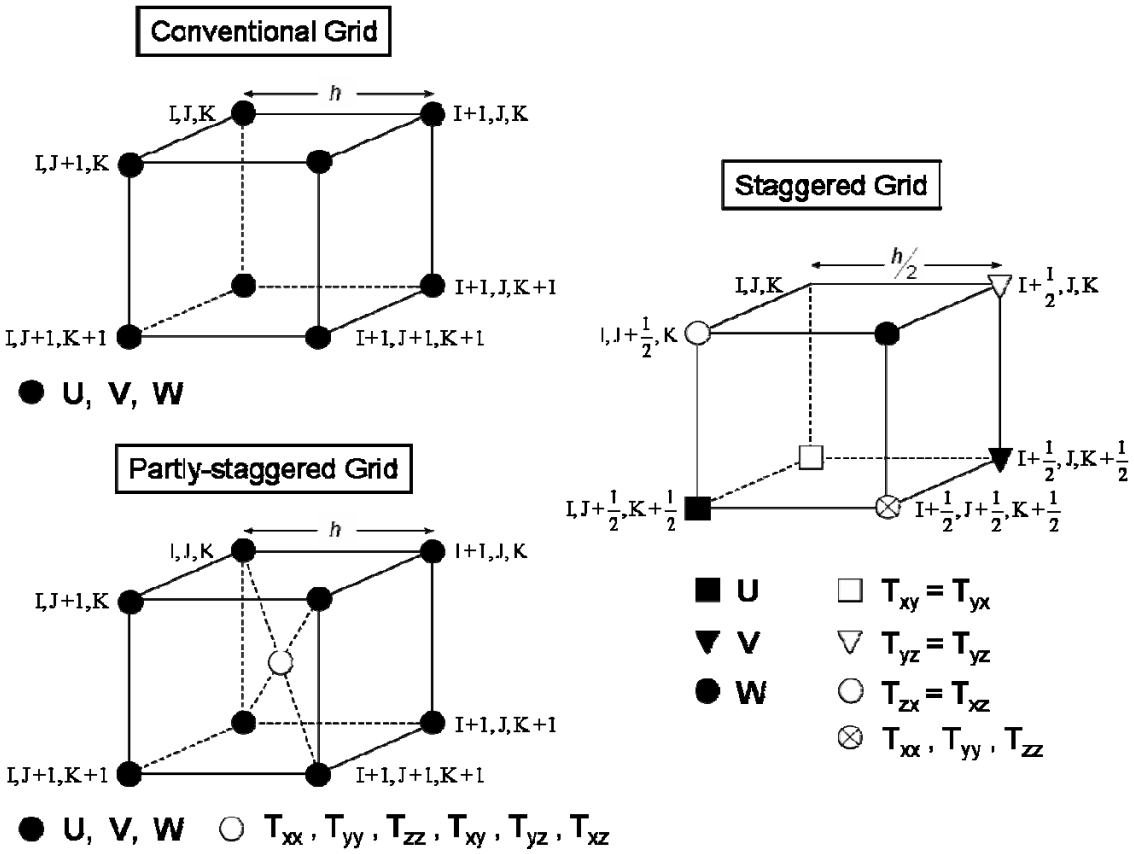

Figure 1. Spatial grid cells in the conventional, partly-staggered and staggered grids. All displacement-vector components U, V and W are located at each grid position in the conventional grid. Either displacement or particle-velocity components U, V and W share the same grid positions whereas stress-tensor components T_{xx}, T_{yy}, T_{zz}, T_{xy}, T_{yz}, and T_{zx} share other grid positions in the partly-staggered grid. Displacement and/or particle-velocity components U, V and W are located at different grid positions as well as stress-tensor components T_{xx}, T_{yy}, T_{zz}, T_{xy}, T_{yz}, and T_{zx} are in the staggered grid. Because the normal stress-tensor components are determined by the same spatial derivatives of the displacement components, they share one grid position.

The FD Approximations to Derivatives

Let the function $\Phi(x)$ have a continuous first derivative. The forward-difference formula

$$\frac{\mathrm{d}\Phi}{\mathrm{d}x}(x_0) \doteq \frac{\Phi(x_0+h)-\Phi(x_0)}{h}\ , \tag{1}$$

the backward-difference formula

$$\frac{\mathrm{d}\Phi}{\mathrm{d}x}(x_0) \doteq \frac{\Phi(x_0)\ -\ \Phi(x_0-h)}{h}\ , \tag{2}$$

and the central-difference formula

$$\frac{\mathrm{d}\Phi}{\mathrm{d}x}(x_0) \doteq \frac{\Phi(x_0+h)\ -\ \Phi(x_0-h)}{2h} \tag{3}$$

are three different approximations to the 1st derivative of function $\Phi(x_0)$. Substituting Taylor expansions of functional values $\Phi(x_0+h)$ and $\Phi(x_0-h)$ about the point x_0 in eqs. (1) and (2) shows that the difference between the first derivative and the value of the right-hand side expression, that is, the truncation error, has the leading term proportional to h^1. The FD formulae (1) and (2) are the 1st -order approximations to the first derivative. Similarly, it is easy to check that the FD formula (3) is the 2nd-order approximation to the first derivative because the truncation error is proportional to h^2. For a chosen derivative, set of the grid points and order of approximation, it is possible to find a FD formula by constructing a system of algebraic equations based on Taylor expansions and equating the coefficients of identical powers of the grid spacing h (e.g., Durran, 1999; Moczo et al., 2004b). This is also true for approximating a derivative in a plane or in a volume.

A frequently used 2nd-order approximation to the second derivative is

$$\frac{\mathrm{d}^2\Phi}{\mathrm{d}x^2}(x_0) \doteq \frac{\Phi(x_0-h)\ -\ 2\Phi(x_0)\ +\ \Phi(x_0+h)}{h^2}\ . \tag{4}$$

The approximation is used in the conventional-grid displacement FD schemes.

An important 4th-order approximation to the 1st derivative is

$$\frac{\mathrm{d}\Phi}{\mathrm{d}x}(x_0) \doteq \frac{1}{h}\left\{a\left[\Phi\left(x_0+\frac{3}{2}h\right)-\Phi\left(x_0-\frac{3}{2}h\right)\right]+b\left[\Phi\left(x_0+\frac{1}{2}h\right)-\Phi\left(x_0-\frac{1}{2}h\right)\right]\right\} \tag{5}$$

with $a=-1/24$, $b=9/8$. The approximation is used in the staggered-grid FD schemes.

For other FD approximations, higher-order FD approximations and FD approximations on arbitrary spaced grids see also Anderson et al. (1984), Dablain (1986), Fornberg (1988), Geller and Takeuchi (1995, 1998), Klimeš (1996), and Cohen (2002).

Basic Properties of the FD Equations and their Solution

Denote a partial differential equation as *PDE* and a FD equation(s) as *FDE* (a FD scheme may be used instead of *FDE*). A *FDE* is consistent with the PDE if the difference between the *FDE* and the *PDE* (the truncation error) vanishes as the sizes of the time step and spatial grid spacing go to zero independently, that is, $|PDE - FDE| \to 0$ if $\Delta t \to 0,\ h \to 0$. If this is true only when a certain relationship is satisfied between Δt and h, the *FDE* is conditionally consistent.

A *FDE* is stable if it produces a bounded solution when the exact solution is bounded, and is unstable if it produces an unbounded solution when the exact solution is bounded. If the solution of the *FDE* is bounded for all values of Δt and h, the *FDE* is unconditionally stable. If the solution of the *FDE* is bounded only for certain values of Δt and h, the *FDE* is conditionally stable. If the solution of the *FDE* is unbounded for all values of Δt and h, the *FDE* is unconditionally unstable. The stability analysis can be performed only for linear *PDE*. A nonlinear *PDE* must be first linearized locally. The *FDE* of the linearized *PDE* can be analyzed for stability. The most commonly used method for the stability analysis is the von Neumann method. The basic idea of the von Neumann method is to represent a discrete solution at a time $m\Delta t$ and spatial point Ih, that is at one grid point, by a finite Fourier series, and examine stability of the individual Fourier components. Thus, the method investigates the local stability. The discrete solution is stable if and only if each Fourier component is stable. Von Neumann analysis is applicable to linear *FDE* with constant coefficients. Though a spatial periodicity is assumed for the finite Fourier series, the analysis can give a useful result even if this is not the case.

A *FDE* is convergent if the solution of the *FDE* approaches the exact solution of the *PDE* as the sizes of the time step and spatial grid spacing go to zero. Denoting the solutions obtained by the *PDE* and *FDE* as $u^m_{I,J,K}$ and $U^m_{I,J,K}$, respectively, the convergence means that $U^m_{I,J,K} \to u^m_{I,J,K}$ if $\Delta t \to 0,\ h \to 0$.

Whereas the consistency is the property of the *FDE* because it relates the *FDE* to the *PDE*, stability and convergence are properties of the numerical solution of the *FDE*. In general, while it is easy to analyze the consistency, proving convergence can be a very difficult mathematical problem. Therefore, it is very helpful that the convergence is related to the consistency and the stability: It follows from the Lax equivalence theorem that if the *FDE* is consistent and stable, it is also convergent.

Due to the discrete nature of the FD solution, the phase and group velocity in the grid differ from the true velocities in the medium. The grid velocities depend on the spatial sampling ratio $s = h/\lambda$, where λ is the wavelength that is to be propagated in the grid, and also on Courant number $c\Delta t/h$, where c is the velocity. The grid dispersion is a very important grid phenomenon. It has a cumulative effect on the wave propagation – the longer the travel distance, the larger the effect of the difference between the grid and true velocity. Therefore, the grid dispersion has to be analyzed prior to the numerical calculations. This is especially important if the medium is viscoelastic. The viscoelastic medium is intrinsically dispersive and thus a possible superposition of two dispersion effects has to be prevented by minimizing the grid dispersion; see Robertsson et al. (1994). The grid-dispersion relation can be obtained from the stability analysis. The grid dispersion has to be taken into account in planning the numerical calculation. For a detailed analysis of stability, grid dispersion and accuracy of the FD schemes solving the equation of motion on the conventional and

staggered-grid schemes in 2D and 3D problems in homogeneous media see, for example, papers by Marfurt (1984), Crase et al. (1992), Igel et al. (1995), Geller and Takeuchi (1995, 1998), Klimeš (1996), Takeuchi and Geller (2000), Mizutani et al. (2000), Moczo et al. (2000).

Explicit and Implicit FD Schemes

In an explicit scheme, the motion at any (one) spatial grid point can be updated for the next time level using an explicit FD formula which uses only values of motion at previous time levels (and, obviously, using also material grid parameters). In the case of an implicit scheme, there is no explicit formula for updating motion only in one grid point. In an implicit scheme, the motion at a given time level is calculated simultaneously at all spatial grid points from the motion values at previous time levels using the inverse of a matrix. Obviously, the explicit schemes are computationally simpler. A vast majority of earthquake ground motion modeling and exploration seismology studies use explicit FD schemes. For the implicit schemes see, e.g., Emerman et al. (1982), Mufti (1985).

Homogeneous and Heterogeneous FD Schemes

Motion in a smoothly heterogeneous elastic or viscoelastic continuum is governed by the equation of motion. The equation can be solved using a proper FD scheme. If the medium contains a material discontinuity, i.e., an interface between two homogeneous or smoothly heterogeneous media, at which density and elastic moduli change discontinuously, the equation of motion still governs motion away from the discontinuity but boundary conditions apply at the discontinuity. There are two approaches to deal with this situation – the homogeneous and heterogeneous approaches. In the homogeneous approach, a FD scheme for the smoothly heterogeneous medium is applied at grid points away from the material discontinuity while a FD scheme obtained by a proper discretization of the boundary conditions is applied at grid points at or near the material discontinuity. In the alternative heterogeneous approach only one FD scheme is used for all interior grid points (points not lying on boundaries of a grid) no matter what their positions are with respect to the material discontinuity. The presence of the material discontinuity is accounted for only by assigning appropriate values of elastic moduli and density. Therefore, except for treating the free surface, the heterogeneous approach has been much more popular since the beginning of the seventies.

A homogeneous FD scheme is specific for a particular problem. Its application to complex models with curved material discontinuities is difficult and therefore impractical. Moreover, finding a stable and sufficiently accurate FD approximation to the boundary conditions is not a trivial problem, see, e.g., Kummer and Behle (1982), Slawinski and Krebes (2002).

While widely used, the heterogeneous approach has not been addressed properly until very recently. The point is that the heterogeneous approach can be justified only when a heterogeneous formulation of the equation of motion and Hooke's law, that is, the same form of the equations for both a point away from the material discontinuity and a point at the material discontinuity, can be found. This question will be analyzed in the next section.

The Equation of Motion, Hooke's Law, and FD Schemes

Given a model, the equation of motion and Hooke's law (the stress-strain relation, constitutive law) together with the initial and boundary conditions fully describe a problem of seismic wave propagation and motion. Consider a Cartesian coordinate system (x_1, x_2, x_3), for example, with the x_1-axis horizontal and positive to the right, and the x_3-axis positive downward. Let $\rho(x_i)$; $i \in \{1,2,3\}$ be density, $c_{ijkl}\left(x_q\right)$ tensor of elastic coefficients, $\kappa(x_i)$ bulk modulus, $\mu(x_i)$ shear modulus, $\vec{u}(x_i,t)$ displacement vector, $\vec{v}(x_i,t)$ particle-velocity vector, $\vec{f}(x_i,t)$ body force per unit volume, $\sigma_{ij}(x_k,t)$ and $\varepsilon_{ij}(x_k,t)$; $i, j, k \in \{1,2,3\}$ stress- and strain-tensors (from now on, x_1, x_2, x_3 and x, y, z may be used interchangeably; similarly, 1, 2, 3 and x, y, z in the subscripts of the displacement and stress-tensor components), δ_{ij} Kronecker delta. A partial time derivative will be denoted by a dot above the symbol or the operator ∂_t; for example, $\partial u_i / \partial t = \dot{u}_i = \partial_t u_i$. A derivative with respect to the coordinate x_j will be denoted by a comma followed by x_j or the operator ∂_j; for example, $\partial \sigma_{ij} / \partial x_j = \sigma_{ij,j} = \partial_j \sigma_{ij}$. The Einstein summation convention for repeated indices will be assumed unless stated otherwise.

With reference to the FD schemes developed during the last decades, the following alternative formulations of the equation of motion and Hooke's law for anisotropic or isotropic media can be used as a starting point for deriving the FD schemes:

displacement-stress

$$\begin{aligned} &\rho \ddot{u}_i = \sigma_{ij,j} + f_i \\ &\sigma_{ij} = c_{ijkl}\varepsilon_{kl} \\ &\quad or \\ &\sigma_{ij} = \kappa \varepsilon_{kk}\delta_{ij} + 2\mu\left(\varepsilon_{ij} - \tfrac{1}{3}\varepsilon_{kk}\delta_{ij}\right) \end{aligned} \tag{6}$$

displacement-velocity-stress

$$\begin{aligned} &\rho \dot{v}_i = \sigma_{ij,j} + f_i \\ &v_i = \dot{u}_i \\ &\sigma_{ij} = c_{ijkl}\varepsilon_{kl} \\ &\quad or \\ &\sigma_{ij} = \kappa \varepsilon_{kk}\delta_{ij} + 2\mu\left(\varepsilon_{ij} - \tfrac{1}{3}\varepsilon_{kk}\delta_{ij}\right) \end{aligned} \tag{7}$$

velocity-stress

$$\begin{aligned} &\rho \dot{v}_i = \sigma_{ij,j} + f_i \\ &\dot{\sigma}_{ij} = c_{ijkl}\dot{\varepsilon}_{kl} \\ &\quad or \\ &\dot{\sigma}_{ij} = \kappa \dot{\varepsilon}_{kk}\delta_{ij} + 2\mu\left(\dot{\varepsilon}_{ij} - \tfrac{1}{3}\dot{\varepsilon}_{kk}\delta_{ij}\right) \end{aligned} \tag{8}$$

displacement

$$\rho \ddot{u}_i = \left[\left(\kappa - \tfrac{2}{3}\mu\right) u_{k,k}\right]_{,i} + \left(\mu u_{i,j}\right)_{,j} + \left(\mu u_{j,i}\right)_{,j} + f_i$$

or

$$\rho \ddot{u}_i = \left(c_{ijkl} u_{k,l}\right)_{,j} + f_i \qquad (9)$$

Because it is not differentiated with respect to the spatial coordinates, the strain tensor $\varepsilon_{ij} = \frac{1}{2}\left(u_{i,j} + u_{j,i}\right)$ was used here in the first three formulations for brevity.

The above are so-called strong formulations of the equation of motion. However, a FD method can also be applied to a (integral) weak form of the equation of motion. For example, a weak form of the Galerkin type is typical for the standard finite-element method (e.g., Zienkiewicz and Taylor, 1989; Ottosen and Petersson, 1992).

When solving the strong form of the equation of motion, the boundary conditions at material discontinuities must be explicitly satisfied. The traction continuity at internal discontinuities and vanishing traction at the free surface are automatically satisfied by the weak-form solution (this is an advantage of the weak form). In contrast, continuity of displacement is an essential continuity condition that must be explicitly satisfied by the weak-form solutions.

Whereas most of the recent FD schemes solve one of the strong forms, Geller and Takeuchi (1995, 1998) developed their optimally accurate FD schemes in application to the weak form of Strang and Fix (1973) and Geller and Ohminato (1994).

In principle, any formulation can be used with any of the three types of the grids (conventional, partly-staggered, staggered). However, it is obvious that the displacement formulation is naturally connected with the conventional grid. This is because only displacement values are explicitly present both in the equations and grid. Similarly, the velocity-stress formulation is naturally connected with the staggered grid as all field quantities in the equation of motion and Hooke's law are explicitly present in the grid. The particular structure (i.e., relative positions of the field quantities in space and time) of the staggered grid is unambiguously determined by the structure of the equation of motion and Hooke's law, that is, by the temporal and spatial derivatives of the field quantities.

In the early days of the FD method applied to seismology and seismics, the displacement formulation and conventional grid were used; for example, Alterman and Karal (1968), Boore (1970, 1972), Kelly et al. (1976). Because the conventional-grid displacement FD schemes had problems with instabilities in models with high-velocity contrasts and with grid dispersion in media with high Poisson's ratio, Virieux (1984, 1986) introduced the staggered-grid velocity-stress FD schemes for modeling seismic wave propagation. Virieux followed Madariaga (1976) who introduced the staggered-grid formulation in his dynamic modeling of the earthquake rupture. Bayliss et al. (1986) and Levander (1988) introduced the 4th-order staggered-grid FD schemes which in 2D and 3D need at least four and eight times less memory, respectively, compared to the 2nd-order schemes. In terms of CPU the improvement is 5-8 times in 2D and 10-16 in 3D. This is related to the grid dispersion. The staggered-grid FD schemes have become the dominant type of schemes in the FD modeling of seismic wave propagation and earthquake motion. In order to further reduce the memory requirements, Luo and Schuster (1990) suggested a staggered-grid displacement-stress 2D P-SV FD scheme which they called a parsimonious scheme. Because the scheme does not integrate stress in time, the stress-tensor components are only temporary quantities. Thus, the

displacement-stress scheme in 3D needs only 75% of the memory needed by the velocity-stress scheme. Rodrigues (1993), and Yomogida and Etgen (1993) used the 8^{th}-order 3D displacement-stress FD schemes, Ohminato and Chouet (1997) applied the 2^{nd}-order while Moczo et al. (2000, 2002) the 4^{th}-order approximations. Moczo et al. (2000) analyzed the grid dispersion of the displacement-stress schemes (4^{th} and 2^{nd} order) and pointed out that the stability and grid dispersion of the displacement-stress, displacement-velocity stress and velocity-stress schemes are the same. The advantage of the displacement-velocity-stress scheme is that both displacement and particle-velocity are calculated at no extra cost.

The partly-staggered grid was probably first used in seismology by Andrews (1973) who applied it in modeling the fault rupture using his traction-at-split-node method. Magnier et al. (1994) realized disadvantages of the staggered-grid schemes in treating the anisotropic media and used the partly-staggered grid. Zhang (1997) used the partly-staggered grid in his 2D velocity-stress FD modeling. However, the developed schemes have not attracted much attention. Recently, the use of the partly-staggered grid was promoted by Saenger et al. (2000) and Saenger and Bohlen (2004). They called the grid rotated staggered grid since they obtained the spatial FD operator by the rotation of the standard staggered-grid operator. The term 'rotated staggered grid' is somewhat unfortunate because assuming one spatial grid position for the stress tensor and another position for the displacement vector, it is possible to find a variety of FD schemes - depending on the order of approximation. Only in one particular case can the spatial FD operator be obtained by the rotation of the standard staggered-grid operator though it is also easy to obtain it without explicit consideration of the rotation. In fact, the particular scheme used by Saenger et al. (2000) is a simple consequence of requirement of the same truncation error with respect to all coordinate axes.

While the reason to use the partly-staggered grids for anisotropic media is obvious (all stress-tensor components located at the same grid position thus requiring no interpolation of particle velocities or strains), the application of the partly-staggered grid to account for the material heterogeneity has not been analyzed. Therefore, this application still needs to be theoretically more rigorously analyzed.

A special aspect of the development is the FD schemes formulated for non-uniform grids. These will be mentioned in the section on the memory optimization and parallelization.

Apart from the recent dominance of the staggered-grid FD schemes, Geller and his co-workers developed another important approach to the FD modeling of seismic wave propagation based on the weak form of the equation of motion. In their schemes displacement is the sole dependent variable, as opposed to the staggered-grid schemes. Geller and Takeuchi (1995) derived a general criterion for optimally accurate numerical operators, and used it to derive an optimally accurate frequency-domain scheme. Geller and Takeuchi (1998) used the criterion to derive an optimally accurate FDTD scheme for 1D problems. Takeuchi and Geller (2000) then developed optimally accurate FDTD operators for 2D and 3D problems. These derivations yield implicit schemes which are solved using a predictor-corrector algorithm, so that the actual computational schemes are explicit. Whereas optimally accurate FDTD schemes require at least twice the CPU time per grid point and time step compared to 2^{nd}-order staggered-grid FD schemes, they yield accuracy improvements on the order of 10 (for 1-D), 50 (for 2-D), or 100 (for 3-D). From this point of view they are cost-effective. The optimally accurate schemes have not yet been widely used in practical FD modeling. The likely reasons are a) the theory might appear relatively complicated compared to that of the standard staggered-grid schemes, b) the fact that quantification and minimization of computational error

have not heretofore been widely viewed as high priorities, c) inertia with respect to traditional approaches and the lack of user-friendly codes for optimally accurate schemes. However, it is likely that optimally accurate FD schemes will be more widely used in the future.

An interesting approach to develop alternative FD scheme was presented by Holberg (1987). Instead of minimizing the error measured in terms of higher-order derivatives he minimized the relative error in group velocity caused by the grid dispersion within a specific frequency band emitted by active sources. Therefore he did not develop the FD operator with the predetermined order of the truncation error using the Taylor expansions. Holberg defined the FD operator as a differentiator realized by a convolutory (FIR) operator.

Whereas most of the recent FD schemes are 2^{nd}-order accurate in time, it is possible to increase the order of accuracy by employing the Lax-Wendroff correction (Lax and Wendroff, 1964; Dablain, 1986). The leading term in the truncation error for the 2^{nd}-order FD approximation to time derivative is replaced by a term with only spatial derivatives using the equation of motion. Although the form of the Lax-Wendroff schemes is quite different from the optimally accurate schemes of Geller and co-workers, Mizutani et al. (2000) have shown that these two types of scheme are in fact essentially identical. An efficient implementation of the approach for viscoelastic media was presented by Blanch and Robertsson (1997). An alternative approach for the time stepping is to use the Chebychev expansion method by Tal-Ezer et al. (1990) which combines computational efficiency with spectral accuracy in time.

Algorithms for Enhancing Computational Performance

A significant part of the literature has been devoted to enhancing the computational efficiency of FDTD by taking a more holistic view as to how FDTD are applied to solve a computational problem. Several methods for hybrid modeling were developed in the eighties and nineties where different computational techniques are used either for temporal/spatial dependences (e.g., Alexeev and Mikhailenko, 1980) or in different parts of the model appropriate for the local wave propagation regime (e.g., Shtivelman, 1984, 1985; Kummer et al., 1987; Stead and Helmberger, 1988; Emmerich, 1989, 1992; Fäh, 1992; Robertsson et al., 1996; Zahradník and Moczo, 1996; Moczo et al., 1997; Lecomte et al., 2004). For instance, for a reflection seismic problem, in a smoothly varying overburden a ray-based solution may be appropriate whereas FDTD are needed only in the vicinity of a complex target where the energy reflects and is reverberated back towards the surface. Such an approach can enable computational savings of several orders of magnitude depending on the specific application and model and will be particularly significant in 3D. Problems with implementing and using such methods are related to model generation and interfacing the different methods which tend to be different from problem to problem making the process very difficult to implement in an automatic fashion.

A somewhat different approach was taken by, for instance, Robertsson and Chapman (2000) and Robertsson et al. (2000) who proposed to use a technique, referred to as FD-injection, fully based on finite differences for regenerating the FD response in a model following local model alterations. The computational savings can be very significant, particularly for applications such as full waveform inversion or time-lapse seismic analyses.

Recently, van Manen et al. (2005) have proposed a method based on concepts from time-reversal acoustics (Fink, 1997), that may become an important tool in synthesizing seismic data. The approach relies on a representation theorem of the wave equation to express the Green's function between points in the interior as an integral over the response in those points due to sources on a surface surrounding the medium. Following a predictable initial computational effort, Green's functions between arbitrary points in the medium can be computed as needed using a simple cross-correlation algorithm.

Optimally Accurate FD Operators

A linear mechanical system or a finite volume of elastic continuum preferably supports oscillatory motion at certain frequencies which are called eigenfrequencies or resonant frequencies, i.e. at normal modes. In other words, the oscillatory motion is naturally most amplified at these frequencies. The same is also true about a numerical error in a discrete numerical system which is a numerical approximation to the true physical system. The basic idea of Geller and Takeuchi (1995) therefore seems quite obvious: to minimize the error of the numerical solution first of all at eigenfrequencies.

Geller and Takeuchi (1995) used first-order Born theory and a normal mode expansion to obtain formal estimates of the relative error of the numerical solution and a general criterion for what they called optimally accurate operators. The criterion requires that the inner product of an eigenfunction and the net error of the discretized equation of motion should be approximately equal to zero when the operand is the eigenfunction and the frequency is equal to the corresponding eigenfrequency. An important aspect of the approach is that it is not necessary to know the actual values of the eigenfrequencies and eigenfunctions to use the criterion to derive optimally accurate operators. Geller and Takeuchi (1995) showed that in the case of a heterogeneous medium the criterion is the logical extension of the criterion to minimize grid dispersion of phase velocity for a homogeneous medium. Based on this criterion, Geller and Takeuchi (1998) derived optimally accurate 2nd-order weak-form FDTD scheme for the elastic 1D case. Takeuchi and Geller (2000) then generalized their approach to the 2D and 3D cases.

Though the optimally accurate FD operators are not applicable to the staggered-grid schemes (they would lead to apparently intractable implicit schemes – according to Geller and Takeuchi, 1998), we consider them important and assume their wider applications in future FDTD modeling. Therefore, we briefly present the basics of Geller and Takeuchi's approach, closely following Geller and Takeuchi (1995, 1998).

General Criterion for Optimally Accurate FD Operators

In the Direct Solution Method (DSM; Geller and Ohminato, 1994) the equation of motion for an anelastic solid is transformed into its Galerkin weak form (Strang and Fix, 1973),

$$\left(\omega^2 \mathbf{T} - \mathbf{H} \right) \vec{c} \; = \; - \vec{g} \;\; , \tag{10}$$

where ω is the angular frequency, $\mathbf{T}$ mass matrix, $\mathbf{H}$ stiffness matrix, $\vec{c}$ vector of expansion coefficients for the trial functions, $\vec{g}$ force vector,

$$T_{rs} = \int_V \left[\phi_i^{(r)} \right]^* \rho \, \phi_i^{(s)} dV \;\; , \quad H_{rs} = \int_V \left[\phi_i^{(r)}{}_{,j} \right]^* c_{ijkl} \, \phi_k^{(s)}{}_{,l} \, dV \;\; ,$$
$$g_r = \int_V \left[\phi_i^{(r)} \right]^* f_i \, dV \;\; , \tag{11}$$

$\phi_i^{(r)}$ is the i-th component of the r-th trial function, and $*$ means complex conjugate quantity. The displacement is represented as

$$u_i = \sum\nolimits_r c_r \, \phi_i^{(r)} \, . \tag{12}$$

If an infinite trial function expansion were used, equation (10) would yield exact solutions. In any practical application the trial function expansion will be finite and there will be some numerical error. The exact equation of motion can be formally written as

$$\left(\omega^2 \, \mathbf{T}^e - \mathbf{H}^e \right) \vec{c}^{\, e} \; = \; - \vec{g} \; . \tag{13}$$

The relation between the numerical and exact quantities is assumed in a form

$$\mathbf{T} = \mathbf{T}^e + \delta\mathbf{T} \, , \quad \mathbf{H} = \mathbf{H}^e + \delta\mathbf{H} \, , \quad \vec{c} = \vec{c}^{\, e} + \overrightarrow{\delta c} \; , \tag{14}$$

where $\delta\mathbf{T}$, $\delta\mathbf{H}$ and $\overrightarrow{\delta c}$ are errors of the numerical operators and solution, respectively.

The normal modes satisfy equation

$$\left(\omega_p^2 \, \mathbf{T}^e - \mathbf{H}^e \right) \vec{c}_{\, p} \; = \; 0 \, , \tag{15}$$

where ω_p is an eigenfrequency of the p-th mode and $\vec{c}_{\, p}$ is the eigenvector. Orthonormalization is assumed in a form

$$\vec{c}_{\, p}^{\, *} \, \mathbf{H}^e \, \vec{c}_{\, q} \; = \; \omega_p^2 \, \vec{c}_{\, p}^{\, *} \, \mathbf{T}^e \, \vec{c}_{\, q} \; = \; \omega_p^2 \, \delta_{pq} \; . \tag{16}$$

Substituting eqs. (14) into the l.h.s. of eq. (10), replacing the r.h.s. of eq. (10) by the l.h.s. of eq. (13), and neglecting terms with products of errors (the first-order Born approximation) leads to

$$\left(\omega^2 \, \mathbf{T}^e - \mathbf{H}^e \right) \overrightarrow{\delta c} \; = \; - \left(\omega^2 \, \delta\mathbf{T} - \delta\mathbf{H} \right) \vec{c}^{\, e} \; . \tag{17}$$

Eq. (17) enables to determine the error of the numerical solution, $\overrightarrow{\delta c}$, if the exact solution and errors of the operators, i.e., $\vec{c}^{\, e}$, $\delta\mathbf{T}$ and $\delta\mathbf{H}$ are known.

The solution of eq. (13) can be represented in terms of an eigenfunction expansion

$$\vec{c}^{\, e} = \sum\nolimits_p d_p^e \, \vec{c}_{\, p} \; . \tag{18}$$

Substituting eq. (18) into eq. (13), and using eq. (16) leads to

$$d_p^e \; = \; \vec{c}_{\, p}^{\, *} \, \vec{g} \, \Big/ \left(\omega^2 - \omega_p^2 \right) \, . \tag{19}$$

The expansion coefficient d_p^e will be large, when ω is close to ω_p. Otherwise, it will be negligible.

The solution of eq. (17) can also be represented in terms of an eigenfunction expansion

$$\overrightarrow{\delta c} = \sum\nolimits_p \delta d_p \vec{c}_p \ . \tag{20}$$

Substituting expansions (18) and (20) into eq. (17), and using eqs. (16) leads to

$$\delta d_p \ = \ -\sum\nolimits_q \left(\omega^2 \vec{c}_p^{\,*} \delta \mathbf{T} \vec{c}_q \ - \ \vec{c}_p^{\,*} \delta \mathbf{H} \vec{c}_q \right) d_q^e \Big/ \left(\omega^2 - \omega_p^2 \right) . \tag{21}$$

The expansion coefficient δd_p will be large only when ω is close to ω_p. In such a case obviously only d_p^e will be large. Therefore, in the vicinity of $\omega = \omega_p$, the $q \neq p$ terms in eq. (21) can be neglected, i.e., the relative error of the numerical solution in the vicinity of ω_p will approximately be

$$\frac{\delta d_p}{d_p^e} \ = \ -\left(\omega^2 \vec{c}_p^{\,*} \delta \mathbf{T} \vec{c}_p - \vec{c}_p^{\,*} \delta \mathbf{H} \vec{c}_p \right) \Big/ \left(\omega^2 - \omega_p^2 \right) . \tag{22}$$

It follows from eq. (22) that the relative error will in general greatly increase with $\omega \to \omega_p$. However, if the numerator of eq. (22) is also proportional to $\omega - \omega_p$, the relative error will remain approximately constant as $\omega \to \omega_p$. Such proportionality can be achieved if and only if

$$\omega_p^2 \vec{c}_p^{\,*} \delta \mathbf{T} \vec{c}_p \ - \ \vec{c}_p^{\,*} \delta \mathbf{H} \vec{c}_p \ \doteq \ 0 \tag{23}$$

for each mode. If eq. (23) is approximately satisfied, then eq. (22) can be simplified:

$$\left| \frac{\delta d_p}{d_p^e} \right| \ \approx \ \vec{c}_p^{\,*} \delta \mathbf{T} \vec{c}_p \ . \tag{24}$$

This means that the relative error for a given grid can be reliably estimated in advance of calculation.

Geller and Takeuchi (1995) defined optimally accurate operators, say $\mathbf{T}'$ and $\mathbf{H}'$, as operators that satisfy eq. (23):

$$\vec{c}_p^{\,*} \left(\omega_p^2 \, \delta \mathbf{T}' - \delta \mathbf{H}' \right) \vec{c}_p \ \doteq \ 0 \ . \tag{25}$$

Substituting first two of eqs. (14) for operators $\mathbf{T}'$ and $\mathbf{H}'$ into eq. (25) and using eq. (15) leads to equivalent equation

$$\vec{c}_p^{\,*}\left(\omega_p^2 \mathbf{T}' - \mathbf{H}' \right) \vec{c}_p \doteq 0 \ . \tag{26}$$

Eq. (25) will be satisfied if the leading term of the truncation error of the discretized equation is zero when the operand is an eigenfunction and the frequency is equal to the corresponding eigenfrequency, in other words if

$$\left(\omega_p^2 \delta\mathbf{T}' - \delta\mathbf{H}' \right) \vec{c}_p \doteq 0 \ . \tag{27}$$

On the other hand, however, it is not necessary for eq. (27) to be satisfied in order for eq. (25) to be satisfied, because even if the quantity on the l.h.s. of eq. (27) is non-zero, its inner product with $\vec{c}_p$ can still be approximately zero. Geller and Takeuchi (1995, 1998) and Takeuchi and Geller (2000) take advantage of this fact to derive optimally accurate operators using a two-step methodology. First, for interior points, they derived optimally accurate operators that satisfy eq. (27). Second, to complete the derivation of the optimally accurate operators, they "fill in" the few remaining degrees of freedom (corresponding to boundary points or their neighbors) so that eq. (25) is approximately satisfied, even though eq. (27) is not necessarily satisfied.

In this review, for simplicity, we discuss only the simplest case of optimally accurate 1-D TDFD operators for interior points only. For a discussion of the treatment of the boundary operators, see, for example, sections 3 and 4 of Geller and Takeuchi (1995).

Consider the equation

$$exact\ LHS(\omega,u) = \vec{f} \tag{28}$$

and such its discretization which gives

$$discretized\ LHS(\omega,u) = exact\ LHS(\omega,u) + \frac{h^2}{a}\left[exact\ LHS(\omega,u)\right]'' + \ldots \ , \tag{29}$$

where the primes denote spatial differentiation. The normal modes satisfy the equation

$$exact\ LHS\left(\omega_p,u_p\right) = 0 \ , \tag{30}$$

which implies

$$\left[exact\ LHS\left(\omega_p,u_p\right)\right]'' = 0 \ . \tag{31}$$

Considering normal modes in eq. (29), and substituting eqs. (30) and (31) into eq. (29) leads to

$$discretized\ LHS\left(\omega_p,u_p\right) \doteq 0 \ , \tag{32}$$

which corresponds to condition (26). This shows that the leading term of the truncation error of each FD approximation used to discretize the l.h.s. of eq. (28) has the same

coefficient, h^2/a, and the displacement 2 times more differentiated than in the approximated term. Thus, we have an indication for constructing optimally accurate discretization.

Optimally Accurate FD Operators for 1D problem in a Homogeneous Medium

In order to illustrate the above theory, we closely follow the 1D problem for a homogeneous medium in Geller and Takeuchi (1998). Consider 1D equation

$$\rho \ddot{u} = C \frac{\partial^2 u}{\partial x^2} + f \ . \tag{33}$$

A weak-form FDTD approximation to the equation can be written as

$$\left[A_I^m(M,i) - K_I^m(M,i) \right] U(M,i) = F_I^m \ , \tag{34}$$

where m is the time level, at which eq. (34) is approximated, I index of the spatial position at which eq. (34) is approximated, M time summation index, i spatial summation index. Matrix $\mathbf{A}_I^m$ has the form

$$\mathbf{A}_I^m(M,i) = \begin{bmatrix} A_I^m(m+1,I-1) & A_I^m(m+1,I) & A_I^m(m+1,I+1) \\ A_I^m(m\quad,I-1) & A_I^m(m\quad,I) & A_I^m(m\quad,I+1) \\ A_I^m(m-1,I-1) & A_I^m(m-1,I) & A_I^m(m-1,I+1) \end{bmatrix}, \tag{35}$$

matrix $\mathbf{K}_I^m$ has an analogous structure. The conventional operators, corresponding to the standard difference formula (4), are

$$\mathbf{A}_I^m = \frac{\rho}{\Delta^2 t} \begin{bmatrix} 0 & 1 & 0 \\ 0 & -2 & 0 \\ 0 & 1 & 0 \end{bmatrix}, \quad \mathbf{K}_I^m = \frac{C}{h^2} \begin{bmatrix} 0 & 0 & 0 \\ 1 & -2 & 1 \\ 0 & 0 & 0 \end{bmatrix}. \tag{36}$$

The operator error at a single point in space and time approximately is (only the leading term is given)

$$\left[\delta A_I^m(M,i) - \delta K_I^m(M,i) \right] U(M,i) \doteq \left[\frac{\Delta^2 t}{12} \rho \frac{\partial^4 u}{\partial t^4} - \frac{h^2}{12} C \frac{\partial^4 u}{\partial x^4} \right]_{m,I}, \tag{37}$$

where $\delta \mathbf{A}_I^m$ and $\delta \mathbf{K}_I^m$ are differences between the conventional and exact operators.

In order to derive an optimally accurate FDTD scheme, Geller and Takeuchi (1998) take the Fourier transform of eq. (34), to obtain the FD equation in the frequency domain for purposes of error analysis:

$$\left[\tilde{A}_I(i) - \tilde{K}_I(i) \right] \tilde{U}(i) = \tilde{F}_I \ . \tag{38}$$

Because eq. (38) has essentially the same form as eq. (10), the above theory of the error of the numerical solution can be applied. The difference is that the operator errors here depend on frequency and wavenumber.

The Fourier transform of eq. (37) is

$$\left[\delta\tilde{A}_I(i) - \delta\tilde{K}_I(i) \right] \tilde{U}(i) \doteq \left[\frac{\omega^2 \Delta^2 t}{12} \rho \omega^2 u - \frac{h^2}{12} \frac{d^2}{dx^2} \left(C \frac{d^2 u}{dx^2} \right) \right]_I . \tag{39}$$

It is clear from eq. (39) that the error is not equal to zero when the operand is an eigenfunction and frequency is equal to eigenfrequency. This would be the case if

$$\left[\delta\tilde{A}_I(i) - \delta\tilde{K}_I(i) \right] \tilde{U}(i) \doteq \left(\frac{\omega^2 \Delta^2 t}{12} - \frac{h^2}{12} \frac{d^2}{dx^2} \right) \left[\rho \omega^2 u + C \frac{d^2 u}{dx^2} \right]_I \tag{40}$$

because the expression inside the brackets is the l.h.s. of the exact homogeneous equation of motion in the frequency domain, which is zero when the operand is an eigenfunction and the frequency is the corresponding eigenfrequency. A time-domain equivalent to eq. (40) can be obtained by applying the inverse Fourier transform to eq. (40):

$$\begin{aligned} &\left[\delta A_I^m(M,i) - \delta K_I^m(M,i) \right] U(M,i) \doteq \\ &\qquad \doteq \left\{ \frac{\Delta^2 t}{12} \frac{\partial^2}{\partial t^2} \left[\rho \frac{\partial^2 u}{\partial t^2} - C \frac{\partial^2 u}{\partial x^2} \right] + \frac{h^2}{12} \frac{\partial^2}{\partial x^2} \left[\rho \frac{\partial^2 u}{\partial t^2} - C \frac{\partial^2 u}{\partial x^2} \right] \right\}_{m,I} . \end{aligned} \tag{41}$$

The operators that yield error (41) are

$$\mathbf{A}_I^m = \frac{\rho}{\Delta^2 t} \begin{bmatrix} 1/12 & 10/12 & 1/12 \\ -2/12 & -20/12 & -2/12 \\ 1/12 & 10/12 & 1/12 \end{bmatrix}, \quad \mathbf{K}_I^m = \frac{C}{h^2} \begin{bmatrix} 1/12 & -2/12 & 1/12 \\ 10/12 & -20/12 & 10/12 \\ 1/12 & -2/12 & 1/12 \end{bmatrix} . \tag{42}$$

Though, obviously, the operators (42) come from the condition (41), which corresponds to conditions (25) and (26), it is now easy to see relation to the conventional operators. Consider, e.g., approximation to the second time derivative at time level m and spatial position I. While the conventional approximation, formula (4), is

$$\left. \frac{\partial^2 u}{\partial t^2} \right|_{m,I} \doteq \frac{1}{\Delta^2 t} \left(U_I^{m-1} - 2U_I^m + U_I^{m+1} \right) , \tag{43}$$

the approximation corresponding to the optimally accurate operator $\mathbf{A}_I^m$ in eq. (42) is

$$\left.\frac{\partial^2 u}{\partial t^2}\right|_{m,I} \doteq \frac{1}{12}\left(\left.\frac{\partial^2 u}{\partial t^2}\right|_{m,I-1} + 10\left.\frac{\partial^2 u}{\partial t^2}\right|_{m,I} + \left.\frac{\partial^2 u}{\partial t^2}\right|_{m,I+1} \right) \tag{44}$$

where the conventional approximation (43) is used to approximate derivatives at time level m at all three spatial positions $I-1$, I and $I+1$. Similarly, the optimally accurate spatial second derivative is approximated over three time levels $m-1$, m and $m+1$.

It is obvious that optimally accurate operators yield an implicit FD scheme. In order to avoid necessity to solve a system of simultaneous linear equations at each time step, Geller and Takeuchi (1998) applied a predictor-corrector scheme. Note that the predictor-corrector optimally accurate scheme and the Lax-Wendroff scheme are essentially the same (Mizutani et al., 2000).

As already mentioned, Takeuchi and Geller (2000) generalized the approach based on the optimally accurate operators to solve 2D and 3D problems.

Complex Viscoelastic Media with Material Discontinuities

As already mentioned, accounting for realistic attenuation and heterogeneity of the medium, particularly in the presence of material discontinuities in the Earth's interior, is of crucial importance in modeling seismic wave propagation and earthquake motion. While seismologists tried to model material discontinuities from the very beginning of the application of the FDM in seismology, the incorporation of the realistic attenuation was made possible considerably later. We first briefly review the problem of material heterogeneity and material discontinuities in the strong formulation of the equation of motion.

A Material Discontinuity in the Elastic Medium

In one of the pioneering efforts on the application of the FDM to seismic wave propagation, Alterman and Karal (1968) introduced the concept of fictitious grid points in order to approximate boundary conditions on material discontinuities in their displacement FD scheme. Difficulties in application of the homogeneous approach to curved discontinuities led Boore (1972) to explicitly include a stress-continuity condition on discontinuities differently from the homogeneous and heterogeneous approaches. Due to poor numerical properties of his explicit continuous stress method, Boore (1972) applied the heterogeneous approach in his SH modeling. In order to follow detailed variation of the torsion modulus and, at the same time, to avoid derivatives of the modulus, he used the mathematical trick of Tikhonov and Samarskii (see, e.g., Mitchell 1969, p.23) and calculated effective grid moduli as integral harmonic averages along a grid line between two neighboring grid points. Ilan et al. (1975) and Ilan and Loewenthal (1976) applied the homogeneous approach to the 2D P-SV problem on horizontal and vertical planar discontinuities. They used Taylor expansions of displacement to couple the equation of motion with the boundary conditions. Kelly et al. (1976) presented their heterogeneous P-SV schemes with simple intuitive averaging of material parameters. They numerically compared the heterogeneous approach with the homogeneous one and showed unacceptable difference between the two approaches in the case of the corner-edge model. Kummer and Behle (1982) followed the approach of Ilan et al. (1975) and derived the 2^{nd}-order SH schemes for grid points lying on different types of segments of the step-like polygonal discontinuity. Virieux (1984, 1986) used the velocity-stress formulation and staggered grid introduced to seismology by Madariaga (1976). His P-SV FD scheme did not suffer from stability problems caused by large values of Poisson's ratio, which was the case of all displacement schemes on conventional grids. Since the work by Virieux, the staggered-grid FD schemes became the dominant schemes applied to seismic wave propagation in heterogeneous media. Virieux also discussed the discrepancy between the homogeneous and heterogeneous approaches found by Kelly et al. (1976). He found it difficult to explain features of the solution obtained by the homogeneous approach.

An attempt to incorporate internal boundary conditions into a displacement FD scheme was made by Sochacki *et al*. (1991) who integrated the equation of motion over a grid cell that could possibly contain a material discontinuity. The integrated equation of motion was then discretized. Schoenberg and Muir (1989) developed a calculus to replace a stack of thin flat elastic anisotropic homogeneous layers by an equivalent (in

the long-wavelength limit) homogeneous anisotropic medium. As a result, they found that stress-strain relation for an averaged medium satisfies the boundary conditions at interfaces. Applying the Schoenberg-Muir calculus simplifies modeling of wave propagation and, at the same time, accounts for transversal anisotropy. Muir et al. (1992) applied the Schoenberg-Muir calculus to a grid cell containing material discontinuity, i.e., in general, they treated contents of the cell as a stack of thin flat layers that can be averaged by the Schoenberg-Muir calculus. The two papers did not have the impact on the heterogeneous FD schemes that they deserved - likely because the authors did not make explicit reference to the question of the heterogeneous FD schemes. Zahradník and Priolo (1995) explicitly pointed out the problem of heterogeneous FD schemes. Assuming discontinuous material parameters in the equation of motion they obtained an expression whose dominant term is equivalent to the traction continuity condition. As other developers of the heterogeneous FD schemes they were not aware of the work by Schoenberg and Muir. Graves (1996) intuitively suggested a formula for determination of effective material grid parameters in the 3D 4^{th}-order velocity-stress staggered-grid schemes and numerically demonstrated the good level of accuracy. Zhang and Symes (1998) developed a 2D 4^{th}-order full-stencil immersed interface technique to account for a curved material discontinuity. In the first step, all grid points are solved using a standard FD scheme. In the second step, each grid point whose stencil includes grid points from both sides of the discontinuity is recalculated using previous time step's values with a special 25-point scheme determined using local boundary conditions. Moczo et al. (2002) analyzed the 1D problem in a medium consisting of two halfspaces. They demonstrated their method on a simple physical model of the contact of two media, found a heterogeneous formulation of the equation of motion and Hooke's law, and derived a heterogeneous FD scheme. Finally they analyzed the 3D problem, suggested a 4^{th}-order heterogeneous staggered-grid FD scheme, and demonstrated its accuracy compared to the standard staggered-grid FD schemes. Their analysis will be followed in the next sections.

1D problem

Consider two elastic halfspaces with a welded interface in the plane $x = 0$. The wave propagation in the halfspaces is described by equations

$$\rho^{\pm}\ddot{u}^{\pm} = \sigma^{\pm}{}_{,x} + f^{\pm} \quad , \qquad \sigma^{\pm} = C^{\pm}u^{\pm}{}_{,x} \tag{45}$$

where the superscript $^{+}$ refers to one halfspace and superscript $^{-}$ to the other. Either $u(x,t)$ is the *x*-component of the displacement $\vec{u}(u_x,0,0)$, $\sigma(x,t)$ the *xx*-component of the stress tensor, $f(x,t)$ the *x*-component of the body force per unit volume $\vec{f}(f_x,0,0)$ and $C(x)=\lambda(x)+2\mu(x)$ in the case of P wave, or $u(x,t)$ is the *y*-component of the displacement $\vec{u}(0,u_y,0)$, $\sigma(x,t)$ the *xy*-component of the stress tensor, $f(x,t)$ the *y*-component of the body force per unit volume $\vec{f}(0,f_y,0)$ and $C(x)=\mu(x)$ in the case of the SH wave (the coordinate system can always be rotated so that the S wave could be the SH wave). At the welded interface the continuity of displacement and traction applies: $u^{-}(0)=u^{+}(0)$, $\sigma^{-}(0)=\sigma^{+}(0)$. Because a

heterogeneous FD scheme should be nothing else than a discrete approximation to a differential problem, a heterogeneous formulation of the differential problem is to be found. This means the same form of the equation of motion and Hooke's law for a point at a material discontinuity as a point away from the material discontinuity.

Let $\varphi^{\pm}(x)$, $c^{\pm}(x)$ and $g^{\pm}(x)$ be real functions of a real argument x such that

$$\varphi^{\pm}(x) = c^{\pm}(x)\, g^{\pm}(x) \tag{46}$$

and

$$\varphi^{-}(0) = \varphi^{+}(0) \,. \tag{47}$$

Functions $c^{\pm}(x)$ and $g^{\pm}(x)$ may have discontinuities of the first order at $x = 0$. Define

$$\overline{g}(0) = 0.5 \cdot \left[g^{-}(0) + g^{+}(0) \right] \,. \tag{48}$$

Then it follows that

$$\varphi^{-}(0) = \varphi^{+}(0) = \overline{c}(0)\, \overline{g}(0) \quad ; \quad \overline{c}(0) = 2 \Big/ \left[1/c^{-}(0) + 1/c^{+}(0) \right] \,. \tag{49}$$

If $c^{\pm}(x) = 1/r^{\pm}(x)$, then

$$\varphi^{-}(0) = \varphi^{+}(0) = \frac{1}{\overline{r}(0)}\, \overline{g}(0) \quad ; \quad \overline{r}(0) = 0.5 \cdot \left[r^{-}(0) + r^{+}(0) \right] \,. \tag{50}$$

It follows from eqs. (46) to (50) that the equation of motion and Hooke's law for a point at the material discontinuity have the form

$$\overline{\rho}(0)\ \ddot{u}(0) = \overline{\sigma_{,x}}(0) + \overline{f}(0) \tag{51}$$

and

$$\sigma(0) = \overline{C}(0)\ \overline{u_{,x}}(0) \,, \tag{52}$$

respectively, with a density equal to the arithmetic average of the densities in the two halfspaces, and elastic modulus equal to the harmonic average of the moduli in the two halfspaces:

$$\overline{\rho}(0) = 0.5 \cdot \left[\rho^{-}(0) + \rho^{+}(0) \right] \quad , \quad \overline{C}(0) = 2 \Big/ \left[1/C^{-}(0) + 1/C^{+}(0) \right]. \tag{53}$$

The average spatial derivatives of the stress and displacement are

$$\begin{aligned} \overline{\sigma_{,x}}(0) + \overline{f}(0) &= 0.5 \cdot \left[\sigma^{-}{}_{,x}(0) + \sigma^{+}{}_{,x}(0) + f^{-}(0) + f^{+}(0) \right] \\ \overline{u_{,x}}(0) &= 0.5 \cdot \left[u^{-}{}_{,x}(0) + u^{+}{}_{,x}(0) \right] \quad . \end{aligned} \tag{54}$$

It is obvious that eqs. (51) and (52) for a point at the material discontinuity have the same form as the equation of motion and Hooke's law (45), at a point away from the material discontinuity. This provides a basis for the heterogeneous 1D FD scheme.

Moczo et al. (2002) also showed that two Hooke elements (elastic springs) connected in series make an appropriate rheological model for considering traction continuity at the welded interface of two elastic materials.

Consider, for example, the velocity-stress formulation. Let V_I^m, T_I^m and F_I^m be the discrete approximations to particle velocity $v_I^m = v\left(Ih, m\Delta t\right)$, stress $\sigma_I^m = \sigma\left(Ih, m\Delta t\right)$ and body force $f_I^m = f\left(Ih, m\Delta t\right)$. One possible heterogeneous 4th-order staggered-grid FD scheme for the 1D problem is

$$\begin{aligned} T_{I+1/2}^m &= T_{I+1/2}^{m-1} \\ &\quad + C_{I+1/2}^H \frac{\Delta t}{h}\left[a\left(V_{I+2}^{m-1/2} - V_{I-1}^{m-1/2}\right) + b\left(V_{I+1}^{m-1/2} - V_I^{m-1/2}\right)\right] \\ V_I^{m+1/2} &= V_I^{m-1/2} \\ &\quad + \frac{1}{\rho_I^A}\frac{\Delta t}{h}\left[a\left(T_{I+3/2}^m - T_{I-3/2}^m\right) + b\left(T_{I+1/2}^m - T_{I-1/2}^m\right)\right] + \frac{\Delta t}{\rho_I^A} F_I^m \end{aligned} \tag{55}$$

with

$$\rho_I^A = \frac{1}{h}\int_{x_{I-1/2}}^{x_{I+1/2}} \rho(x)\, dx \quad , \quad C_{I+1/2}^H = \left[\frac{1}{h}\int_{x_I}^{x_{I+1}} \frac{1}{C(x)}\, dx\right]^{-1} . \tag{56}$$

The coefficients in eqs. (55) are $a = -1/24$ and $b = 9/8$. In the scheme, the averaging of the spatial derivatives of the functions at the material discontinuity is neglected while the harmonic averaging of the elastic moduli and arithmetic averaging of densities at the material discontinuity is taken into account (see Moczo et al., 2002 for details). In general, the integrals are evaluated numerically. It is easy to check that the scheme yields very good accuracy in smoothly and/or discontinuously heterogeneous media. The scheme is capable to sense a true position of the material discontinuity no matter what the position of the discontinuity is with respect to the grid points.

While Tikhonov and Samarski (e.g., Mitchell 1969, p.23) obtained the harmonic averaging as a result of the mathematical 'trick' to avoid spatial derivatives of the coefficients in the 2nd-order displacement formulation, the harmonic average in the heterogeneous formulation (52) is due to traction-continuity condition at the material discontinuity.

3D problem

Define stress and strain vectors

$$\vec{\sigma} = \left[\sigma_{xx}, \sigma_{yy}, \sigma_{zz}, \sigma_{xy}, \sigma_{yz}, \sigma_{zx}\right]^T , \quad \vec{\varepsilon} = \left[\varepsilon_{xx}, \varepsilon_{yy}, \varepsilon_{zz}, \varepsilon_{xy}, \varepsilon_{yz}, \varepsilon_{zx}\right]^T . \tag{57}$$

Hooke's law for an isotropic medium can be written as

$$\vec{\sigma} = \mathbf{E}\,\vec{\varepsilon} \tag{58}$$

where

$$\mathbf{E} = \begin{bmatrix} \kappa+\frac{4}{3}\mu & \kappa-\frac{2}{3}\mu & \kappa-\frac{2}{3}\mu & 0 & 0 & 0 \\ \kappa-\frac{2}{3}\mu & \kappa+\frac{4}{3}\mu & \kappa-\frac{2}{3}\mu & 0 & 0 & 0 \\ \kappa-\frac{2}{3}\mu & \kappa-\frac{2}{3}\mu & \kappa+\frac{4}{3}\mu & 0 & 0 & 0 \\ 0 & 0 & 0 & 2\mu & 0 & 0 \\ 0 & 0 & 0 & 0 & 2\mu & 0 \\ 0 & 0 & 0 & 0 & 0 & 2\mu \end{bmatrix} \tag{59}$$

is the elasticity matrix. Let moduli κ and μ have a discontinuity of the first order across a surface *S* with normal vector $\vec{n}$. The surface *S* defines the geometry of the material discontinuity (interface). The welded-interface boundary conditions are continuity of displacement $\vec{u}(\vec{\eta})$ and traction $\vec{T}(\vec{\eta},\vec{n})$ across the surface:

$$\vec{u}^{+}(\vec{\eta}) = \vec{u}^{-}(\vec{\eta}) \quad , \quad \vec{T}^{+}(\vec{\eta},\vec{n}) = \vec{T}^{-}(\vec{\eta},\vec{n}) \; . \tag{60}$$

For simplicity, consider first the planar surface *S* parallel to the *xy*-coordinate plane with a normal vector $\vec{n} = (0,0,1)$. The conditions (60) imply

$$\sigma_{zx}^{+} = \sigma_{zx}^{-}, \quad \sigma_{zy}^{+} = \sigma_{zy}^{-}, \quad \sigma_{zz}^{+} = \sigma_{zz}^{-}, \qquad \varepsilon_{xx}^{+} = \varepsilon_{xx}^{-}, \quad \varepsilon_{yy}^{+} = \varepsilon_{yy}^{-}, \quad \varepsilon_{xy}^{+} = \varepsilon_{xy}^{-}. \tag{61}$$

The components σ_{xx}, σ_{yy}, σ_{xy}, ε_{zx}, ε_{zy} and ε_{zz} may be discontinuous across the material discontinuity. Define averaged stress and strain vectors at the material discontinuity:

$$\vec{\sigma}^{A} = \tfrac{1}{2}\left(\vec{\sigma}^{+} + \vec{\sigma}^{-}\right) \quad , \quad \vec{\varepsilon}^{A} = \tfrac{1}{2}\left(\vec{\varepsilon}^{+} + \vec{\varepsilon}^{-}\right) . \tag{62}$$

Due to the boundary conditions,

$$\vec{\sigma}^{A} = \left[\sigma_{xx}^{A}, \sigma_{yy}^{A}, \sigma_{zz}, \sigma_{xy}^{A}, \sigma_{yz}, \sigma_{zx}\right]^{T}, \quad \vec{\varepsilon}^{A} = \left[\varepsilon_{xx}, \varepsilon_{yy}, \varepsilon_{zz}^{A}, \varepsilon_{xy}, \varepsilon_{yz}^{A}, \varepsilon_{zx}^{A}\right]^{T}. \tag{63}$$

Then Hooke's law for a point on the material discontinuity is

$$\vec{\sigma}^{A} = \tilde{\mathbf{E}}\;\vec{\varepsilon}^{A} \tag{64}$$

with the elasticity matrix

$$\tilde{\mathbf{E}} = \begin{bmatrix} \Lambda + 2\mu^A & \Lambda & \Psi & 0 & 0 & 0 \\ \Lambda & \Lambda + 2\mu^A & \Psi & 0 & 0 & 0 \\ \Psi & \Psi & \left(\kappa + \frac{4}{3}\mu\right)^H & 0 & 0 & 0 \\ 0 & 0 & 0 & 2\mu^A & 0 & 0 \\ 0 & 0 & 0 & 0 & 2\mu^H & 0 \\ 0 & 0 & 0 & 0 & 0 & 2\mu^H \end{bmatrix} \tag{65}$$

and

$$\begin{aligned} \Lambda &= \left[\left(\frac{\kappa - \frac{2}{3}\mu}{\kappa + \frac{4}{3}\mu}\right)^A\right]^2 \cdot \left(\kappa + \frac{4}{3}\mu\right)^H + 2 \cdot \left(\frac{\left(\kappa - \frac{2}{3}\mu\right)\mu}{\kappa + \frac{4}{3}\mu}\right)^A , \\ \Psi &= \left(\frac{\kappa - \frac{2}{3}\mu}{\kappa + \frac{4}{3}\mu}\right)^A \cdot \left(\kappa + \frac{4}{3}\mu\right)^H . \end{aligned} \tag{66}$$

Superscripts *A* and *H* denote arithmetic and harmonic averages, respectively.

Relation (64) means that for a point on the material discontinuity it is possible to find the same form of Hooke's law as for a point inside a homogeneous or smoothly heterogeneous medium, given by eq. (58). Considering the point on the discontinuity as a point of the averaged medium characterized by matrix $\tilde{\mathbf{E}}$ assures traction continuity at the point. There is, however, an important difference between laws (64) and (58). The matrix $\tilde{\mathbf{E}}$ for the averaged medium given by eq. (65) has 5 independent nonzero elements and the averaged medium is transversely isotropic. Matrix $\mathbf{E}$ for any of the two isotropic media in contact has only 2 independent nonzero elements. This means that the exact heterogeneous formulation for a planar material discontinuity parallel with a coordinate plane increases the number of elastic coefficients necessary to describe the medium.

Next let us consider a planar material discontinuity in a general position in a Cartesian coordinate system. Let the normal vector be $\vec{n} = \left(n_x, n_y, n_z\right)$ with all non-zero elements. Find a Cartesian coordinate system *x'y'z'* in which $\vec{n}$ is parallel to the *z'*-axis. Then it is possible to find a matrix $\tilde{\mathbf{E}}'$ with 5 independent non-zero elements. Transforming the matrix $\tilde{\mathbf{E}}'$ into a matrix $\tilde{\mathbf{E}}$ in the original coordinate system *xyz* yields a symmetric elasticity matrix $\tilde{\mathbf{E}}$ which has, in general, all elements non-zero (5 being independent). This means that all strain-tensor components are necessary to calculate each stress-tensor component at a point of the interface (not the case with the standard staggered grid), and 21 non-zero elastic coefficients are necessary at the point.

If the geometry of a material discontinuity is defined by a non-planar smooth surface *S*, the surface may be locally approximated by a planar surface tangential to surface *S* at a given point.

It is obvious that finding a heterogeneous formulation of the differential problem as a basis for a heterogeneous FD scheme for a medium with a material discontinuity in a general 3D problem is far more complicated than that in the 1D problem. A non-simplified treatment and a corresponding FD scheme would lead to a substantial increase in memory requirement.

Therefore, Moczo et al. (2002) suggested a simplified approach: a) They wanted to keep the structure, number of operations and memory requirements of the standard 4th-order staggered-grid scheme. b) At the same time, they chose to determine an effective grid elastic modulus (κ or μ) at each grid position of the stress-tensor components as volume harmonic average of the modulus within a volume of the grid cell centered at the grid position. The latter choice was based on the fact that harmonic averaging is exact in the 1D case, see eq. (49), and is a part of exact averaging in the 3D case, see eqs. (64) - (66).

At each position of the displacement or particle-velocity component an effective grid density is determined as a volume arithmetic average of density within a volume of the grid cell centered at the grid position. The averaging applies to both smoothly and discontinuously heterogeneous media. The averages are evaluated by numerical integration.

Let $T^{xx,m}_{I+1/2,J+1/2,K+1/2}$ be the discrete approximation to the stress-tensor component $\sigma_{xx}\left[(I+1/2)h,(J+1/2)h,(K+1/2)h,m\Delta t\right]$. Similarly, let $V^{x,m}_{I,J+1/2,K+1/2}$, $V^{y,m}_{I+1/2,J,K+1/2}$, $V^{z,m}_{I+1/2,J+1/2,K}$ and $F^{x,m}_{I,J+1/2,K+1/2}$ be discrete approximations to the particle-velocity and body-force components. Examples of the FD schemes for the stress-tensor and particle-velocity components σ_{xx} and v_x are

$$
\begin{aligned}
&T^{xx,m}_{I+1/2,\,\mathrm{J}+1/2,\,\mathrm{K}+1/2} = T^{xx,m-1}_{I+1/2,\,\mathrm{J}+1/2,\,\mathrm{K}+1/2} \; + \\
&\frac{\Delta t}{h}\left\{\left(\kappa^{H}_{I+1/2,\,\mathrm{J}+1/2,\,\mathrm{K}+1/2}+\tfrac{4}{3}\mu^{H}_{I+1/2,\,\mathrm{J}+1/2,\,\mathrm{K}+1/2}\right)\cdot\right. \\
&\quad\left[\; a\left(V^{x,m-1/2}_{I+2,\,\mathrm{J}+1/2,\,\mathrm{K}+1/2}-V^{x,m-1/2}_{I-1,\,\mathrm{J}+1/2,\,\mathrm{K}+1/2}\right)+b\left(V^{x,m-1/2}_{I+1,\,\mathrm{J}+1/2,\,\mathrm{K}+1/2}-V^{x,m-1/2}_{I,\,\mathrm{J}+1/2,\,\mathrm{K}+1/2}\right)\right] \\
&+\left(\kappa^{H}_{I+1/2,\,\mathrm{J}+1/2,\,\mathrm{K}+1/2}-\tfrac{2}{3}\mu^{H}_{I+1/2,\,\mathrm{J}+1/2,\,\mathrm{K}+1/2}\right)\cdot \\
&\quad\left[\; a\left(V^{y,m-1/2}_{I+1/2,\,\mathrm{J}+2,\,\mathrm{K}+1/2}-V^{y,m-1/2}_{I+1/2,\,\mathrm{J}-1,\,\mathrm{K}+1/2}\right)+b\left(V^{y,m-1/2}_{I+1/2,\,\mathrm{J}+1,\,\mathrm{K}+1/2}-V^{y,m-1/2}_{I+1/2,\,\mathrm{J},\,\mathrm{K}+1/2}\right)\right. \\
&\quad\left.\left.+\,a\left(V^{z,m-1/2}_{I+1/2,\,\mathrm{J}+1/2,\,\mathrm{K}+2}-V^{z,m-1/2}_{I+1/2,\,\mathrm{J}+1/2,\,\mathrm{K}-1}\right)+b\left(V^{z,m-1/2}_{I+1/2,\,\mathrm{J}+1/2,\,\mathrm{K}+1}-V^{z,m-1/2}_{I+1/2,\,\mathrm{J}+1/2,\,\mathrm{K}}\right)\right]\right\}
\end{aligned}
\tag{67}
$$

with

$$
\kappa^{H}_{I+1/2,\,\mathrm{J}+1/2,\,\mathrm{K}+1/2}=\left[\frac{1}{h^3}\int_{x_I}^{x_{I+1}}\int_{y_J}^{y_{J+1}}\int_{z_K}^{z_{K+1}}\frac{1}{\kappa}\,\mathrm{d}x\,\mathrm{d}y\,\mathrm{d}z\right]^{-1} \tag{68}
$$

$$
\mu^{H}_{I+1/2,\,\mathrm{J}+1/2,\,\mathrm{K}+1/2}=\left[\frac{1}{h^3}\int_{x_I}^{x_{I+1}}\int_{y_J}^{y_{J+1}}\int_{z_K}^{z_{K+1}}\frac{1}{\mu}\,\mathrm{d}x\,\mathrm{d}y\,\mathrm{d}z\right]^{-1} \tag{69}
$$

and

$$
\begin{aligned}
V^{x,m+1/2}_{I,\,\mathrm{J+1/2},\,\mathrm{K+1/2}} = V^{x,m-1/2}_{I,\,\mathrm{J+1/2},\,\mathrm{K+1/2}} \quad + \quad & \left[\Delta t \Big/ \left(h\,\rho^{A}_{I,\,\mathrm{J+1/2},\,\mathrm{K+1/2}}\right)\right] \cdot \\
\Big[\; & a\left(T^{xx,m}_{I+3/2,\,\mathrm{J+1/2},\,\mathrm{K+1/2}} - T^{xx,m}_{I-3/2,\,\mathrm{J+1/2},\,\mathrm{K+1/2}}\right) + b\left(T^{xx,m}_{I+1/2,\,\mathrm{J+1/2},\,\mathrm{K+1/2}} - T^{xx,m}_{I-1/2,\,\mathrm{J+1/2},\,\mathrm{K+1/2}}\right) \\
& + a\left(T^{xy,m}_{I,\,\mathrm{J+2},\,\mathrm{K+1/2}} - T^{xy,m}_{I,\,\mathrm{J-1},\,\mathrm{K+1/2}}\right) + b\left(T^{xy,m}_{I,\,\mathrm{J+1},\,\mathrm{K+1/2}} - T^{xy,m}_{I,\,\mathrm{J},\,\mathrm{K+1/2}}\right) \\
& + a\left(T^{zx,m}_{I,\,\mathrm{J+1/2},\,\mathrm{K+2}} - T^{zx,m}_{I,\,\mathrm{J+1/2},\,\mathrm{K-1}}\right) + b\left(T^{zx,m}_{I,\,\mathrm{J+1/2},\,\mathrm{K+1}} - T^{zx,m}_{I,\,\mathrm{J+1/2},\,\mathrm{K}}\right) \Big] \\
& + \left(\Delta t \Big/ \rho^{A}_{I,\,\mathrm{J+1/2},\,\mathrm{K+1/2}}\right) F^{x,m}_{I,\,\mathrm{J+1/2},\,\mathrm{K+1/2}}
\end{aligned}
\tag{70}
$$

with

$$
\rho^{A}_{I,\,\mathrm{J+1/2},\,\mathrm{K+1/2}} = \frac{1}{h^3} \int_{x_{I-\frac{1}{2}}}^{x_{I+\frac{1}{2}}} \int_{y_J}^{y_{J+1}} \int_{z_K}^{z_{K+1}} \rho \; \mathrm{d}x \; \mathrm{d}y \; \mathrm{d}z \tag{71}
$$

Moczo et al. (2002) used a set of models to numerically test the scheme. The tests demonstrated its very good numerical accuracy. Here we illustrate an important property of the scheme - the capability to sense the position of a material discontinuity regardless of its position with respect to the spatial grid. Five different models of a single horizontal homogeneous layer located in between two homogeneous halfspaces differ from each other by the thickness of the layer. The spatial grid is one and the same in all five models (see the upper part of Fig. 2). A double-couple point source was located in the lower halfspace. The FD synthetics (u_x component) are compared with those calculated by the discrete wavenumber (DWN) method (Bouchon, 1981; computer code Axitra by Coutant, 1989), see the lower part of Fig. 2. The FD and DWN synthetics agree very well regardless of the position of the upper layer-halfspace interface with respect to the spatial grid. It is also clear from Fig. 2 that differences in thickness of the layer - smaller than one grid spacing - cause considerable changes in seismic motion. This often is underestimated by many modelers who consider the size of one grid cell as „atom of resolution" within which a FD scheme cannot see differences. This and other examples given by Moczo et al. (2002) clearly show that this is not the case if the scheme is sufficiently accurate.

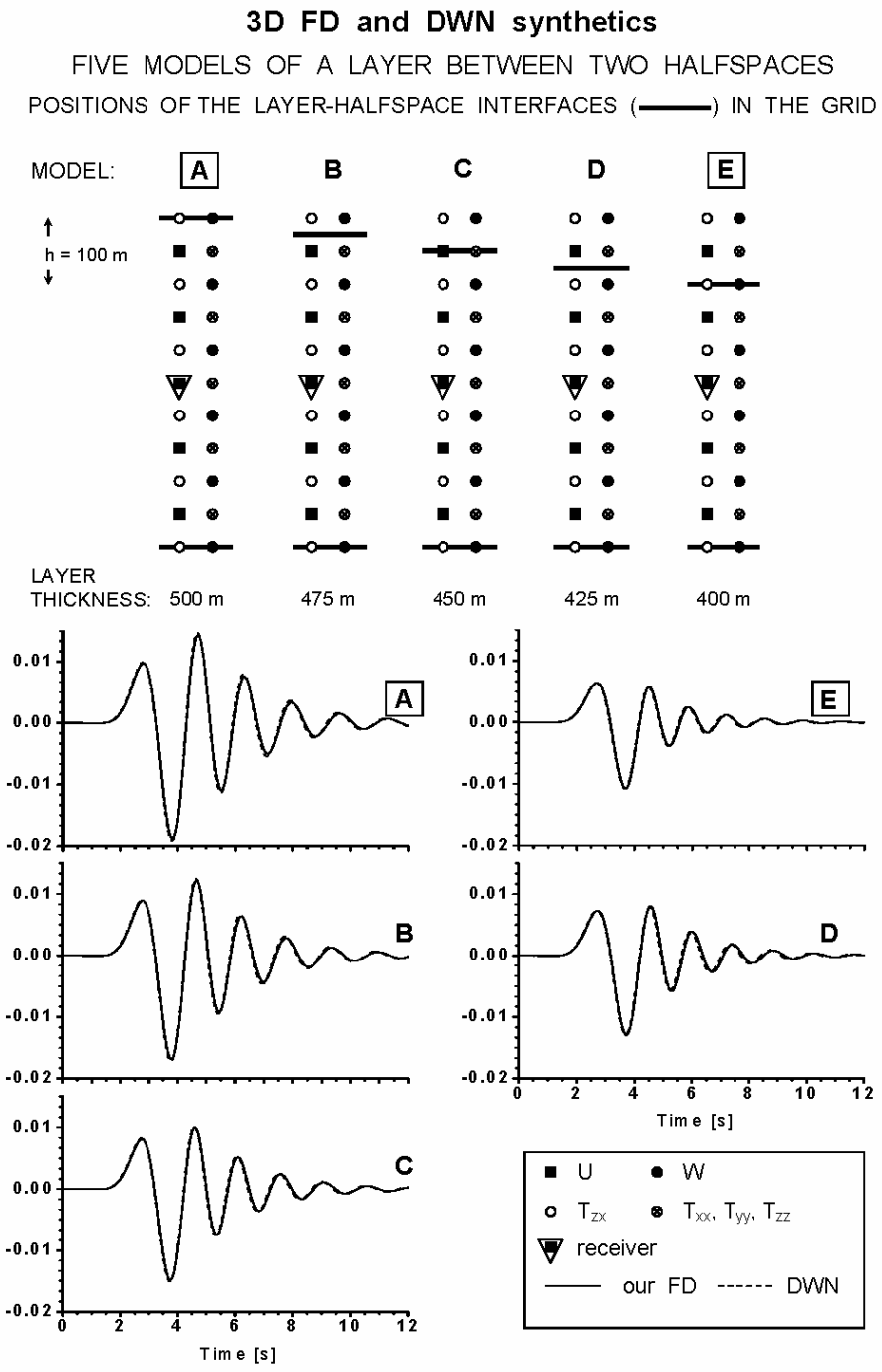

Figure 2. The upper part: Positions of the upper and lower layer-halfspace interfaces in five models of a layer between two halfspaces - shown schematically in one vertical grid plane. The five models differ from each other by position of the upper layer-halfspace interface in the spatial grid (the same for all models) and thus by the layer thickness. (For the parameters of the models see Tab. 1.) The lower part: Comparison of our FD and DWN synthetics for the five models. Note very good accuracy of the FD synthetics for any position of the layer-halfspace interface with respect to the spatial grid. Also note considerable differences between synthetics due to variations in the layer thickness that is smaller than one grid spacing. Reproduced from Moczo et al. (2002).

Incorporation of the Realistic Attenuation

Stress-Strain Relation in Viscoelastic Medium – the 1D Case

The behavior of real Earth's material can be described as a combination of elastic solids and viscous fluids. The stress-strain relation therefore also should depend on time. The rheology of a viscoelastic medium seems appropriate for quantitative description of seismic wave propagation. Observations show that the internal friction in the Earth is nearly constant over the seismic frequency range, e.g. McDonal et al. (1958), Liu et al. (1976), Spencer (1981), Murphy (1982).

The stress-strain relation in a linear isotropic viscoelastic material is given by the Boltzmann superposition principle. For the 1D problem this is

$$\sigma(t) = \int_{-\infty}^{t} \psi(t-\tau)\dot{\varepsilon}(\tau)\,d\tau\,, \tag{72}$$

where $\sigma(t)$ is the stress, $\dot{\varepsilon}(t)$ the time derivative of the strain, and $\psi(t)$ the stress relaxation function defined as a stress response to a Heaviside unit step function in strain. According to eq. (72), the stress at a given time t is determined by the entire history of the strain until time t. The integral in eq. (72) represents a time convolution of the relaxation function and the strain rate. Using the symbol $*$ for the convolution, eq. (72) can be written as

$$\sigma(t) = \psi(t) * \dot{\varepsilon}(t)\ . \tag{73}$$

It follows from the definition of the relaxation function that its time derivative

$$M(t) = \dot{\psi}(t) \tag{74}$$

is the stress response to the Dirac δ-function in strain and that

$$\sigma(t) = M(t) * \varepsilon(t)\ . \tag{75}$$

Let $\mathcal{F}$ and $\mathcal{F}^{-1}$ denote the direct and inverse Fourier transforms

$$\mathcal{F}\{x(t)\} = \int_{-\infty}^{\infty} x(t)\exp(-i\omega t)\,dt\ ,\quad \mathcal{F}^{-1}\{X(\omega)\} = \frac{1}{2\pi}\int_{-\infty}^{\infty} X(\omega)\exp(i\omega t)\,d\omega\ ,$$

where ω is the angular frequency. Relation (75) can be Fourier-transformed into the frequency domain:

$$\sigma(\omega) = M(\omega)\cdot\varepsilon(\omega)\ . \tag{76}$$

In general, $M(\omega)$ is a complex, frequency-dependent viscoleastic modulus. Due to properties of the Fourier transform

$$\psi(t) = \mathcal{F}^{-1}\left\{\frac{M(\omega)}{i\omega}\right\} . \tag{77}$$

Equation (76) indicates the correspondence principle in the linear theory of viscoelasticity - in the frequency-domain, relations for the viscoelastic medium are obtained by replacing real frequency-independent moduli by complex, frequency-dependent quantities. Thus, the incorporation of the attenuation into the frequency-domain computations is much easier than that in the time domain.

The time derivative of the stress is

$$\dot{\sigma}(t) = M(t) * \dot{\varepsilon}(t) . \tag{78}$$

An instantaneous elastic response of the viscoelastic material is given by the so-called unrelaxed modulus M_U, a long-term equilibrium response is given by the relaxed modulus M_R:

$$M_U = \lim_{t\to 0}\psi(t) = \lim_{\omega\to\infty} M(\omega) \quad , \quad M_R = \lim_{t\to\infty}\psi(t) = \lim_{\omega\to 0} M(\omega) . \tag{79}$$

The modulus defect or relaxation of modulus is

$$\delta M = M_U - M_R . \tag{80}$$

Given the viscoelastic modulus, the quality factor $Q(\omega)$ is defined as

$$Q(\omega) = \mathrm{Re}\,M(\omega) / \mathrm{Im}\,M(\omega) . \tag{81}$$

Due to large computer time and memory requirements, the stress-strain relation (72) in some cases only allowed simplified $Q(\omega)$ laws, e.g. linear $Q(\omega)$.

Conversion of the Convolutory Stress-Strain Relation into a Differential Form

If $M(\omega)$ is a rational function, the inverse Fourier transform of eq. (76) yields the n^{th}-order differential equation for $\sigma(t)$, which can be numerically solved much more easily than the convolution integral. Day and Minster (1984) assumed that, in general, the viscoelastic modulus is not a rational function. Therefore they suggested approximating a viscoelastic modulus by an n^{th}-order rational function and determining its coefficients by the Padé approximant method. They obtained *n* ordinary differential equations for *n* additional internal variables, which replace the convolution integral. The sum of the internal variables multiplied by the unrelaxed modulus gives an additional viscoelastic term to the elastic stress. The work of Day and Minster not only developed one

particular approach but, in fact, indirectly suggested the future evolution – a direct use of the rheological models whose $M(\omega)$ is a rational function of $i\omega$. In response to work by Day and Minster (1984), Emmerich and Korn (1987) realized that an acceptable relaxation function corresponds to a rheology of what they defined as the generalized Maxwell body – *n* Maxwell bodies and one Hooke element (elastic spring) connected in parallel; Fig. 3. Because in the rheological literature the generalized Maxwell body is defined without the additional single Hooke element, the abbreviation GMB-EK will hereafter be used for the model defined by Emmerich and Korn. Because the viscoelastic modulus of the GMB-EK has a form of a rational function, Emmerich and Korn (1987) obtained similar differential equations as Day and Minster (1984). In order to fit an arbitrary $Q(\omega)$ law they chose the relaxation frequencies logarithmically equidistant over a desired frequency range and used the least-square method to determine weight factors of the relaxation mechanisms (classical Maxwell bodies). Emmerich and Korn (1987) demonstrated that their approach is better than the approach based on the Padé approximant method both in accuracy and computational efficiency. Independently, Carcione et al. (1988a, b), in accordance with the approach by Liu et al. (1976), assumed the generalized Zener body (GZB) - *n* Zener bodies (ZB, standard linear bodies), connected in parallel; Fig. 4. Carcione et al. (1988a, b) developed a theory for the GZB and introduced the term memory variables for the obtained additional variables.

After publications by Emmerich and Korn (1987) and Carcione et al. (1988a, b) different authors chose to use either the GMB-EK (for example, Emmerich, 1992; Fäh, 1992; Moczo and Bard, 1993; Moczo et al., 1997; Kay and Krebes, 1999) or GZB (for example, Robertsson et al., 1994; Blanch et al., 1995; Xu and McMechan, 1995; Robertsson, 1996; Hestholm 1999). In both cases the authors followed the corresponding mathematical formalisms. Moczo et al. (1997) applied the GMB-EK approach also in the finite-element method and hybrid FD-finite-element method. Emmerich and Korn (1987), Emmerich (1992), Fäh (1992), and Moczo and Bard (1993) defined one memory variable for one displacement component. Robertsson et al. (1994) introduced the memory variables based on the GZB rheology into the staggered-grid velocity-stress FD scheme. Blanch et al. (1995) suggested an approximate single-parameter method, τ-method, to approximate the constant $Q(\omega)$ law. Xu and McMechan (1998) used simulated annealing for determining a best combination of relaxation mechanisms to approximate a desired $Q(\omega)$ law.

There appears to have been no or little comments by the authors using the GZB on the rheology of the GMB-EK and the corresponding algorithms, and vice versa. Thus, two parallel sets of publications and algorithms had been developed during years. Therefore, Moczo and Kristek (2005) addressed this development and showed relation between the two rheologies.

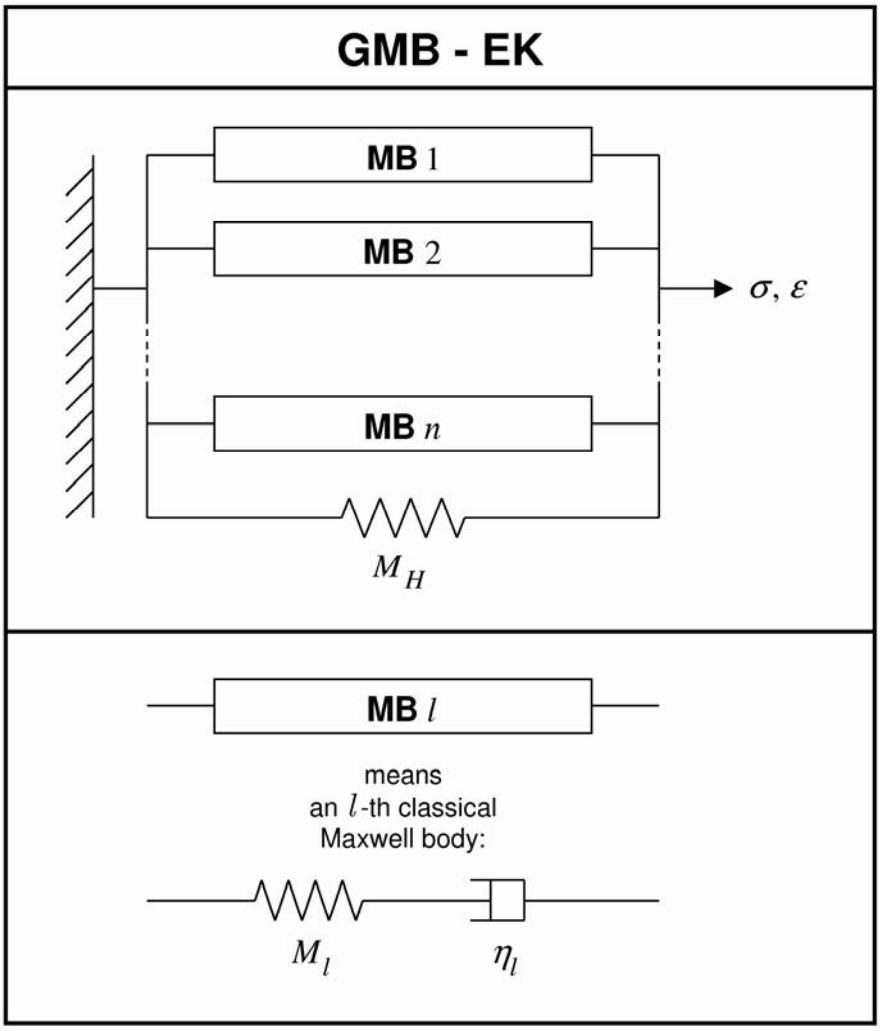

Figure 3. Rheological model of the Generalized Maxwell Body (GMB-EK) defined by Emmerich and Korn (1987). M_H and M_l denote elastic moduli, η_l viscosity.

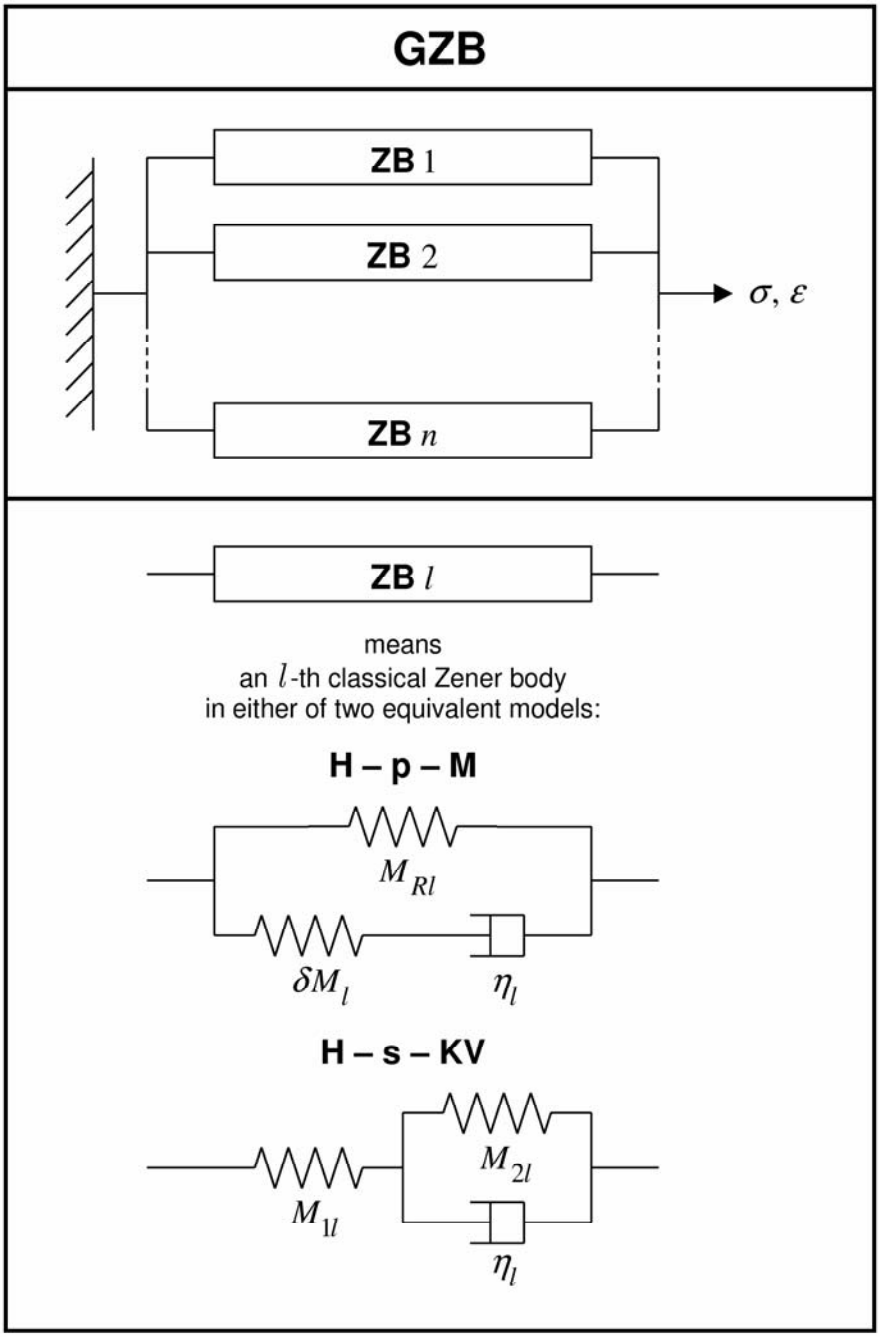

Figure 4. Rheological model of the Generalized Zener Body (GZB). For a classical Zener body (standard linear body) there are two equivalent models: H-p-M , that is, Hooke element connected in parallel with Maxwell body, and H-s-KV, that is, Hooke element connected in series with Kelvin-Voigt body. In the H-p-M model it is easier to recognize the relaxed modulus M_{Rl} and modulus defect δM_l. M_{1l} and M_{2l} in the H-s-KV model denote elastic moduli. In both models η_l stands for viscosity.

Rheologies of the GMB-EK and GZB

There are simple rules in the time and frequency domains for the mathematical representation of the linear rheological models consisting of Hooke and Stokes elements (springs and dashpots) connected in parallel or series. In the frequency domain, the stress-strain relations for the Hooke and Stokes elements are $\sigma(\omega) = M \cdot \varepsilon(\omega)$ and $\sigma(\omega) = i\omega\eta \cdot \varepsilon(\omega)$, respectively, where M is the elastic modulus, and η viscosity. If two elements are connected in series, stresses are equal while strains additive. If two elements are connected in parallel, stresses are additive while strains are equal.

The application of the frequency-domain rules to the GMB-EK yields

$$M(\omega) = M_H + \sum_{l=1}^{n} \frac{iM_l\omega}{\omega_l + i\omega} \quad , \quad \omega_l = M_l/\eta_l \; ; \quad l = 1,...,n \quad , \tag{82}$$

where ω_l is a relaxation frequency. The relaxed and unrelaxed moduli are

$$M_R \equiv \lim_{\omega\to 0} M(\omega) = M_H \quad , \quad M_U \equiv \lim_{\omega\to\infty} M(\omega) = M_R + \sum_{l=1}^{n} M_l \; . \tag{83}$$

Since $M_U = M_R + \delta M$, we get $M_l = \delta M_l$, and it is possible to assume

$$\delta M_l = a_l \, \delta M \quad ; \quad \sum_{l=1}^{n} a_l = 1 \tag{84}$$

without any simplification. Then

$$M(\omega) = M_R + \delta M \sum_{l=1}^{n} \frac{ia_l\omega}{\omega_l + i\omega} \; . \tag{85}$$

Using relation (77) it is straightforward to obtain the relaxation function

$$\psi(t) = \left[M_R + \delta M \sum_{l=1}^{n} a_l e^{-\omega_l t} \right] \cdot H(t) \; , \tag{86}$$

where $H(t)$ is the Heaviside unit step function. The above formulae were presented by Emmerich and Korn (1987).

From the two equivalent models of the ZB, shown in Fig. 4, we choose the H-p-M type to obtain $M(\omega)$. This is because it is easy to recognize the relaxed modulus and modulus defect in the ZB. The application of the frequency-domain rules to the GZB results in

$$M(\omega) = \sum_{l=1}^{n} M_{Rl} \frac{1 + i\tau_{\varepsilon l}\omega}{1 + i\tau_{\sigma l}\omega} \tag{87}$$

with relaxation times

$$\tau_{\varepsilon l}=\frac{\eta_l}{\delta M_l}\frac{M_{Ul}}{M_{Rl}} \quad , \quad \tau_{\sigma l}=\frac{\eta_l}{\delta M_l} \quad , \quad \frac{\tau_{\varepsilon l}}{\tau_{\sigma l}}=\frac{M_{Ul}}{M_{Rl}} \tag{88}$$

and

$$M_{Ul}=M_{Rl}+\delta M_l \ . \tag{89}$$

The unrelaxed and relaxed moduli are

$$M_R=\sum_{l=1}^{n}M_{Rl} \quad , \quad M_U=\sum_{l=1}^{n}M_{Rl}\frac{\tau_{\varepsilon l}}{\tau_{\sigma l}}=M_R+\sum_{l=1}^{n}\delta M_l \quad . \tag{90}$$

Relations (77) and (87) yield the relaxation function

$$\psi(t)=\left\{\sum_{l=1}^{n}M_{Rl}\left[1-\left(1-\frac{\tau_{\varepsilon l}}{\tau_{\sigma l}}\right)\exp\left(-t/\tau_{\sigma l}\right)\right]\right\}\cdot H(t) \quad . \tag{91}$$

Assumption of simplification (Carcione, 2001)

$$M_{Rl}=\frac{1}{n}M_R \tag{92}$$

leads to

$$M(\omega)=\frac{M_R}{n}\sum_{l=1}^{n}\frac{1+i\tau_{\varepsilon l}\omega}{1+i\tau_{\sigma l}\omega}, \quad \psi(t)=M_R\left[1-\frac{1}{n}\sum_{l=1}^{n}\left(1-\frac{\tau_{\varepsilon l}}{\tau_{\sigma l}}\right)\exp\left(-t/\tau_{\sigma l}\right)\right]\cdot H(t) \ . \tag{93}$$

Formulae (92) and (93) were presented by Carcione (2001). Unfortunately, all papers dealing with the incorporation of the attenuation based on the GZB, starting from Liu et al. (1976) until now, despite the book by Carcione (2001), have the same error – the missing factor $1/n$ in the viscoelastic modulus and relaxation function.

The Relation Between the GZB and GMB-EK

Following Moczo and Kristek (2005), consider again the ZB (H-p-M) model. The application of the frequency-domain rules to the *l*-th ZB yields

$$\sigma_l(\omega)\cdot\left(\frac{1}{\delta M_l}+\frac{1}{i\eta_l\omega}\right)=\left(1+\frac{M_{Rl}}{\delta M_l}+\frac{M_{Rl}}{i\eta_l\omega}\right)\cdot\varepsilon(\omega) \ . \tag{94}$$

Defining

$$\omega_l=\delta M_l/\eta_l \tag{95}$$

and rearranging eq. (94) gives

$$\sigma_l(\omega)=M_l(\omega)\cdot\varepsilon(\omega) \quad ; \quad M_l(\omega)=M_{Rl}+\frac{i\delta M_l\omega}{\omega_l+i\omega} \ . \tag{96}$$

For *n* ZB connected in parallel, that is, for the GZB (Fig. 4), the stress is

$$\sigma(\omega)=\sum_{l=1}^{n}\sigma_l(\omega)=\left[\sum_{l=1}^{n}M_l(\omega)\right]\cdot\varepsilon(\omega) \tag{97}$$

and thus

$$M(\omega)=\sum_{l=1}^{n}M_{Rl}+\sum_{l=1}^{n}\frac{i\delta M_l\omega}{\omega_l+i\omega}\ . \tag{98}$$

Since

$$M_R=\sum_{l=1}^{n}M_{Rl}\quad,\quad M_U=M_R+\sum_{l=1}^{n}\delta M_l\quad,\quad M_U=M_R+\delta M\ , \tag{99}$$

it is possible to define

$$\delta M_l=a_l\delta M\quad;\quad\sum_{l=1}^{n}a_l=1 \tag{100}$$

without loss of generality and obtain

$$M(\omega)=M_R+\delta M\sum_{l=1}^{n}\frac{ia_l\omega}{\omega_l+i\omega}\ . \tag{101}$$

The viscoelastic modulus (101) obtained for the GZB (H-p-M), Fig. 4, is exactly the same as it has been obtained by Emmerich and Korn (1987) for their GMB-EK, Fig. 3. Obviously, $M(\omega)$ for the GZB (H-s-KV) would be the same. It is also easy to rewrite the non-simplified $\psi(t)$ for the GZB, eq. (91), into the form of $\psi(t)$ for the GMB-EK, eq. (86), without any simplification. In other words, the rheology of the GMB-EK and GZB is one and the same. As a consequence, the GMB-EK will be used in the following.

Introduction of the Anelastic Functions (Memory Variables) – the 1D Case

In order to focus on the essential aspects of the implementation of the realistic attenuation in the time-domain computations, we continue by considering the 1D case with one stress and one strain component. Using the unrelaxed modulus, the viscoelastic modulus (101) and relaxation function (86) are rewritten as

$$M(\omega)=M_U-\delta M\sum_{l=1}^{n}\frac{a_l\omega_l}{\omega_l+i\omega}\quad,\quad\psi(t)=\left[M_U-\delta M\sum_{l=1}^{n}a_l\left(1-e^{-\omega_l t}\right)\right]\cdot H(t). \tag{102}$$

The time derivative of the relaxation function (time-dependent modulus) is

$$M(t)=\dot{\psi}(t)=-\delta M\sum_{l=1}^{n}a_l\omega_l e^{-\omega_l t}\cdot H(t)+\left[M_U-\delta M\sum_{l=1}^{n}a_l\left(1-e^{-\omega_l t}\right)\right]\cdot\delta(t). \tag{103}$$

Inserting eq. (103) into eq. (75) yields

$$\sigma(t) = M_U \cdot \varepsilon(t) - \delta M \sum_{l=1}^{n} a_l \omega_l \int_{-\infty}^{t} \varepsilon(\tau) \cdot e^{-\omega_l (t-\tau)} d\tau \ . \tag{104}$$

The convolution integral can be replaced by additional functions (internal variables, new variables, memory variables, anelastic functions). While Day and Minster (1984), Emmerich and Korn (1987), and Carcione et al. (1988a, b) defined the additional functions as material-dependent, Kristek and Moczo (2003) defined their anelastic functions as material-independent (the reason will be explained later):

$$\zeta_l(t) = \omega_l \int_{-\infty}^{t} \varepsilon(\tau) \cdot e^{-\omega_l (t-\tau)} d\tau \quad , \quad l = 1,...,n \, . \tag{105}$$

The stress-strain relation then becomes

$$\sigma(t) = M_U \cdot \varepsilon(t) - \sum_{l=1}^{n} \delta M \, a_l \, \zeta_l(t) \ . \tag{106}$$

Equations necessary to solve for the anelastic functions are easily obtained by taking the time derivative of eq. (105):

$$\dot{\zeta}_l(t) = \omega_l \frac{d}{dt} \int_{-\infty}^{t} \varepsilon(\tau) \cdot e^{-\omega_l (t-\tau)} d\tau = \omega_l \left[-\zeta_l(t) + \varepsilon(t) \right] \tag{107}$$

and

$$\dot{\zeta}_l(t) + \omega_l \zeta_l(t) = \omega_l \varepsilon(t) \quad ; \quad l = 1,...,n \, . \tag{108}$$

Eqs. (106) and (108) define the time-domain stress-strain relation for the viscoelastic medium whose rheology corresponds to the rheology of the GMB-EK (and to its equivalent – the GZB). If the staggered-grid velocity-stress FD scheme is to be used, then the time derivative of the stress is needed. It is easy to obtain

$$\dot{\sigma}(t) = M_U \cdot \dot{\varepsilon}(t) - \sum_{l=1}^{n} \delta M \, a_l \, \xi_l(t) \tag{109}$$

and

$$\dot{\xi}_l(t) + \omega_l \xi_l(t) = \omega_l \dot{\varepsilon}(t) \quad ; \quad l = 1,...,n \ . \tag{110}$$

As mentioned before, formalism developed specifically for the GZB was used in many papers. Therefore we give here equations equivalent to those presented by Robertsson et al. (1994). Using eqs. (91), (74), (78) and (90) it is easy to obtain

$$\dot{\sigma}(t) \ = \ M_U \cdot \dot{\varepsilon}(t) \ - \ \sum_{l=1}^{n} r_l(t) \ , \tag{111}$$

$$r_l(t) = \frac{M_{Rl}}{\tau_{\sigma l}}\left(1-\frac{\tau_{\varepsilon l}}{\tau_{\sigma l}}\right)\int_{-\infty}^{t}\dot{\varepsilon}(\tau)\cdot\exp\left[-(t-\tau)/\tau_{\sigma l}\right]d\tau \quad , \quad l=1,...,n, \tag{112}$$

$$\dot{r}_l(t) + \frac{1}{\tau_{\sigma l}} r_l(t) = \frac{M_{Rl}}{\tau_{\sigma l}}\left(1-\frac{\tau_{\varepsilon l}}{\tau_{\sigma l}}\right)\dot{\varepsilon}(t) \quad , \quad l=1,...,n. \tag{113}$$

Note that anelastic functions (memory variables) $r_l(t)$ are material-dependent.

Defining anelastic coefficients (different from those used by Emmerich and Korn, 1987)

$$Y_l = a_l\,\delta M/M_U \quad ; \quad l=1,...,n\ , \tag{114}$$

the stress-strain relations (106) and (109) become

$$\sigma(t)=M_U\cdot\varepsilon(t)-\sum_{l=1}^{n}M_U\,Y_l\,\zeta_l(t) \quad , \quad \dot{\sigma}(t)=M_U\cdot\dot{\varepsilon}(t)-\sum_{l=1}^{n}M_U\,Y_l\,\xi_l(t)\ . \tag{115}$$

The related eqs. (108) and (110) remain unchanged.

It is clear that the stress or its time derivative can be calculated if the anelastic coefficients and unrelaxed modulus are known.

The anelastic coefficients $Y_l\,; l=1,...,n$ have to be determined from $Q(\omega)$-law. Using the anelastic coefficients, the viscoelastic modulus and quality factor (81) are

$$M(\omega)=M_U\left[1-\sum_{l=1}^{n}Y_l\,\frac{\omega_l}{\omega_l+i\omega}\right] \tag{116}$$

and

$$\frac{1}{Q(\omega)}=\left[\sum_{l=1}^{n}Y_l\,\frac{\omega_l\omega}{\omega_l^2+\omega^2}\right]\Bigg/\left[1-\sum_{l=1}^{n}Y_l\,\frac{\omega_l^2}{\omega_l^2+\omega^2}\right]. \tag{117}$$

Eq. (117) yields

$$Q^{-1}(\omega)=\sum_{l=1}^{n}\frac{\omega_l\omega+\omega_l^2Q^{-1}(\omega)}{\omega_l^2+\omega^2}Y_l\,. \tag{118}$$

Eq. (118) can be used to numerically fit any $Q(\omega)$-law. A sufficiently accurate approximation to nearly constant $Q(\omega)$ is obtained if the relaxation frequencies ω_l are distributed logarithmically equidistant over the frequency range of interest. If, for example, $Q(\omega)$ values are known at frequencies $\tilde{\omega}_k\,; k=1,...,2n-1$, with $\tilde{\omega}_1=\omega_1,\ \tilde{\omega}_{2n-1}=\omega_n$, eq. (118) can be solved for $Y_l\,; l=1,...,n$ using the least square

method. A more detailed discussion of the frequency range and its sampling at frequencies $\tilde{\omega}_k$ can be found in the papers by Blanch et al. (1995) and Graves and Day (2003; eqs. 13 and 14).

If an elastic P-wave velocity α or S-wave velocity β is known, then, in the considered 1D problem, $M_U = \rho\alpha^2$ for the P-wave or $M_U = 2\rho\beta^2$ for the S-wave. In practice, a phase velocity at a certain reference frequency ω_r can be measured or estimated. The P-wave or S-wave phase velocity $c(\omega)$ is given by

$$1/c(\omega) = \mathrm{Re}\left\{\left[M(\omega)/\rho\right]^{-1/2}\right\} . \tag{119}$$

It follows (Moczo et al., 1997) from eqs. (116) and (119) that

$$M_U = \rho c^2(\omega_r)\frac{R+\Theta_1}{2R^2} \quad ; \; R = \left(\Theta_1^2 + \Theta_2^2\right)^{1/2} , \tag{120}$$

$$\Theta_1 = 1 - \sum_{l=1}^{n} Y_l \frac{1}{1+\left(\omega_r/\omega_l\right)^2} , \quad \Theta_2 = \sum_{l=1}^{n} Y_l \frac{\omega_r/\omega_l}{1+\left(\omega_r/\omega_l\right)^2} \quad . \tag{121}$$

As already pointed out, a constant or almost constant Q is of great importance. Therefore, Blanch et al. (1995) addressed the question of an efficient and sufficiently accurate curve-fitting procedure in the case of constant Q. Their τ-method is based on the fact that the level of attenuation caused by a ZB can be determined by a dimensionless variable $\tau = \left(\tau_\varepsilon - \tau_\sigma\right)/\tau_\sigma$. Blanch et al. (1995) derived explicit closed formula to determine parameters of the GZB for a desired constant Q, for P- and S-waves, respectively. The GZB obtained by tuning through a single parameter τ yields a very good constant-Q approximation.

A FD Scheme for the Anelastic Functions in the 1D Case

The 2nd-order approximations to the anelastic functions ζ_l and $\dot{\zeta}_l$; $l = 1,...,n$ give

$$\zeta_l(t_m) \doteq \tfrac{1}{2}\left(\zeta_l(t_{m+1/2}) + \zeta_l(t_{m-1/2})\right) , \; \dot{\zeta}_l(t_m) \doteq \frac{1}{\Delta t}\left(\zeta_l(t_{m+1/2}) - \zeta_l(t_{m-1/2})\right), \tag{122}$$

where t_m denotes the *m*-th time level. Then each of the equations for the anelastic functions can be solved by

$$\zeta_l(t_{m+1/2}) = \frac{2\,\omega_l\,\Delta t}{2+\omega_l\,\Delta t}\,\varepsilon(t_m) \; + \; \frac{2-\omega_l\,\Delta t}{2+\omega_l\,\Delta t}\,\zeta_l(t_{m-1/2}) \; . \tag{123}$$

The value of $\zeta_l(t_m)$ needed in the stress-strain relation

$$\sigma(t_m) = M_U \cdot \varepsilon(t_m) - \sum_{l=1}^{n} M_U\, Y_l^M\, \zeta_l(t_m)\ , \tag{124}$$

is obtained from $\zeta_l(t_{m-1/2})$ and $\zeta_l(t_{m+1/2})$ using eq. (122). This means that two values have to be kept in memory for one spatial position at one time. It is, however, possible (Kristek and Moczo, 2003) to avoid the necessity to keep in memory both values. It follows from eqs. (123) and (122) that

$$\zeta_l(t_m) = -\frac{\omega_l\,\Delta t}{2-\omega_l\,\Delta t}\,\varepsilon(t_m) \ + \ \frac{2}{2-\omega_l\,\Delta t}\,\zeta_l(t_{m+1/2})\ . \tag{125}$$

Then the stress-strain relation (124) can be obtained in the form

$$\sigma(t_m) = \tilde{M}\,\varepsilon(t_m) - \sum_{l=1}^{n} \tilde{Y}_l^M\,\zeta_l(t_{m+1/2}) \tag{126}$$

where

$$\begin{aligned} \tilde{M} &= M_U\left(1+\sum_{l=1}^{n} G_{1l}\,Y_l^M\right)\quad ,\quad \tilde{Y}_l^M = G_{2l}\,M_U\,Y_l^M \\ G_{1l} &= \frac{\omega_l\,\Delta t}{2-\omega_l\,\Delta t}\quad ,\quad G_{2l} = \frac{2}{2-\omega_l\,\Delta t}\quad . \end{aligned} \tag{127}$$

Using scheme (123) and a proper scheme for eq. (126) it is sufficient to have only one variable for one anelastic function at one grid position at one time. In the case of the staggered-grid velocity-stress FD scheme, the form of equations is the same; only ζ_l and ε have to be replaced by ξ_l and $\dot{\varepsilon}$, respectively.

A Material Discontinuity in the Viscoelastic Medium – the 1D Case

It is not a trivial task to find a heterogeneous formulation to the differential problem if the stress is given in the form of eq. (115). Kristek and Moczo (2003) suggested an approximate approach which has been shown sufficiently accurate using numerical tests against the discrete wavenumber method (Bouchon, 1981; Coutant, 1989).

Consider a contact of two viscoelastic media with the GMB-EK rheology. Each of the two media is described by a real density and complex frequency-dependent modulus given by eq. (116). The question is how to determine density, elastic (unrelaxed) modulus $\bar{M}_U$, and anelastic coefficients $Y_l^{\bar{M}}\ ; l=1,...,n$ for an averaged medium that should represent the contact of two media (that is the boundary conditions at the interface between the two media) if a material discontinuity goes through a grid cell. There is no reason to consider other than volume arithmetic averaging for the density using formula (56). An averaged viscoelastic modulus $\bar{M}$ can be obtained by numerical averaging in the frequency domain over the grid cell. From the averaged viscoelastic modulus, the quality factor corresponding to this modulus can be determined, eq. (81), for example, at frequencies $\tilde{\omega}_k\ ; k=1,...,2n-1$:

$Q_{\bar{M}}(\tilde{\omega}_k) = \mathrm{Re}\,\bar{M}(\tilde{\omega}_k)/\mathrm{Im}\,\bar{M}(\tilde{\omega}_k)$. Assuming that the rheology of the averaged medium can be approximated by the GMB-EK rheology, the anelastic coefficients $Y_l^{\bar{M}}\ ; l = 1,...,n$ for the averaged medium can be obtained using eq. (118).

It follows from eq. (79) that $\bar{M}_U = \lim_{\omega\to\infty} \bar{M}(\omega)$. An implication is that, in the limit, the averaging of the viscoelastic modulus gives the averaging of the unrelaxed modulus. This means that the unrelaxed (elastic) modulus $\bar{M}_U$ for the averaged viscoelastic medium can be obtained in the same way as in the perfectly elastic medium.

A Summary of Equations in the 3D Case

In the 3D case it is assumed that the rheology of the medium is described by one GMB-EK (or, equivalently, GZB) for the complex frequency-dependent bulk modulus and one GMB-EK for the complex frequency-dependent shear modulus. The stress-strain relation is (Kristek and Moczo, 2003)

$$\sigma_{ij} = \kappa\,\varepsilon_{kk}\delta_{ij} + 2\mu\left(\varepsilon_{ij} - \tfrac{1}{3}\varepsilon_{kk}\delta_{ij}\right) - \sum_l^n \left[\kappa Y_l^{\kappa}\zeta_l^{kk}\delta_{ij} + 2\mu Y_l^{\mu}\left(\zeta_l^{ij} - \tfrac{1}{3}\zeta_l^{kk}\delta_{ij}\right)\right] \tag{128}$$

where $i, j, k \in \{1,2,3\}$, the equal-index summation convention does not apply to l, $\kappa(x_i)$ and $\mu(x_i)$ are unrelaxed (elastic) bulk and shear moduli, and Y_l^{κ} and Y_l^{μ} are the corresponding anelastic coefficients. Assuming a measured or estimated $Q_\alpha(\omega)$ for the P- and $Q_\beta(\omega)$ for the S-waves, the corresponding anelastic coefficients Y_l^{α} and Y_l^{β} are obtained using eq. (118). Then the anelastic coefficients Y_l^{κ} and Y_l^{μ} are

$$Y_l^{\kappa} = \left(\alpha^2 Y_l^{\alpha} - \tfrac{4}{3}\beta^2 Y_l^{\beta}\right)\Big/\left(\alpha^2 - \tfrac{4}{3}\beta^2\right) \quad , \quad Y_l^{\mu} = Y_l^{\beta} \quad ; l = 1,...,n\,. \tag{129}$$

There are n material-independent anelastic functions ζ_l^{ij} for each of 6 strain-tensor components satisfying equations

$$\dot{\zeta}_l^{ij} + \omega_l \zeta_l^{ij} = \omega_l \varepsilon_{ij} \quad ; \quad l = 1,...,n\ , \tag{130}$$

where the equal-index summation convention does not apply to l.

While eqs. (128) and (130) are applicable to the conventional displacement, or staggered-grid displacement-stress and displacement-velocity-stress FD schemes, equations

$$\dot{\sigma}_{ij} = \kappa\,\dot{\varepsilon}_{kk}\delta_{ij} + 2\mu\left(\dot{\varepsilon}_{ij} - \tfrac{1}{3}\dot{\varepsilon}_{kk}\delta_{ij}\right) - \sum_l^n \left[\kappa Y_l^{\kappa}\xi_l^{kk}\delta_{ij} + 2\mu Y_l^{\mu}\left(\xi_l^{ij} - \tfrac{1}{3}\xi_l^{kk}\delta_{ij}\right)\right] \tag{131}$$

and

$$\dot{\xi}_l^{ij} + \omega_l \xi_l^{ij} = \omega_l \dot{\varepsilon}_{ij} \quad ; \quad l = 1,...,n \tag{132}$$

are needed for the staggered-grid velocity-stress FD schemes.

In analogy to the 1D case, it is possible to obtain

$$\zeta_l^{ij}(t_{m+1/2}) = \frac{2\omega_l \Delta t}{2+\omega_l \Delta t}\, \varepsilon_{ij}(t_m) \; + \; \frac{2-\omega_l \Delta t}{2+\omega_l \Delta t}\, \zeta_l^{ij}(t_{m-1/2}) \quad ; \quad l = 1,...,n \tag{133}$$

and

$$\begin{aligned} \sigma_{ij}(t_m) = \; & \tilde{\kappa}\, \varepsilon_{kk}(t_m)\, \delta_{ij} + \; 2\tilde{\mu} \left(\varepsilon_{ij}(t_m) - \tfrac{1}{3} \varepsilon_{kk}(t_m)\, \delta_{ij} \right) - \\ & \sum_{l=1}^{n} \left[\tilde{Y}_l^{\kappa}\, \zeta_l^{kk}(t_{m+1/2})\, \delta_{ij} \; + 2\, \tilde{Y}_l^{\mu} \left(\zeta_l^{ij}(t_{m+1/2}) - \tfrac{1}{3} \zeta_l^{kk}(t_{m+1/2})\, \delta_{ij} \right) \right] , \end{aligned} \tag{134}$$

where

$$\begin{aligned} \tilde{\kappa} &= \kappa \left(1 + \sum_{l=1}^{n} G_{1l}\, Y_l^{\kappa} \right) \quad , \quad \tilde{\mu} &= \mu \left(1 + \sum_{l=1}^{n} G_{1l}\, Y_l^{\mu} \right) \\ \tilde{Y}_l^{\kappa} &= G_{2l}\, \kappa Y_l^{\kappa} \qquad\qquad , \quad \tilde{Y}_l^{\mu} &= G_{2l}\, \mu Y_l^{\mu} \\ G_{1l} &= \frac{\omega_l\, \Delta t}{2 - \omega_l\, \Delta t} \qquad , \quad G_{2l} &= \frac{2}{2 - \omega_l\, \Delta t} \quad . \end{aligned} \tag{135}$$

Eqs. (133) to (135) are ready for programming. In the case of the staggered-grid velocity-stress FD scheme, the form of equations is the same; only ζ_l^{ij} and ε_{ij} are replaced by ξ_l^{ij} and $\dot{\varepsilon}_{ij}$.

Coarse Spatial Sampling

The incorporation of realistic attenuation considerably increases the number of operations and variables/parameters that have to be kept in computer (core) memory. In order to reduce the increased memory requirements and also computational time, Zeng (1996), independently Day (1998) and Day and Bradley (2001) introduced coarse spatial sampling of the anelastic functions and coefficients. In Day's (1998) approach, one anelastic function ξ_l^{ij} for one relaxation frequency ω_l is distributed with a spatial period of $2h$, h being a grid spacing. Consequently, $n = 8$. Considering, for example, location of the stress-tensor component T^{zx} at 8 corners of a grid cube $h \times h \times h$, only one of the 8 ξ_l^{zx} anelastic functions is assigned to one of the 8 corners (say, ξ_1^{zx} is assigned to one position, ξ_2^{zx} to other position, and so on). Consequently, the total number of ξ_l^{zx} ; $l = 1,2,...,8$ in the whole grid is $\frac{MX}{2} \cdot \frac{MY}{2} \cdot \frac{MZ}{2} \cdot 8 = MX \cdot MY \cdot MZ$, *MX*, *MY* and *MZ* being the numbers of the grid cells in the three Cartesian directions. Because there are 6 independent stress-tensor components, the total number of all the anelastic functions in the whole grid is $MX \cdot MY \cdot MZ \cdot 6$. Since the anelastic

coefficients Y_l^{κ} and Y_l^{μ} at the grid positions of the normal stress-tensor components, and $Y_l^{\mu xy}$, $Y_l^{\mu yz}$ and $Y_l^{\mu zx}$ at the grid positions of the shear stress-tensor components are distributed in the same coarse manner, the total number of the anelastic coefficients in the grid is $MX \cdot MY \cdot MZ \cdot 5$. Thus, the additional memory due to attenuation in Day's (1998) approach in the staggered-grid scheme in the case of 8 relaxation frequencies is equivalent to the case of just one relaxation frequency without coarse sampling, which is significant.

Graves and Day (2003) analyzed stability and accuracy of the scheme with the coarse spatial sampling and defined the effective modulus and the quality factor necessary to achieve sufficient accuracy.

As discussed earlier, Moczo et al. (2002) demonstrated that a position of a material discontinuity within one grid cell can be sensed by a sufficiently accurate FD scheme. In a structurally complex model there are material discontinuities going through grid cells in different orientations with respect to the coordinate system. In such a case and with the originally suggested spatial sampling (Day, 1998; Day and Bradley, 2001) it can happen that the medium from one side of the material discontinuity is characterized over one half of the whole considered frequency range while the medium from the other side of the discontinuity is characterized over the other half of the considered frequency range. Since the behavior of the two media in contact is characterized in two disjunctive frequency sub-intervals, the two media cannot physically interact. Consequently, the two media cannot be averaged.

In principle, the geometry of the coarse spatial sampling shown in the papers by Day (1998) and Day and Bradley (2001) is not the only one possible. Keeping the same spatial periodicity of the anelastic quantities, it is possible to avoid division of a grid cell into two parts characterized in two disjunctive frequency sub-intervals. Still the best possible alternative situation would be characterization of one medium in contact using, for example, relaxation frequencies $\omega_1, \omega_3, \omega_5, \omega_7$ and characterization of the other medium in contact using $\omega_2, \omega_4, \omega_6, \omega_8$, which again is not satisfactory.

In evaluating the sum that makes an anelastic term in the stress-strain relation, eqs. (128), (131) or (134), at a given spatial grid position, it would be possible to account for the anelastic coefficients and functions which are not located at that grid point by their properly weighted values. Such averaging, however, poses a problem: Because the anelastic functions (that is, internal variables or memory variables) introduced by Day and Minster (1984), Emmerich and Korn (1987), Carcione et al. (1988a, b) and Robertsson et al. (1994) are material-dependent, any such spatial averaging (accounting for the functions missing at the considered grid point) would introduce and additional artificial averaging of the material parameters. There is no reason for such an additional averaging.

There would be no problem with the coarse spatial sampling and at the same time with weighted spatial averaging of the anelastic functions at a grid point with only one of the all anelastic functions if the anelastic functions were material-independent. Therefore Kristek and Moczo (2003) introduced material-independent anelastic functions (as given above). Moreover, they also suggested an alternative coarse spatial distribution of the anelastic functions which only requires $n = 4$ relaxation frequencies, keeping the same memory requirements as in Day (1998), and Day and Bradley (2001). The distribution is shown in Fig. 5. Kristek and Moczo (2003) demonstrated accuracy of their FD scheme with the material-independent anelastic functions and new coarse distribution of the anelastic functions.

Incorporation of Attenuation in Anisotropic Media

FD modeling in anisotropic media is addressed in the following section. Here we only point out the main difference between incorporating attenuation in the isotropic and anisotropic media. In the isotropic medium it is possible to consider that the rheology of the medium is described by two separate viscoelastic bodies – one for the complex frequency-dependent bulk modulus (corresponding to the dilatational part of the strain) and one for the complex frequency-dependent shear modulus (corresponding to the deviatoric part of the strain). In terms of the quality factors for P- and S-waves, the quality factors can be strictly separated. This makes the incorporation of the attenuation in the isotropic medium much easier compared to the anisotropic medium, where the two quality factors cannot be simply separated if they are not equal.

Robertsson and Coates (1997) presented a 2D velocity-stress staggered-grid FD scheme for modeling qP- and qS wave propagation in anisotropic media based on the rheological model described by Carcione and Cavallini (1994). Through eigenvalue decomposition of the stress and stiffness tensors, relaxation functions and memory variables are associated with the so-called eigenstiffness and eigenstresses. The decomposition of stresses and stiffness in this fashion was first observed by Lord Kelvin (Thomson, 1856).

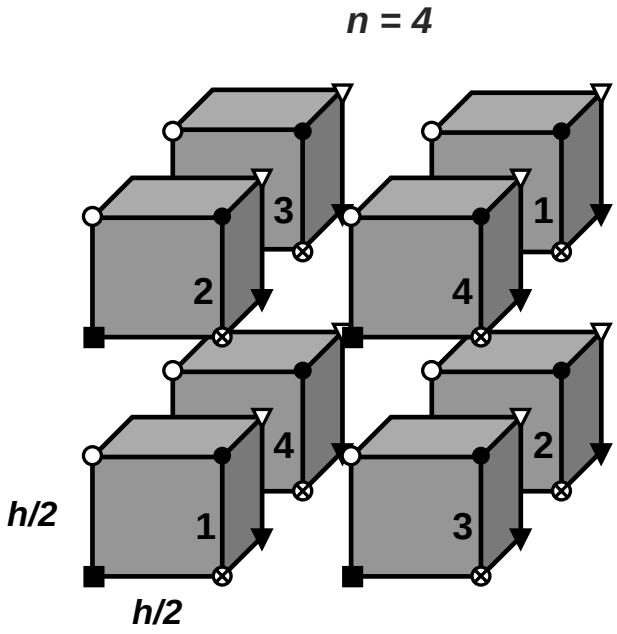

Figure 5. Coarse spatial distribution of grid cells and anelastic functions. The number on a cell face indicates the relaxation frequency of the anelastic functions localized in the cell. For example, grid cell 1 contains $\xi_1^{xx}, \xi_1^{yy}, \xi_1^{zz}, \xi_1^{xy}, \xi_1^{yz}, \xi_1^{zx}$. Reproduced from Kristek and Moczo (2003).

Anisotropic Media

FD modeling of wave propagation in anisotropic media has attracted limited attention as the main focus of both applied and academic studies has been on wave propagation in isotropic heterogeneous models. However, a need for modeling of anisotropic wave propagation arises not only from modeling of wave propagation in truly anisotropic materials such as for instance aligned anisotropic crystals in the upper mantle or shales, but also from wave propagation in an equivalent anisotropic medium, see eq. (65). An equivalent anisotropic medium is a low-frequency approximation for wave propagation in heterogeneous isotropic media (Backus, 1962; Helbig, 1984). An equivalent anisotropic medium can be used to represent for instance fine-scale layering or heterogeneity on a coarse scale appropriate for the scale of discretization of the FD modeling grid. Methods to compute equivalent anisotropic media are well known in 1D (Schoenberg and Muir, 1989) and can applied to FD modeling of smooth interfaces in 2D and 3D (Muir et al., 1992; Moczo et al., 2002). An equivalent anisotropic medium can also be used for modeling of wave propagation through stress induced cracked materials, where equivalent homogeneous anisotropic material represents average orientation and size of cracks (e.g., Crampin and Chastin, 2003). A general equivalent medium theory for 3D heterogeneous media is a formidable challenge and still a topic of research (and likely to remain one for quite some time).

Another reason for the limited use of FD modeling in anisotropic media is the lack of suitable formulation of anisotropic finite differencing. Whereas the conventional-grid schemes allow modeling of arbitrary anisotropic propagation, they may become unstable at fluid/solid boundaries (among other problems). The staggered-grid schemes are stable at fluid/solid boundaries but wave propagation in general anisotropic media is significantly more difficult. For example, Hooke's law for the general anisotropic medium has the form

$$\sigma_{ij} = c_{ijkl}\, u_{k,l} \ .$$

Tensor of elastic constants c_{ijkl} is symmetric in *i* and *j*, *k* and *l*, *ij* and *kl* indexes. The stress tensor σ_{ij} requires evaluation of terms such as $c_{1112}\, u_{1,2}$. Fig. 6 illustrates that the derivative of u_1 along the 2nd axis is not centered on the stress component σ_{11}. In fact, in 3D anisotropic media all derivatives with coefficients

$$c_{1112}, c_{1113}, c_{1123}, c_{2212}, c_{2213}, c_{2223}, c_{3312}, c_{3313}, c_{3323}, c_{2313}, c_{2312}, c_{1312}$$

are not centered on the corresponding stress components with the standard staggered-grid formulation. Therefore only wave propagation in an orthorhombic anisotropic medium with axis of symmetry aligned along the Cartesian coordinate system does not require any interpolation and is easily implemented. Neglecting the shift of the derivatives for a generally anisotropic medium introduces significant errors. Igel et al. (1995) therefore proposed interpolation operators that shift the derivatives to the corresponding stress positions on the staggered grid. Analogously to the differential operators, the higher-order interpolation operators are more accurate, but require more floating point operations. In fact the interpolation significantly increases the number of operations at every time-step. In general anisotropic media we must carry out 15 interpolations (12 for every coefficient shown above and three of these coefficients require interpolations in two directions), which leads to a substantial increase in terms

of computational cost. For example, the 3D second-order staggered pressure-velocity scheme, with no attenuation and no source representation, requires 16 floating-point operations per time-step for acoustic media. Analogously, the partly-staggered grid (discussed below) formulation (stress-velocity) requires 51 operations for an isotropic elastic medium and 81 operations per time-step for an anisotropic medium (without the cost interpolation required for staggered grids). The cost of interpolation operators in anisotropic media leads to an increase in the number of operations by 500 or more operations per time step (the number of float operations depends on particular implementation as some of the intermediate variables can be stored and reused for further calculations; if no intermediate variables are reused, each interpolation requires 55 operations for the fourth-order interpolation operator). The total number of operations per grid points is therefore on the order of 600 for the 3D anisotropic case. In other words, anisotropic finite differences on staggered grids are approximately 50 times slower (per time step) than acoustic modeling, and more than 15-20 times slower than isotropic modeling. Note that in addition as elastic simulations typically require shorter time steps and larger simulation times to propagate S-waves thus making acoustic modeling comparably even more computationally inexpensive.

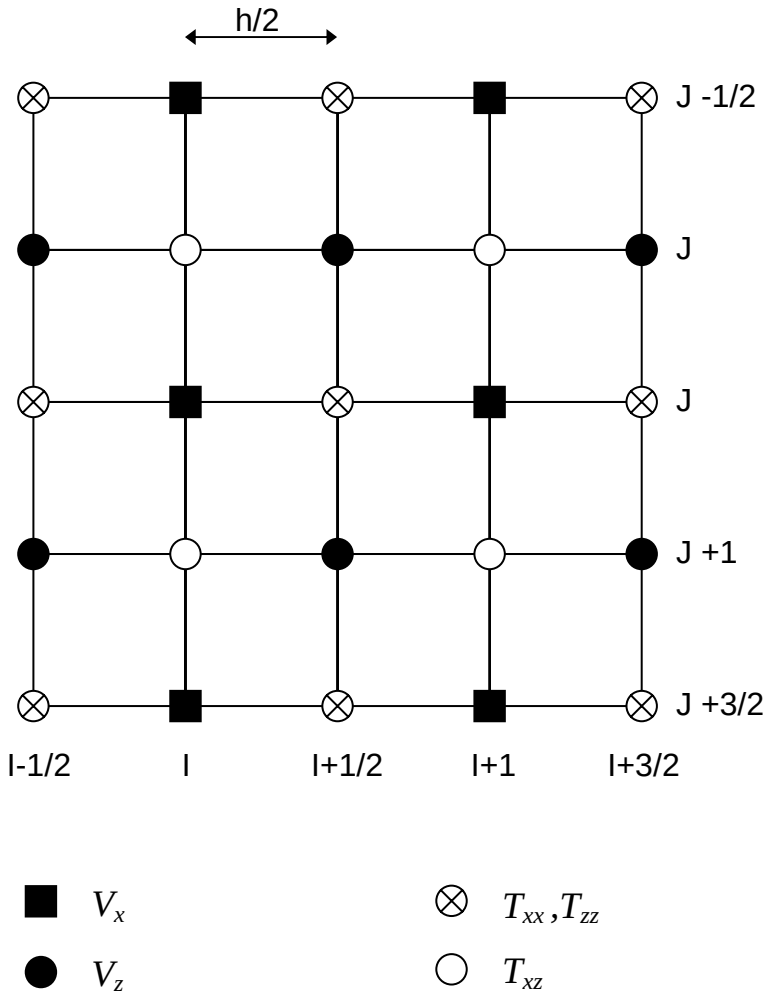

Figure 6. Staggered grid in 2D. V_x and V_z are the particle displacement/velocity components, T_{xx}, T_{zz} and T_{zx} are the stress-tensor components.

A FD formulation on a partly-staggered grid, originally developed for isotropic wave propagation (Andrews, 1973 and Zhang, 1997), was successfully applied to anisotropic wave propagation by Saenger and Bohlen (2004) (they used term rotated staggered). The formulation combines features of the conventional and staggered-grid schemes. In a grid cell, all stress-tensor components are located at one grid position, all displacement or particle-velocity components are located at other grid position. Numerical analysis of the stability condition shows that the formulation is stable for fluid/solid boundaries. For anisotropic finite-differences on the partly-staggered grid the calculation is roughly only 60% slower than isotropic modeling and the relative cost further decreases with the higher-order space derivative operators that are used as both types of media require the same number (18) of spatial derivatives (e.g., for the popular 4^{th}-order in space and 2^{nd}-order in time formulation, the anisotropic calculation requires only 35% additional computations). This comparison illustrates that there is no significant saving in computational cost by modeling only restricted degrees of anisotropy on the partly-staggered grid (e.g., modeling only orthorhombic versus fully anisotropic media). Although the partly-staggered grid appears to have some quite attractive properties it is not widely used today and the properties of the partly-staggered-grid FD schemes, such as stability for various qP-to-qS wave speeds ratio and interfaces, have to our knowledge not been fully analyzed and tested. Further research is therefore required before adapting the partly-staggered grid formulation instead of the standard staggered-grid formulation introduced by Madariaga (1976) and Virieux (1984) that we focus on in our chapter.

Next we shall derive numerical stability conditions for a FD approximation that is 2^{nd}-order accurate in time and of arbitrary order accuracy in space (von Neuman condition; O'Brien et al., 1951) for wave propagation in a fully anisotropic homogeneous medium. We shall follow the derivation of numerical stability by Crase (1990), Igel et al. (1995), and Saenger and Bohlen (2004). The stability conditions for anisotropic heterogeneous media are evaluated by stability of the equivalent homogeneous medium.

The velocity-stress formulation of the equation of motion for a general anisotropic medium is (without the body-force term), eqs. (8),

$$\begin{aligned} \rho \dot{v}_i &= \sigma_{ij,j} \\ \dot{\sigma}_{ij} &= c_{ijkl} v_{k,l} \,. \end{aligned}$$

An approximation to the time derivatives yields

$$\begin{aligned} v_i\left(I,J,K,m+1/2\right) - v_i\left(I,J,K,m-1/2\right) &\doteq \Delta t \frac{1}{\rho} \partial_j \left[\sigma_{ij}\left(I,J,K,m\right)\right], \\ \sigma_{ij}(I,J,K,m) - \sigma_{ij}(I,J,K,m-1) &\doteq \Delta t\, c_{ijkl}\, \partial_l \left[v_k\left(I,J,K,m-1/2\right)\right]. \end{aligned} \tag{136}$$

Here, $\partial_i = \partial / \partial x_i$. Taking the plane-wave ansatz, i.e., a harmonic wave $u_i(t,k) = A_i \exp\left[i\left(\omega t - k_j x_j\right)\right]$, $k = \left|\vec{k}\right|$ being a wavenumber, which satisfies the elastodynamic equation, we can rewrite eq. (136) to contain only particle velocity at one time:

$$-4\sin^2\left(\frac{\omega\Delta t}{2}\right)v_i(I,J,K,m) \;=\; -\Delta t^2\,\frac{1}{\rho}\,\partial_j\left\{\,c_{ijkl}\,\partial_l\left[v_k(I,J,K,m)\right]\right\}. \quad (137)$$

The spatial operators on r.h.s. of eqs. (137) are also discretized. The ansatz solution for the harmonic wave in a homogeneous anisotropic medium allows analytical evaluation of the FD approximation to the real wavenumber (note that we ignore the issue of interpolation here):

$$\partial_i \;\doteq\; \tilde{k}_i \;=\; \frac{2}{\Delta x_i}\sum_{n=1}^{N_S/2} p_n \sin\left(k_i\,\frac{2n-1}{2}\Delta x_i\right), \quad (138)$$

where $\tilde{k}$ is the numerical wavenumber, Δx_i grid spacing in the x_i-direction, N_S the order of the spatial operator, and p_n the coefficients of the spatial operator. Now we can evaluate complete discretized eqs. (137) for the ansatz solution and obtain the following expression for the angular frequency:

$$\omega = \frac{2}{\Delta t}\arcsin\left[\frac{1}{2}\frac{\Delta t^2}{2}\lambda_q\left(\tilde{k}_r, c_{ijkl}\right)\right]^{1/2}. \quad (139)$$

Here λ_p are diagonal elements of the matrix

$$D_{ik} = \frac{1}{\rho}\tilde{k}_j\,c_{ijkl}\,\tilde{k}_l\,. \quad (140)$$

If the expression under the square root in eq. (139) is greater than one or less than zero, the numerical angular frequency is not real and the FD scheme becomes unstable (because the operator on particle velocity of eq. (137) is unstable). Thus a general condition for stability of the FD approximation is

$$0 \;\le\; \frac{\Delta t^2}{4}\lambda_q(\tilde{k}_r, c_{ijkl}) \;\le\; 1\;. \quad (141)$$

To evaluate stability condition (141) we need the eigenvalues of the matrix (140). To evaluate these we bound the FD wavenumbers of eq. (138) by

$$\tilde{k}_i \;\le\; \frac{2}{\Delta x_i}\sum_{n=1}^{N_S/2}\left|p_n\right|, \quad (142)$$

and evaluate eigenvalues of the FD operator (140). In isotropic media the conditions (139-140) can be evaluated analytically and they correspond to the CFL condition (e.g., Mitchell and Griffiths, 1994, p. 167; Taflove and Hagness, 2005, p. 42). The analytic solution exists for isotropic homogeneous media where stability condition (141) is

$$0 \leq -2\sum_{n=1}^{N_t/2}(-1)^n \frac{\Delta t^{2n}\ \alpha^{2n}}{\Delta x_i^{2n}(2n)!}\left(\sum_{j=1}^{N_S/2}\left|p_j\right|\right)^{2n} \leq 1\ , \tag{143}$$

where α is the P-wave velocity. The condition is valid for both P- and S-wave velocities, but P-wave velocity imposes a stricter constraint as it is larger than the S-wave velocity. However, for a general anisotropic medium the stability condition (141) has to be evaluated numerically.

Free Surface

Traction-free Boundary Condition

In exploration and earthquake seismology recordings are often made at or close to the Earth's surface. In most seismological applications, the air/fluid (ocean) or air/solid (land) interface can be thought of as a free surface where a fluid or solid abruptly terminates and is replaced by vacuum, that is, the Earth's surface may be approximated by a surface with vanishing traction. Let the surface *S* with normal vector $\vec{n}$ define the geometry of the Earth's surface. Let $\vec{T}(\vec{u},\vec{n})$ be the traction vector corresponding to the displacement vector $\vec{u}$ and normal vector $\vec{n}$. The traction-free condition is

$$\vec{T}(\vec{u},\vec{n}) = 0 \ . \tag{144}$$

A real location for the seismic recordings can be affected by at least two significant factors causing a large impact on wave propagation that must be modeled or understood in many applications. Apart from the fact that the near-surface medium structure may be highly complex with large velocity variations (e.g., Eisner and Clayton, 2002), the free surface itself may display significant topographic variations. At the same time, the FD method inherently has difficulty to implement traction boundary condition. Therefore the accuracy and efficiency of the free-surface approximation are key issues in FD modeling of seismic wave propagation and earthquake motion.

Though, in principle, the same free-surface boundary condition should be simulated for planar and non-planar (topographic) free surfaces, due to the definition of the FD method and unlike, for example, the finite-element method, the implementation of the traction-free condition in the case of topography is a considerably more difficult problem. This is also reflected in the recent development. Therefore, the two geometries will be addressed separately.

Planar Free Surface

Let the surface *S* be a planar free surface at $z = 0$ with the unit normal vector $\vec{n} = (0,0,-1)$. Then

$$\sigma_{z\eta} = 0 \,, \quad \eta \in \{x, y, z\} \tag{145}$$

is the desired boundary condition at the horizontal (flat) free surface.

Recall the 4th-order approximation to the 1st derivative used in the staggered-grid FD schemes for interior grid points. The 1st derivative of a function $\Phi(\xi)$ at $\xi = \xi_0$ is approximated by eq. (5)

$$\begin{aligned} \Phi'(\xi_0) &= \Phi_{,\xi}(\xi_0) \\ &= \frac{1}{h}\left\{ a\left[\Phi\left(\xi_0 + \frac{3}{2}h\right) - \Phi\left(\xi_0 - \frac{3}{2}h\right)\right] + b\left[\Phi\left(\xi_0 + \frac{1}{2}h\right) - \Phi\left(\xi_0 - \frac{1}{2}h\right)\right]\right\} \end{aligned}$$

with $a = -1/24$, $b = 9/8$ and h being a grid spacing. Evaluation of the z-derivative of a function at $z = 0$ then requires the function values at positions $-h/2$ and $-3h/2$ above the free surface. Similarly, evaluation of the z-derivatives of a function at $z = h/2$ and $z = h$ requires values at $z = -h$ and $z = -h/2$, respectively. This implies two principal possibilities:
- the application of the FD scheme for the interior grid points with the field or material parameters somehow defined above the free surface,
- the application of a different, say, adjusted, FD scheme which does not require any values above the free surface.
Obviously, for the same reason which makes the heterogeneous schemes easier to use than the homogeneous ones, the first approach is preferable.

The first approach either leads to the so-called vacuum formalism, medium taper or imaging method. The vacuum formalism applies zero moduli above the free surface. While this approach gives good accuracy in the displacement formulation, e.g., Zahradník and Priolo (1995) in 2D, Moczo et al. (1999) in 3D, Graves (1996) and other authors did not find the approach satisfactory in the staggered-grid modeling. A density taper was used by Frankel and Leith (1992) in their conventional-grid displacement FD scheme.

Stress Imaging

The stress imaging was introduced by Levander (1988) in his 2D P-SV 4th-order staggered-grid velocity-stress FD scheme. The stress-imaging technique applies explicit boundary conditions to the stress-tensor component(s) located at the grid plane coinciding with the free surface, and uses imaged values of the stress-tensor components above the free surface assuming their antisymmetry about the free surface. The antisymmetry

$$\sigma_{z\eta}(-z) = -\sigma_{z\eta}(z) \quad ; \eta \in \{x, y, z\} \tag{146}$$

ensures that the boundary condition given by eqs. (145) are satisfied.

As summarized by Robertsson (1996), there are three possibilities for treating the displacement or particle-velocity values formally required by the FD scheme:
1. The values are calculated using the 2nd-order approximations to the boundary condition and imaged stress-tensor components. The approach was used by Levander (1988), Graves (1996), Kristek et al. (2002) and others.
2. The values are mirrored as even values with respect to the free surface. The approach was used by Crase (1990) and Rodrigues and Mora (1993). As pointed out by Robertsson (1996), the even values of the particle velocity values violate the boundary conditions.
3. The values are set to zero. This was proposed by Robertsson (1996).

Given the staggered grid, there are two natural options for locating the free surface. In one, say H formulation, the horizontal displacement or particle-velocity components, and stress-tensor components T_{xx}, T_{yy}, T_{zz} and T_{xy} are located at the free surface. In the other, say W formulation, the vertical displacement or particle-velocity component and T_{zx} and T_{zy} are at the free surface. Rodrigues (1993) developed a 3D 8th-order staggered-grid displacement-stress scheme and used the stress-imaging technique in the H

formulation. He found that it is necessary to use more than twice the number of grid points compared to inside the medium in order to avoid a significant numerical dispersion. Therefore, he combined the stress-imaging technique with a vertically refined grid near the free surface and achieved good accuracy. Kristek et al. (2002) numerically tested both the H and W formulations of the stress-imaging technique against the discrete-wavenumber method. They demonstrated that in the 3D case the stress-imaging technique in the 4th-order FD modeling requires at least twice as many grid points per wavelength compared to what is sufficient inside the medium if the Rayleigh waves are to be propagated without significant grid dispersion even in the case of the simple homogeneous halfspace. They also tested the 4th-order version of the Rodrigues (1993) approach. While sufficiently accurate, the approach needs three times smaller time step (the factor of 3 is due to the most natural refinement of the staggered-grid).

It is obvious that either at least twice denser spatial sampling or three times smaller time step degrade the efficiency of the 4th-order staggered-grid modeling inside the medium.

Adjusted FD Approximations (AFDA)

The principle of the AFDA technique used by Kristek et al. (2002) is simple. The technique

1. directly prescribes zero values of σ_{zz} at the free surface in the H formulation or σ_{zx} and σ_{zy} in the W formulation,

2. applies adjusted FD approximations to calculate the z-derivatives at the grid points at the free surface and depths $h/2$ and h; the adjusted approximation uses only function values in the medium.

As a consequence, no imaged (virtual) values above the free surface are needed. Kristek et al. (2002) showed that while H-AFDA results in slightly better phases, W-AFDA results in better amplitudes. They concluded with the recommendation to use W-AFDA for earthquake ground motion modeling. The calculation of the stress-tensor and displacement components in W-AFDA can be summarized as follows (if the velocity-stress formulation is considered, displacement components are simply replaced by the particle-velocity components):

1. Direct application of the boundary condition:
$T_{zx}(0)=0,\ T_{zy}(0)=0$

2. The following 4th-order FD approximations are used to calculate the stress-tensor and displacement vector components:

$$\Phi'(z_0)=\frac{1}{h}\left[-\frac{352}{105}\Phi(z_0)+\frac{35}{8}\Phi\left(z_0+\frac{h}{2}\right)-\frac{35}{24}\Phi\left(z_0+\frac{3}{2}h\right)+\frac{21}{40}\Phi\left(z_0+\frac{5}{2}h\right)-\frac{5}{56}\Phi\left(z_0+\frac{7}{2}h\right)\right]+O\left(h^4\right) \tag{147}$$

$$\Phi'(z_0)=\frac{1}{h}\left[-\frac{11}{12}\Phi\left(z_0-\frac{h}{2}\right)+\frac{17}{24}\Phi\left(z_0+\frac{h}{2}\right)+\frac{3}{8}\Phi\left(z_0+\frac{3}{2}h\right)-\frac{5}{24}\Phi\left(z_0+\frac{5}{2}h\right)+\frac{1}{24}\Phi\left(z_0+\frac{7}{2}h\right)\right]+O\left(h^4\right) \tag{148}$$

$$\Phi'(z_0)=\frac{1}{h}\left[-\frac{h}{22}\Phi'(z_0-h)-\frac{577}{528}\Phi\left(z_0-\frac{h}{2}\right)+\frac{201}{176}\Phi\left(z_0+\frac{h}{2}\right)-\frac{9}{176}\Phi\left(z_0+\frac{3}{2}h\right)+\frac{1}{528}\Phi\left(z_0+\frac{5}{2}h\right)\right]+O\left(h^4\right) \tag{149}$$

$$\Phi'(z_0)=\frac{1}{h}\left[\frac{16}{105}\Phi(z_0-h)-\frac{31}{24}\Phi\left(z_0-\frac{h}{2}\right)+\frac{29}{24}\Phi\left(z_0+\frac{h}{2}\right)-\frac{3}{40}\Phi\left(z_0+\frac{3}{2}h\right)+\frac{1}{168}\Phi\left(z_0+\frac{5}{2}h\right)\right]+O\left(h^4\right) \tag{150}$$

a.) The calculation of the stress-tensor components:
$T_{xx}(h/2)$ is obtained from the 4th-order FD approximation to Hooke's law for σ_{xx}; derivative $u_{z,z}$ is approximated by formula (148);
$T_{yy}(h/2)$ and $T_{zz}(h/2)$ – similar to $T_{xx}(h/2)$;
$T_{zx}(h)$ is obtained from the 4th-order FD approximation to Hooke's law for σ_{zx}; derivative $u_{x,z}$ is approximated by formula (149) in which $u_{x,z}(0)$ is replaced by $u_{z,x}$ due to condition $\sigma_{zx}(0)=0$;
$T_{zy}(h)$ is obtained from the 4th-order FD approximation to Hooke's law for σ_{zy}; derivative $u_{y,z}$ is approximated by formula (149) in which $u_{y,z}(0)$ is replaced by $u_{z,y}$ due to condition $\sigma_{zy}(0)=0$;

b.) The calculation of the displacement-vector components:
$W(0)$ is obtained from the 4th-order FD approximation to the equation of motion for u_z; derivative $\sigma_{zz,z}$ is approximated by formula (147) in which condition $\sigma_{zz}(0)=0$ is used;
$U(h/2)$ is obtained from the 4th-order FD approximation to the equation of motion for u_x; derivative $\sigma_{zx,z}$ is approximated by formula (148);
$V(h/2)$ is obtained from the 4th-order FD approximation to the equation of motion for u_y; derivative $\sigma_{zy,z}$ is approximated by formula (148);
$W(h)$ is obtained from the 4th-order FD approximation to the equation of motion for u_z; derivative $\sigma_{zz,z}$ is approximated by formula (150) in which condition $\sigma_{zz}(0)=0$ is used.

In the W formulation, displacement component W, and stress-tensor components σ_{zx} and σ_{yz} are located at the free surface. The corresponding grid material parameters are evaluated as integral averages in the half grid-cell volumes, that is, the upper half of the volume located above the free surface is not taken into account. For example, density and unrelaxed moduli are evaluated as

$$\rho_W^A = \rho^A_{I+1/2,\, J+1/2,\, 0} = \frac{2}{h^3} \int_{x_I}^{x_{I+1}} \int_{y_J}^{y_{J+1}} \int_{z_0}^{z_{1/2}} \rho \, \mathrm{d}x \, \mathrm{d}y \, \mathrm{d}z \quad , \tag{151}$$

$$\mu_{zx}^H = \mu^H_{I,\, J+1/2,\, 0} = \left[\frac{2}{h^3} \int_{x_{I-1/2}}^{x_{I+1/2}} \int_{y_J}^{y_{J+1}} \int_{z_0}^{z_{1/2}} \frac{1}{\mu} \, \mathrm{d}x \, \mathrm{d}y \, \mathrm{d}z \right]^{-1} , \tag{152}$$

$$\mu_{yz}^H = \mu^H_{I+\frac{1}{2},\, J,\, 0} = \left[\frac{2}{h^3} \int_{x_I}^{x_{I+1}} \int_{y_{J-1/2}}^{y_{J+1/2}} \int_{z_0}^{z_{1/2}} \frac{1}{\mu} \, \mathrm{d}x \, \mathrm{d}y \, \mathrm{d}z \right]^{-1} . \tag{153}$$

Using numerical comparisons against the DWN method, Kristek et al. (2002) demonstrated that with the W-AFDA technique it is possible to apply the same spatial sampling as inside the medium. Because in many realistic models of the Earth's interior lateral material discontinuities reach the free surface, Moczo et al. (2004a) tested the accuracy of the W-AFDA technique against the finite-element method for which it is easy and natural to satisfy boundary condition at the free surface. Detailed numerical tests demonstrated the sufficient accuracy of the W-AFDA technique in models with near-surface material discontinuities and the capability of the FD scheme to 'see' the true position of the material discontinuities in the spatial grid.

Free-surface Topography

Approaches to Model Free-surface Topography

The classification of approaches is similar to that given in the previous section. The approaches based on modifying material properties at or in the vicinity of the free surface to implicitly satisfy the boundary conditions (e.g., Mittet, 2002; Zahradník and Hron, 1992; Zahradník et al., 1993) lend themselves to be generalized to incorporate topographic variations without much difficulty. However, they tend to require significant spatial oversampling. Frankel and Leith (1992) modeled the topographic effects on seismic waves generated at a Russian test site by using a technique where a smoothly varying density taper was used to model the transition from vacuum to the elastic sub-surface. Ohminato and Chouet (1997) describe one of the first techniques implemented in 3D where the exact location of the free surface is chosen such that it follows a staircase approximating the topographic surface. In their technique normal stresses are never located on the free surface. Instead, the location of the surface is chosen such that only the shear stresses which should be zero are at the free surface. The free-surface condition is simulated by setting the shear modulus to zero at the free surface and all elastic moduli to zero in the vacuum above the free surface. In the 2nd-

order FD scheme at least 25 grid spacings per minimum wavelength are needed to achieve an accurate and stable solution. Pitarka and Irikura (1996) also developed a similar method which was applied in 3D to study wave propagation site effects at the Kobe-JMA station.

Robertsson (1996) presented a method of simulating the free surface in staggered-grid FD modeling. The method is based on stress imaging and also results in a staircase-shaped surface approximation to the free-surface topography. By splitting the update at each time step in two iterations (in 2D) that contain spatial derivatives in one direction only, the imaging conditions can be satisfied also in the case of surface topography. The method is relatively simple to implement and yields sufficiently accurate results if at least 15-20 grid points are used per minimum wavelength. The method has been successfully applied both to land seismic applications (e.g., Robertsson and Holliger, 1997; Holliger and Robertsson, 1998) as well as for modeling scattering from a rough sea surface (Laws and Kragh, 2002; Robertsson et al., 2006).

As mentioned above the problem with spatial oversampling the wavefield in the vicinity of the free surface by roughly a factor of three can be circumvented by introducing a simple grid-refinement scheme in the vicinity of the free surface (Rodrigues, 1993; Robertsson and Holliger, 1997). A similar approach was also taken by Hayashi et al. (2001). The technique by Robertsson (1996) and its extension by Robertsson and Holliger (1997) will be described in the next sub-section.

Several authors developed approaches to avoid a staircase-shaped free surface. Ilan (1977) considered an arbitrary polygonal free surface. Ilan's technique did not address the transition points between the segments of various slopes and required a non-uniform grid that decreased accuracy. An improved representation of the arbitrary polygonal free surface was developed by Jih et al. (1988). Following a predefined classification scheme, the different segments were treated using a one-sided approximation of the free-surface condition. Unfortunately, the one-sided difference approximations reduce the accuracy of the method such that a significant spatial oversampling is needed. Another approach to overcome the "staircase problem," initially developed by Fornberg (1988) and then further developed by a number of authors (Tessmer et al., 1992; Carcione and Wang, 1993; Carcione, 1994; Nielsen et al., 1994; Hestholm and Ruud, 1994; Tessmer and Kosloff, 1994; Hestholm, 1999; Hestholm and Ruud, 2002) is to solve the wave equation on a curved grid whose line/surface coincides with the topographic surface (or another internal surface). This is achieved by solving the equation of motion written in Cartesian coordinates and involves first computing the spatial derivatives in the new (conformably mapped) coordinate system (curved grid) and then applying the chain rule to calculate the required Cartesian spatial derivatives. The main drawbacks of the method are stability problems associated with modeling very rough surface topography as well as the computational overhead caused by the chain rule (25% in 2D and 50% in 3D according to Komatitsch et al., 1996). Komatitsch et al. (1996) therefore proposed solving the equation of motion directly on the curved grid and thus avoiding the chain-rule computations. Although the approach addresses the computational efficiency, it requires additional memory.

As the FD method inherently has problems when incorporating the traction-free condition, particularly in the case of an arbitrary surface topography, Moczo et al. (1997) instead used a hybrid approach where a finite-element solution was used in the vicinity of the free-surface topography and a FD solution in the rest of the model. The method was shown to work very well and to be accurate and stable. Obviously, in order not to loose the computational efficiency it is desirable to minimize the region where the finite-element method is applied.

A Method for Modeling Surface Topography in 2D

To summarize the discussion above, a completely accurate and efficient technique applicable in general to model free-surface topography does not exist. Here we describe a relatively robust technique proposed by Robertsson (1996). The method can be viewed as a generalization of the stress-imaging method of Levander (1988) (H formulation) with one important modification. Instead of updating the particle velocities in the vicinity of the free surface such that the free surface condition is explicitly satisfied by using second-order accurate difference approximations, the particle velocities are simply set to zero above the free surface. Stresses on the other hand are imaged such that tractions perpendicular to the free surface always are zero at the free surface. The generalization to the viscoelastic case is straightforward since no spatial derivatives of the memory variables occur.

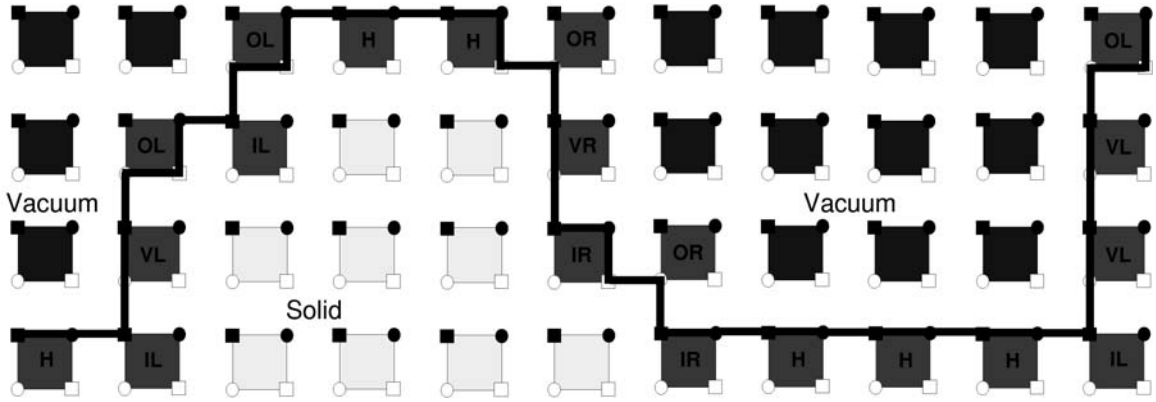

Figure 7. Staggered FD grid in the vicinity of the free-surface boundary where it forms a crest or (left) and a trough (right). The light large squares represent the locations of the grid-cells in the sub-surface. The grey grid-cells are located along the free-surface boundary, which runs exactly along the thick black line. All boundary grid-points are classified H-, VL-, IL-, OL-, VR-, IR-, or OR-points as described in the text. Within the grid-cells, the solid squares represent the σ_{xx} and σ_{zz} components, the light squares the σ_{zx} component, the solid circles the v_x component, and the light circles represent the v_z component. Reproduced from Robertsson (1996).

A description of the staggered grid in the vicinity of the free surface is shown in Fig. 7, for a crest and a trough. The free surface is discretized such that all grey grid-cells belong to it. It is critical where the boundary is located within the staggered grid-cells (see Robertsson, 1996, for a discussion). Numerically, the free surface itself is located along the thick black line. The grid-points along the discretized boundary belong to one and only one of the seven following categories: (1) horizontal boundary (H); (2) vertical boundary with vacuum to the left (VL); (3) inner corner with vacuum above to the left (IL); (4) outer corner with vacuum below to the left (OL); (5) vertical boundary with vacuum to the right (VR); (6) inner corner with vacuum above to the right (IR); and (7) outer corner with vacuum below to the right (OR).

It is worthwhile to recall the physical meaning of the imaging technique. The imaging is carried out to ensure that the normal and shear stresses perpendicular to the

boundary under consideration (σ_{zz} and σ_{zx} for the 2-D case of a flat horizontal surface) are zero. Notice that within all seven categories of boundary grid-cells, the free surface is always parallel to the grid. Imaging, therefore, only takes place in the directions of the x- and z-coordinate axes.

What happens in the vicinity of inner corners, where grid-points are subject to imaging from different directions? Briefly, by calculating separately the vertical and horizontal derivatives of the stress components in the update of the particle velocities, such problems are readily avoided (see below).

Horizontal boundary grid-point (H-point): An H-point has one neighbor on either horizontal side that is either an H-, OL-, OR-, IL- or IR-point. The H-points are treated identically to the flat free-surface approximation. Particle velocities are set to zero in the vacuum. Imaging of stresses only takes place in the vertical direction. Just as for the flat free surface, the σ_{xx} component is updated using the fourth-order accurate central FD approximation along the surface.

Vertical boundary grid-point with vacuum to the left (VL-point): A VL-point has one neighbor on either vertical side that is either a VL-, IL- or OL-point. The VL-points are treated similar to the H-points with the exception that here it is the σ_{xx} component that should be zero at the boundary, and the imaging therefore only takes place in the horizontal direction. The σ_{zz} component is updated in the same way that the σ_{xx} component is updated for the H-points.

Inner corner grid-point with vacuum above to the left (IL-point): An IL-point has one neighbor vertically above that is either an OL- or VL-point, and one horizontally to the left that is either an H- or OL-point. No imaging takes place around the IL-points. The σ_{xx} and σ_{zz} components are located along the boundary, perpendicular to parts of it, and are therefore set to zero.

Outer corner grid-point with vacuum to the left (OL-point): An OL-point has either an IL- or H-point immediately to the right and an IL- or VL-point immediately below. The free surface is located through the v_x, v_z, and σ_{zx} components, while the normal stresses are located in the vacuum above the free surface (Fig. 7). The σ_{zx} component is therefore set to zero. The σ_{xx} and σ_{zx} components are imaged horizontally with respect to the rightmost vertical part of the free surface, and the σ_{zz} and again the σ_{zx} components are imaged vertically with respect to the lowermost horizontal part of the free-surface (Fig. 7). If the OL-point is adjacent to an IL-point, the particle velocity component in between must be set to zero to obtain a stable and accurate solution.

Vertical boundary grid-point with vacuum to the right (VR-point): A VR-point has one neighbor on either vertical side that is either a VR-, IR- or OR-point. The VR-points are treated analogously to the VL-points, with the exception that the imaging takes place in the opposite horizontal direction.

Inner corner grid-point with vacuum above to the right (IR-point): An IR-point has one neighbor vertically above that is either an OR- or VR-point, and one horizontally to the right that is either an H- or OR-point. Only vertical imaging of the σ_{zx} component takes place for the IR-points. The σ_{xx} and σ_{zz} components are located along the boundary, perpendicular to parts of it, and are therefore set to zero.

Outer corner grid-point with vacuum to the right (OR-point): An OR-point has either an IR- or H-point immediately to the left and an IR- or VR-point immediately below. The free-surface makes a step immediately to the left of the OR-point and only

intersects with its v_z component, whereas the other velocity- and stress-fields are located in the vacuum above the free surface (Fig. 7). The σ_{zx} component immediately to the left of the boundary point is set to zero. The σ_{xx} and σ_{zx} components are imaged horizontally with respect to the vertical segment of the free-surface boundary to the left of the grid-point (Fig. 7). The σ_{zz} component is imaged vertically with respect to the step at the v_z component in the OR-point. If the OR-point is adjacent to an IR-point, the particle velocity component in between must be set to zero to obtain a stable and accurate solution.

The free-surface boundary points have to be classified prior the FD. The maximum computational efficiency is obtained by setting the reciprocal values of the densities to zero everywhere in the FD grid above the free surface. The particle velocities will then automatically be zero above the free surface after every update. The imaging algorithm thus does not add a substantial amount of the computational cost. However, computations are wasted in the region occupied by vacuum above the topography in the FD grid.

Each of the equations for the particle velocities, consist of two derivatives (one vertical and one horizontal) of the stress-tensor components. Here we do not show explicitly equations for the considered 2D case as they can be easily obtained from eqs. (8) for the 3D case. By first performing all vertical imaging of the stress-tensor components (H-, OR-, OL-, and IR-points) and then calculating and adding only the vertical derivatives in equations, the free-surface condition is satisfied completely in all grid-cells along the boundary. Next, the horizontal imaging of the stress components (VL-, VR-, OR-, and OL-points) is carried out followed by an update with the remaining horizontal derivatives in equations, again satisfying the free-surface boundary condition. Following the updates of equations it is necessary to set the v_x component to zero in the VR- and OR-points, since the reciprocal velocity is not zero in these points. Subsequently, the stress-fields are updated. This action does not involve any imaging of the variable fields. Following the update, the correction of the normal stress parallel to the surface must be made at the H- (σ_{xx}), VL- and VR-points (σ_{zz}), as described above for the horizontal free-surface.

There is a modeling limit as to how narrow the "troughs" or "crests" in the topography can be. A crest cannot be narrower than the number of grid-points imaged around its horizontal sides. Fig. 7 shows the narrowest crest and trough that are allowed when using fourth-order accurate spatial central-difference approximations.

Since the technique requires approximately three times dense spatial sampling than that inside the medium, Robertsson and Holliger (1997) used a grid-refinement as illustrated in Fig. 8. For the update at grid points of the finer grid close to the coarser grid a simple linear interpolation in the vertical direction is sufficient between the wavefield components in the coarse and fine parts of the grid. However, in the horizontal direction, some care should be taken since waves that propagate close to parallel to the transition region will undergo reflection due to very slight numerical errors in the interpolation between the two regions. An excellent performance can be obtained by using a more accurate sinc interpolation (Martin Musil, personal communication).

To illustrate the accuracy of the method for modeling surface topography we show an acoustic example that has been published elsewhere (Robertsson et al., 2006). The example addresses the problem of modeling scattering from a rough sea surface modeled as a self-similar surface using the method by Pierson and Moskowitz (1964).

The so-called Significant Wave Height (SWH) was set to 2 meters (a moderately rough sea as marine reflection seismic data typically are acquired in seas up to 4m SWH).

Figure 9 shows the reflected response due to a plane wave incident vertically from below as well as at 30° incidence angle with respect to the vertical, recorded 6m below the average level of the sea surface. We show solutions computed using three different methods. First, the FDTD method by Robertsson (1996) described here. Second, a solution computed using the spectral element method (Chaljub et al., 2006) and finally a solution computed using the Kirchhoff approximation (Laws and Kragh, 2002).

Careful convergence tests were carried out to ensure that details of the reflected and scattered response were not contaminated by numerical artifacts in the respective method. The FDTD method determined the spatial discretization of the sea surface used for all three methods, since it required the densest sampled sea surface (15-20 grid-points per minimum wavelength).

As can be seen from Figure 9, there is very good match between the FDTD and the spectral element solutions both in terms of amplitude and phase far into the coda. Although the much simpler (and more efficient Kirchhoff method) provides a reasonably accurate solution, the synthesized coda differs significantly from that computed using the two other methods.

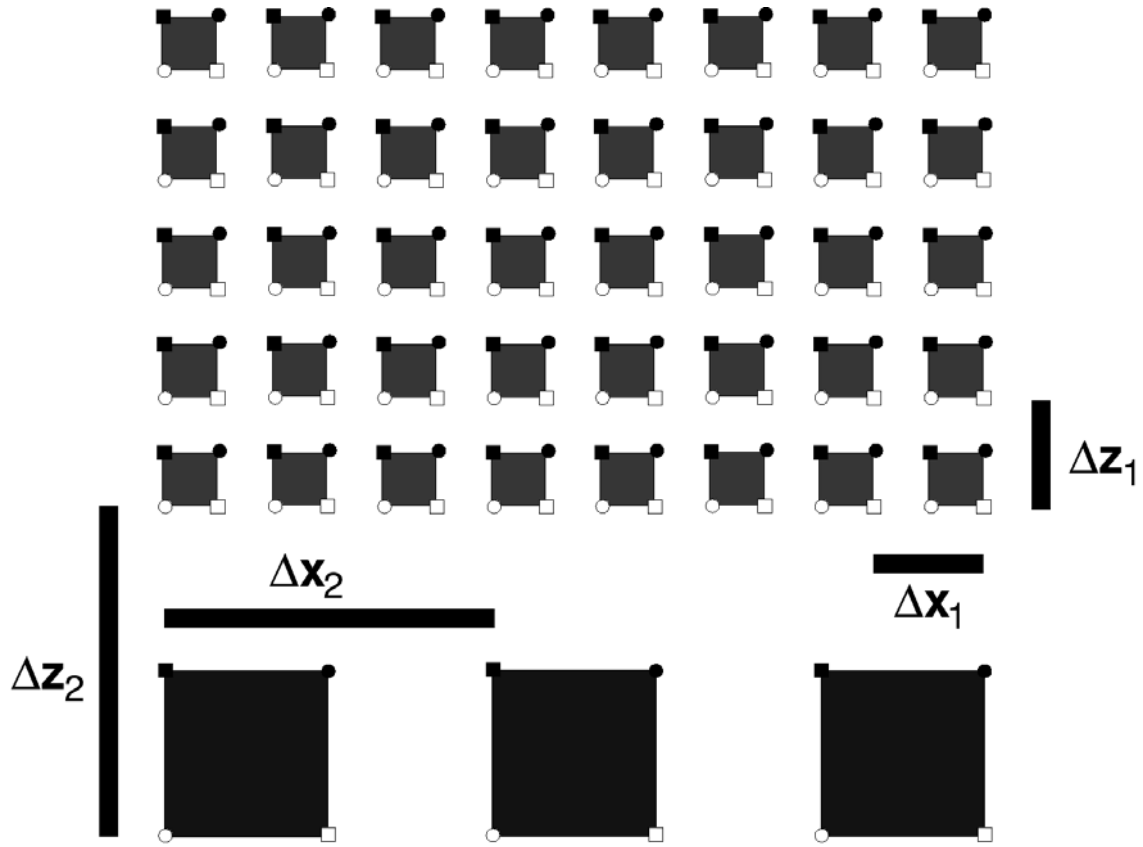

Figure 8. Grid-refinement technique (Robertsson and Holliger, 1997) used together with the method for modeling surface topography (Robertsson, 1996). The upper part of the grid (light grid cells) is three times more densely sampled than the lower part (dark grid cells). Reproduced from Robertsson and Holliger (1997).

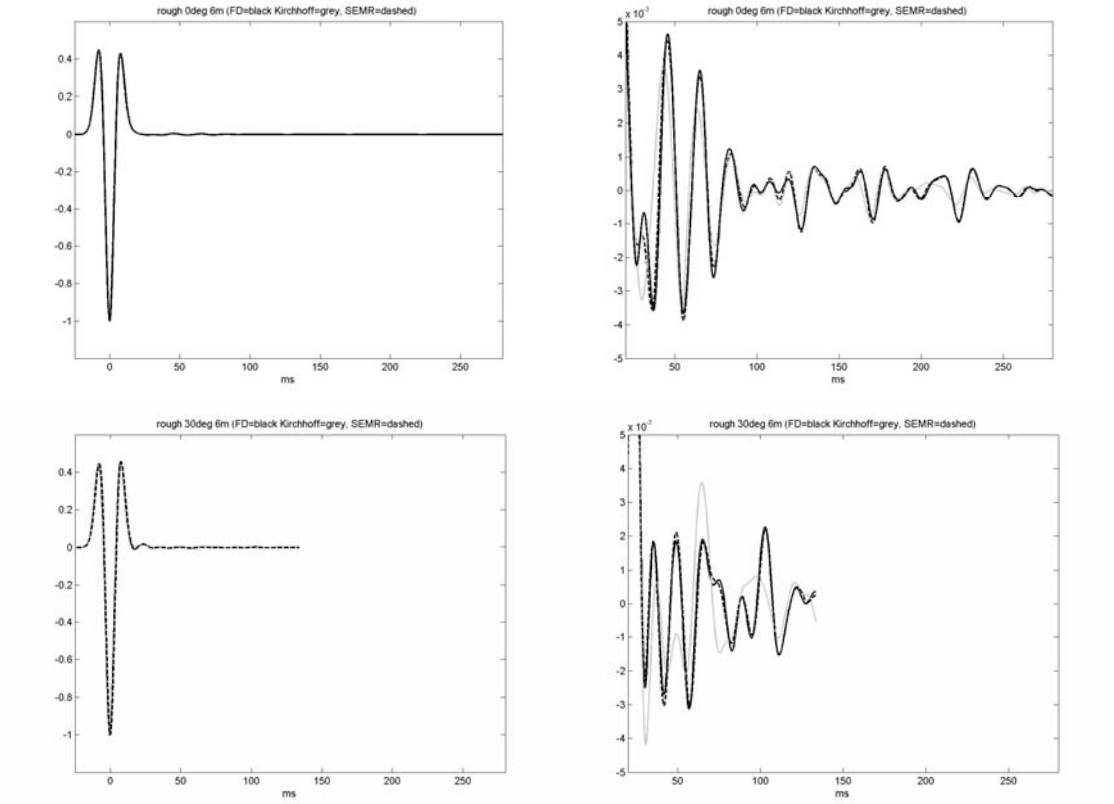

Figure 9. Rough sea surface reflected response for a plane wave incident vertically from below (top row) and at an angle of 30° to the vertical (bottom row). The reflected/scattered field is recorded at a point placed at 6m depth. The plots on the right are enlargements of the scattered coda in the plots on the left. Black: FDTD response. Grey: Response computed using a Kirchhoff method (Laws and Kragh, 2002). Dashed: Response computed using a spectral element method (Chaljub et al., 2006). Figure reproduced from Robertsson et al. (2006).

Wavefield Excitation

Direct modeling of the point sources

The average properties of complex seismic sources are usually represented as point sources in a continuous elastic medium (see, for example, chapter 3 of Aki and Richards, 1980). The two simplest point sources are body forces and moment-tensor sources. A point source representation of a body-force type of source can be implemented directly as the increment of the corresponding components as given by the equation of motion, e.g. eqs. (7) :

$$\rho \dot{v}_i = \sigma_{ij,j} + f_i .$$

Note, that the body force source-time function is not differentiated with respect to time. The usual implementation of the body-force point source at the time t_m is then

$$v_i(t_m) = v_i(t_m) + \frac{1}{\rho} \Delta t \; f_i(t_m).$$

Implementation of the moment-tensor source can be included either by stress (Virieux, 1986; Coutant et al., 1995) or by particle velocity (Frankel, 1993; Yomogida and Etgen, 1993; Graves, 1996). The implementations are equivalent due to the body-force equivalent theorem (e.g., pages 40-44 of Aki and Richards, 1980). In the particle-velocity implementation, each component of the moment tensor is implemented by corresponding couple of the body forces with discrete arm length between the forces. For example, in the staggered-grid velocity-stress formulation the M_{xx} component of the moment tensor is equivalent to couple of the forces $(M_{xx}/\Delta x)$ acting along the x-axis in the opposite directions. Because these forces are applied at one grid point, the appropriate volume is one grid cell, $\Delta x \cdot \Delta y \cdot \Delta z$. Therefore, the particle-velocity update for the M_{xx} component of the moment tensor at grid node (I, J, K) is

$$v_x(I+1/2, J, K, m) = v_x(I+1/2, J, K, m) + \frac{1}{\rho} \Delta t \frac{M_{xx}(I, J, K, m)}{\Delta x^2 \Delta y \Delta z},$$

$$v_x(I-1/2, J, K, m) = v_x(I-1/2, J, K, m) - \frac{1}{\rho} \Delta t \frac{M_{xx}(I, J, K, m)}{\Delta x^2 \Delta y \Delta z}.$$

However, the equivalent body forces for the representation of the M_{xy} component of the moment tensor are not located along the grid line I and they must be averaged from four equivalent body forces $(M_{xy}/2\Delta y)$ acting along the x-axis in the opposite directions with a force arm of length $2\Delta y$ as illustrated in Fig. 10. Therefore the particle velocity update for the M_{xy} component of the moment tensor at grid node (I, J, K) is

$$v_x\left(I \pm 1/2, J+1, K, m\right) = v_x\left(I \pm 1/2, J+1, K, m\right) + \frac{1}{\rho}\Delta t \frac{M_{xy}\left(I, J, K, m\right)}{4\Delta x \Delta y^2 \Delta z},$$

$$v_x\left(I \pm 1/2, J-1, K, m\right) = v_x\left(I \pm 1/2, J-1, K, m\right) - \frac{1}{\rho}\Delta t \frac{M_{xy}\left(I, J, K, m\right)}{4\Delta x \Delta y^2 \Delta z}.$$

Analogously the remaining components of the moment tensor can be implemented as equivalent body forces centered at grid node $\left(I, J, K\right)$. Note that this moment tensor implementation allows modeling of the explosive sources (equal diagonal elements and vanishing non-diagonal elements of the moment tensor), pure shear slip (if the moment tensor is determined from the dip, strike and rake and seismic moment, page 117-118 of Aki and Richards, 1980), or a compensated linear vector dipole (CLVD) source.

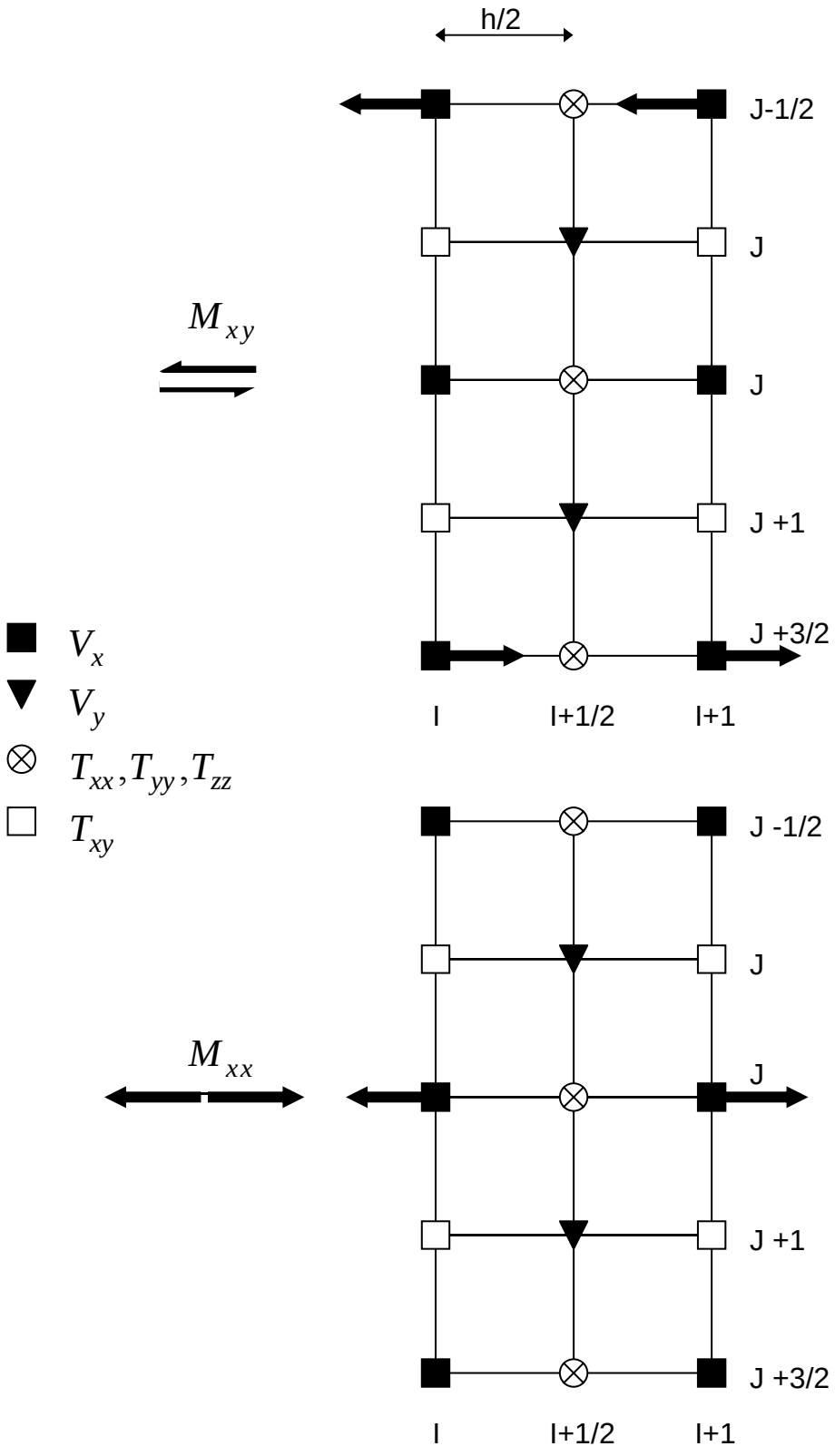

Figure 10. An example of equivalent body force implementation of moment tensor source component M_{xy} (top) and M_{xx} (bottom). The FD grid shows only the XY plane of the 3D grid as all body forces are implemented in the same plane (plane *K*).

Introducing the source wavefield along a boundary internal to the grid

Alterman and Karal (1968), Kelly et al. (1976) and Levander (1989) describe how to introduce a source field into a FD grid by "injecting" an analytical source solution on an internal artificial surface surrounding the source to for instance avoid a (point) source singularity in the FD computation. The source wavefield is introduced so that it radiates from the outside of the surface surrounding the source. In principle, all we need is to satisfy the principle of superposition and the continuity of the superimposed wavefields across the surface. In practice because the FD calculation is discontinuous at the injection surface S, some care must be taken in the FD calculations where the spatial FD stencil intersects the surface.

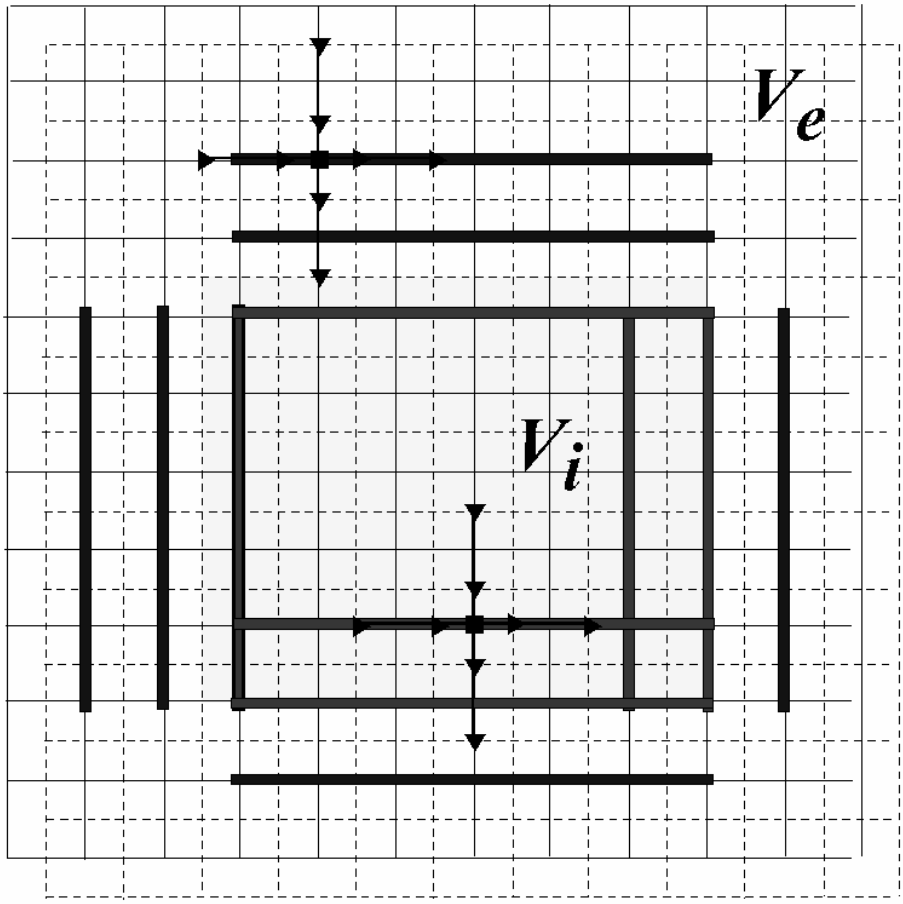

Figure 11. Introduction of a source wavefield along an internal artificial surface in the staggered grid illustrating the update of normal stresses. Normal stresses are located on the solid grid whereas shear stresses are located on the dashed grid. The region with grey background corresponds to V_i whereas the remaining part of the grid (white background) corresponds to V_e. The so-called injection surface S separates the two regions. Two FD stencils are shown in the picture (one updating a point in V_i and one a point in V_e). Bold lines in the grey region correspond to grid points where the source wavefield should be subtracted at the appropriate points during the update whereas bold lines in the white region show grid points where it should be added**.** Reproduced from Robertsson and Chapman (2000).

Fig. 11 shows a 2D staggered FD grid in the vicinity of the injection surface S. The region outside the surface is referred to as the external region V_e (white in Fig. 11) whereas the region inside the surface is referred to as the internal region V_i (grey in Fig. 11). The process of introducing the source wavefield is straightforward and involves manipulating the update of the wavefield only in the vicinity of S for the update of points where the spatial extent of the FD stencil intersects S (where the wavefield in the grid is discontinuous). In Fig. 11 these points have been marked with by the thick bold lines.

The source field to be injected is known (e.g., analytically) in the vicinity of the surface S for all times (this is possible at least if the surface is located entirely within a homogeneous part of the model). The source wavefield will interact with the model throughout the FD grid within V_i and V_e and generate a scattered wavefield. In V_e both the source wavefield and the scattered wavefield is present whereas in V_i only the scattered wavefield is present. Since the source wavefield is known (e.g., analytically) this can be added and subtracted as appropriate for the update of points along the bold lines for the parts of the spatial stencils that intersect S (subtract the source wavefield at the appropriate points when updating points along the bold lines in the grey region and adding the source wavefield at the appropriate points when updating points along the bold lines in the white region).

In each FD time step the stresses (and corresponding memory variables for the viscoelastic case) are first updated in the entire grid. When the update is complete, we go back and correct the update at the points where the spatial FD stencil intersected the surface S. Here we describe how this is done for the normal stresses (illustrated in Fig. 11). Outside S in V_e, the wavefield is updated as if the injected wavefield were propagating through the entire grid. Therefore we must add the injected source wavefield to the particle-velocity components corresponding to the parts of the stencil that are inside S in V_i. In Fig. 11 this occurs when normal stresses along the bold lines in the white region along each side of V_e are updated. For a 4^{th}-order accurate scheme we therefore need to know the source wavefield along the two closest grid points inside S for the upper and left edges of the rectangular injection region shown in Fig. 11, and along the closest grid point for the lower and right edges. Inside S in V_i, the wavefield is updated as if no wavefield were injected. Therefore we must subtract the injected source wavefield from the particle-velocity components corresponding to the parts of the stencil that are outside S in V_e (for update of normal stresses located along the bold lines in the grey region along each side in V_i).

Next, we advance the calculation by half a FD time step and update the particle velocities in the entire grid using equation. The wavefield injection is performed using the same procedure by adding and subtracting the stress components of the injection wavefield at the three grid points around S. In total, we therefore need to know the values at all times of stresses and particle velocities at three grid points around S, staggered appropriately both in time and space. By iterating these two steps of the update, the entire FD simulation is stepped through and the wavefield is injected along the surface S.

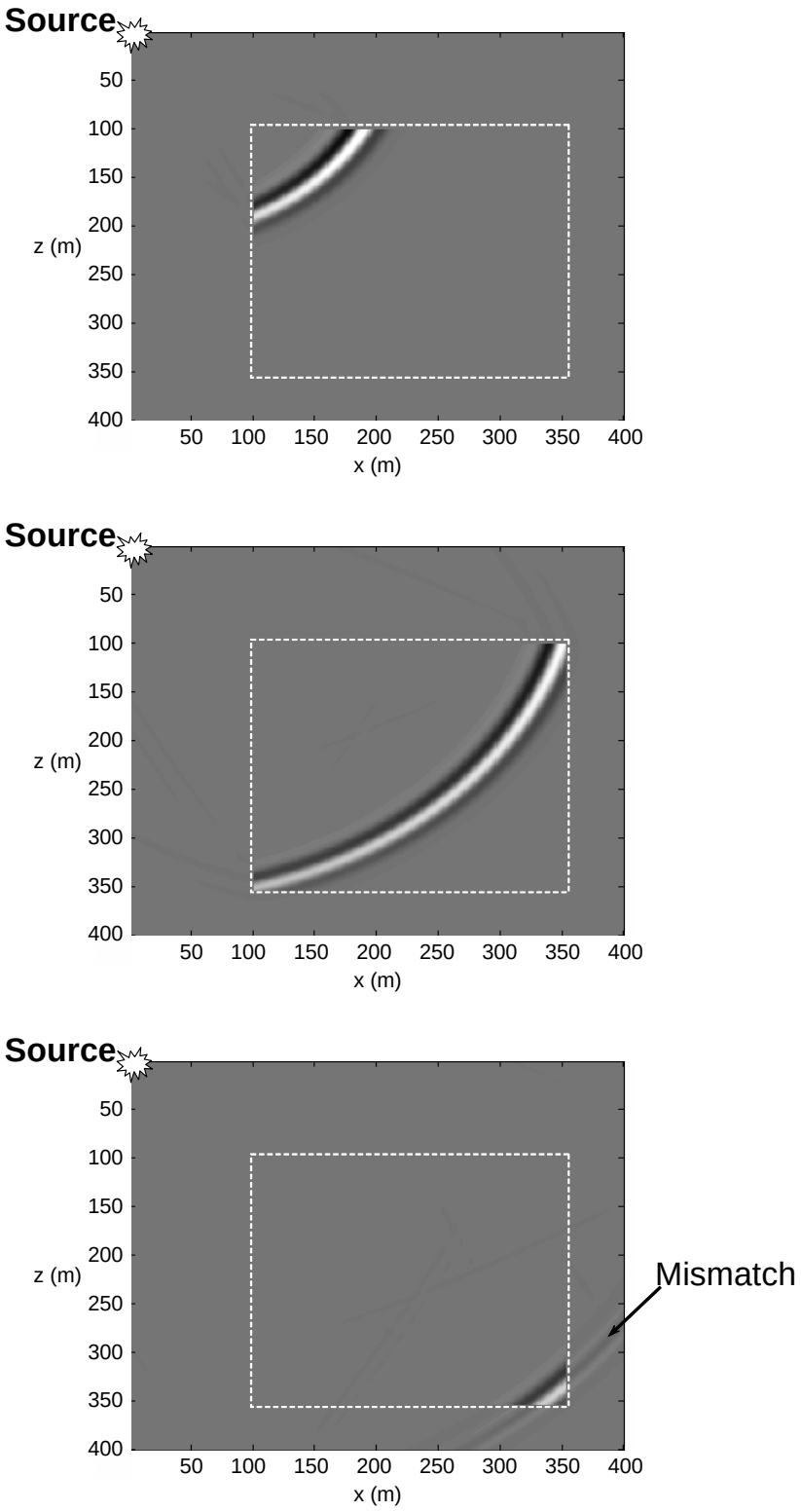

Figure 12. Example of a hybrid simulation in a homogeneous medium, where the FD computation is driven by an analytical wavefield for a point source in a homogeneous medium. The source is located at a fictitious position in the upper corner of the FD grid. The injection surface is outlined as a dashed box. Snapshots from 0.14s, 0.24s and 0.30s are shown.

As noted by for instance Fäh (1992), Zahradník (1995), Robertsson et al. (1996), Zahradník and Moczo (1996), Moczo et al. (1997), Robertsson and Chapman (2000), and Takeuchi and Geller (2003), the same technique for introducing the source wavefield along an internal boundary can be used for hybrid modeling purposes where the wavefield from another computational technique (e.g., discrete-wavenumber or ray method) is introduced inside a FD grid. In that case we reverse the regions V_i and V_e so that the source wavefield is injected inside the surface S.

Fig. 12 shows snapshots from tests of such a hybrid technique. Here the source wavefield is given by an analytical solution for a point source in a homogeneous medium. Since the FD grid also corresponds to a homogeneous medium we would expect the scattered wavefield in V_e to be zero. In the snapshots from 0.14s and 0.24s, we see no evidence of any wavefield being present in V_e. However, in the snapshot from 0.30s, part of the wavefield leaks through into V_e. This is because the wavefront that has propagated in the FD grid has suffered from numerical dispersion and no longer exactly match the wavefield from the analytical solution which ideally should destructively interfere with the FD wavefront as it reaches the injection surface dS.

In the so-called FD-injection technique (Robertsson and Chapman, 2000), the source wavefield is generated by a FD solution in an unperturbed model to drive the update on small FD sub-grids surrounding regions of change to compute the wavefield in a perturbed model. This can provide a powerful method in for instance waveform inversion applications.

Dynamic Modeling of Earthquake Rupture

Fault Boundary Condition

In many seismological problems an earthquake fault may be represented by a surface embedded in heterogeneous elastic or viscoelastic pre-stressed medium. A non-zero initial equilibrium stress is due to tectonic loading and residual stress after previous earthquakes on the fault. An earthquake itself may be modeled as spontaneous rupture propagation along the fault. The rupture generates seismic waves which then propagate from the fault into the embedding medium. In general, several ruptures can propagate along the fault at one time. Inside the rupture displacement and particle-velocity vectors are discontinuous across the fault. At the same time traction is continuous. Let $\vec{n}(x_i)$ be a unit normal vector to the fault surface pointing from the '-' to '+' side of the surface (Fig. 13), $D\vec{u}(x_i,t) = \vec{u}^+(x_i^+,t) - \vec{u}^-(x_i^-,t)$ slip (discontinuity in displacement vector across the fault), $D\vec{v}(x_i,t) = \vec{v}^+(x_i^+,t) - \vec{v}^-(x_i^-,t)$ slip rate (discontinuity in the particle-velocity vector across the fault), $\vec{T}(\vec{n};x_i,t) = \vec{T}^0(\vec{n};x_i) + \Delta\vec{T}(\vec{n};x_i,t)$ total traction on the fault, $\vec{T}^0(\vec{n};x_i)$ initial traction, and $\Delta\vec{T}(\vec{n};x_i,t)$ traction variation. The latter is due to the rupture propagation. Inside the rupture the total traction is related to slip at the same point through the friction law $\vec{T} = \vec{T}^f(D\vec{u},D\vec{v},\theta)$, where $\vec{T}^f$ is frictional traction and θ represents a set of state variables. Given the initial traction and (visco)elastic material parameters of the fault, it is the friction law which controls initialization, propagation and healing of the rupture.

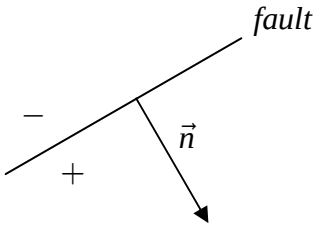

Figure 13. Fault surface and the normal vector $\vec{n}$.

Consider further only shear faulting: there is no opening of the fault and no interpenetrating of the fault materials. Assume a locked fault. If the magnitude of the shear traction is smaller than the frictional strength (product of the normal traction and the friction coefficient) at a point, the fault remains locked and slip rate zero at the point. Should the shear traction exceed the frictional strength, slip occurs. The shear traction decreases over a finite distance from the static down to the dynamic frictional level, following the friction law. The slipping is opposed by the friction.

Let subscripts *sh* and *n* denote the shear and normal components. Let *S* denote frictional strength. The boundary conditions on the fault can be formulated as follows (Day, 1982, 2005; Day et al. 2005).

Shear faulting:

$$D\vec{u}_n = 0, \quad D\vec{v}_n = 0, \quad D\vec{u}_{sh} \neq 0, \quad D\vec{v}_{sh} \neq 0. \tag{154}$$

Shear traction bounded by the frictional strength:

$$\left|\vec{T}_{sh}\right| \leq S \ . \tag{155}$$

Colinearity of the shear traction and slip rate:

$$S\, D\vec{v}_{sh} - \vec{T}_{sh}(\vec{n})\left|D\vec{v}_{sh}\right| = 0 . \tag{156}$$

The fact that the frictional traction opposes the slipping is consistent with the colinearity requirement because we consider vector $\vec{n}$ oriented in the direction from the '-' to '+' side of the fault and slip as the relative motion of the '+' side with respect to the '-' side of the fault: both $\vec{T}(\vec{n})$ and $D\vec{v}$ are viewed from the same side of the fault. If slip was defined as the relative motion of the '-' side with respect to the '+' side of the fault, requirement of the antiparallelism with the '+' sign in eq. (156) would be consistent with the frictional traction opposing the relative motion of the fault faces.

While semi-analytical boundary integral equation (BIE) method is perhaps the most accurate method to account for the fault boundary conditions, especially on non-planar faults (e.g., Aochi and Fukuyama, 2002), its application is limited because it cannot include heterogeneity of the medium. Because the FDM can account for material heterogeneity and is computationally more efficient, it has been extensively applied to study source dynamics particularly on planar faults parallel to grid planes.

The FDM has been applied to the dynamic rupture propagation independently by Andrews (1973, 1976), and Madariaga (1976), and then by many others. Two main

approaches have been developed and applied. In the split-node approach the fault is represented by a grid surface of split (partial) nodes. At a grid point, each of the two partial nodes belongs to only one side of the fault and the two nodes may experience a relative motion (slip) along the fault. In the zone approach the fault is represented by a „thick" zone and slip is evaluated either using inelastic strain or as a difference between displacements at grid points separated by the fault zone. Before we mention other approaches we explain the split-node and zone methods in some detail.

Traction-at-Split-Nodes (TSN) Method

The TSN method has been developed independently by Andrews (1973, 1976, 1999), Day (1977, 1982, 2005); see also Day et al. (2005). Consider a halfspace H^- covered by a FD grid and a grid node $p.n.^-$ on the free surface of the halfspace. Similarly, consider halfspace H^+ and a grid node $p.n.^+$ on its free surface (Fig. 14). Define an outer normal vector $\vec{n}$ to the surface of the halfspace H^- pointing to the halfspace H^+ (i.e., $\vec{n}$ is in the ' $p.n.^- \rightarrow p.n.^+$ ' direction).

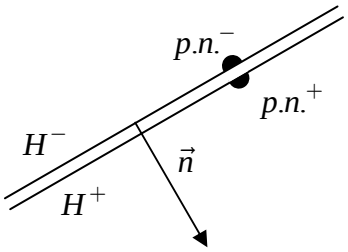

Figure 14. Halfspaces H^- and H^+, partial nodes $p.n.^+$ and $p.n.^-$, and the normal vector $\vec{n}$.

Let M^- and M^+ be masses of the two partial nodes. The partial node $p.n.^-$ is accelerated by a force $\vec{F}^-$ which is due to deformation in the halfspace H^- and, possibly, by body forces acting in the halfspace. Similarly, the partial node $p.n.^+$ is accelerated by a force $\vec{F}^+$. Thus, the accelerations are $\vec{a}^{\pm} = \vec{F}^{\pm} / M^{\pm}$. Couple the halfspaces H^- and H^+ along their surfaces in order to simulate a fault. The coupling can be accomplished by a constraint surface traction acting at the contact. Consider a traction $\vec{T}^c(\vec{n})$ quantifying a contact force with which material in H^+ acts upon material in H^-. Let A be an area of the fault surface associated with each partial node. Then the acceleration $\vec{a}^-$ of the partial node $p.n.^-$ is contributed by the force $\vec{F}^-$ (which is due to deformation in the halfspace H^-) and by the constraint force $\vec{F}^{c,-} = \vec{F}^c = A \cdot \vec{T}^c(\vec{n})$ (which is due to the action of the halfspace H^+): $\vec{a}^- = \left(\vec{F}^- + \vec{F}^{c,-}\right) / M^- = \left(\vec{F}^- + A \cdot \vec{T}^c\right) / M^-$. Similarly, the acceleration $\vec{a}^+$ of the partial node $p.n.^+$ is contributed by the force $\vec{F}^+$ (due to deformation in the halfspace H^+) and by the constraint force $\vec{F}^{c,+} = -\vec{F}^c = -A \cdot \vec{T}^c(\vec{n})$ (due to the action of the halfspace H^-): $\vec{a}^+ = \left(\vec{F}^+ + \vec{F}^{c,+}\right) / M^+ = \left(\vec{F}^+ - A \cdot \vec{T}^c\right) / M^+$. Consider some initial

equilibrium state with traction $\vec{T}^0(\vec{n})$. The traction does not contribute to the acceleration of the partial node $p.n.^-$. If $\vec{T}^c$ is the total traction, only the difference $\vec{T}^c - \vec{T}^0$ contributes to the acceleration. Considering the accelerations at time t,

$$\vec{a}^{\pm}(t) = \left\{ \vec{F}^{\pm}(t) \mp A \cdot \left[\vec{T}^c(t) - \vec{T}^0 \right] \right\} \Big/ M^{\pm}. \tag{157}$$

Though the initial traction is nonzero, the initial strain is considered zero. Then forces $\vec{F}^{\pm}$ correspond to deformations caused only by the dynamic changes due to rupture. The particle velocities and displacements of the partial nodes in the 2nd-order approximation are then

$$\vec{v}^{\pm}(t + dt/2) = \vec{v}^{\pm}(t - dt/2) + dt \left\{ \vec{F}^{\pm}(t) \mp A \cdot \left[\vec{T}^c(t) - \vec{T}^0 \right] \right\} \Big/ M^{\pm} \tag{158}$$

and

$$\vec{u}^{\pm}(t + dt) = \vec{u}^{\pm}(t) + dt \cdot \vec{v}^{\pm}(t + dt/2). \tag{159}$$

For the slip rate we obtain from eq. (158)

$$D\vec{v}(t + dt/2) \doteq D\vec{v}(t - dt/2) + dt\, B \left\{ \frac{M^- \vec{F}^+(t) - M^+ \vec{F}^-(t)}{A \cdot \left(M^- + M^+ \right)} - \left[\vec{T}^c(t) + \vec{T}^0 \right] \right\}, \tag{160}$$

where $B = A\left(M^- + M^+\right) \Big/ \left(M^- M^+\right)$. Find a constraint traction $\vec{T}^c(t) = \vec{T}^{ct}(t)$ that assures zero slip rate before two partial nodes start slipping as well as vanishing slip rate when the slipping ceases. The question is how to time condition $D\vec{v} = 0$. If $D\vec{v}(t) = 0$ is required, the trial traction acts for the interval from $t - dt/2$ to $t + dt/2$ and can reverse the slipping (i.e., produce back-slip) by the time it is integrated all the way up to $t + dt/2$. This results in the traction driving slip rather than opposing it and thus in violating conservation of energy. Therefore, $D\vec{v}(t + dt/2) = 0$ has to be required. Assume $D\vec{v}(t + dt/2) = 0$ in eq. (160) and obtain the trial traction

$$\vec{T}^{ct}(t) \doteq \vec{T}^0 + \frac{dt^{-1} M^- M^+ D\vec{v}(t - dt/2) + M^- \vec{F}^+(t) - M^+ \vec{F}^-(t)}{A \cdot \left(M^- + M^+ \right)}. \tag{161}$$

Find a constraint traction during the slip, that is, frictional traction $\vec{T}^c_{sh}(t) = \vec{T}^f_{sh}(t)$ such that $D\vec{v}(t + dt/2) \neq 0$. Assuming first $D\vec{v}(t + dt/2) \neq 0$ for $\vec{T}^c_{sh}(t) = \vec{T}^f_{sh}(t)$ in eq. (160), and then $D\vec{v}(t + dt/2) = 0$ for $\vec{T}^c(t) = \vec{T}^{ct}(t)$ leads to

$$D\vec{v}_{sh}(t + dt/2) \doteq dt\, B \left[\vec{T}^{ct}_{sh}(t) - \vec{T}^f_{sh}(t) \right]. \tag{162}$$

Recalling the colinearity condition (156)

$$S(t)\, D\vec{v}_{sh}(t) \;-\; \vec{T}^{f}_{sh}(t)\,\big|\, D\vec{v}_{sh}(t)\big| \;=\; 0\,. \tag{163}$$

Using approximation $D\vec{v}_{sh}(t) \;=\; \frac{1}{2}\big[\; D\vec{v}_{sh}(t-dt/2) \;+\; D\vec{v}_{sh}(t+dt/2)\;\big]$ and eq. (162) we obtain from the colinearity (163)

$$\left[\; \big|D\vec{v}_{sh}(t)\big| \;+\; S(t)\frac{dt}{2}\,B\;\right]\vec{T}^{f}_{sh}(t) \doteq \frac{S(t)}{2}\big[\; D\vec{v}_{sh}(t-dt/2) \;+\; dt\; B\,\vec{T}^{ct}_{sh}(t)\;\big]. \tag{164}$$

Define an auxiliary vector $\vec{\gamma}$

$$\vec{\gamma} \;=\; D\vec{v}_{sh}(t-dt/2) \;+\; dt\,B\,\vec{T}^{ct}_{sh}(t)\;. \tag{165}$$

Eqs. (164) and (165) imply that $\vec{T}^{f}_{sh}(t)$ has the direction of the vector $\vec{\Upsilon} \;=\; \vec{\gamma}\big/\big|\vec{\gamma}\big|$. Therefore, enforcing the boundary conditions on the fault can be formulated as follows:

$$\text{If}\quad \big|\vec{T}^{ct}_{sh}(t)\big| \;\le\; S(t)\quad \text{then}\quad \vec{T}^{c}(t) \;=\; \vec{T}^{ct}(t). \tag{166}$$

$$\text{If}\quad \big|\vec{T}^{ct}_{sh}(t)\big| \;>\; S(t)\quad \text{then}\quad \vec{T}^{c}_{sh}(t) \;=\; S(t)\,\vec{\Upsilon}\;,\quad \vec{T}^{c}_{n}(t) \;=\; \vec{T}^{ct}_{n}(t). \tag{167}$$

The above approach, based on finding a trial traction $\vec{T}^{ct}(t)$ ensuring $D\vec{v}(t+dt/2)=0$, and colinearity requirement at time t, can cause in some rare cases large oscillations of rake direction just around the time of rupture arrest (Day 2005). It is possible to avoid this problem by the modification of the colinearity condition (Day 2005):

$$S(t)\, D\vec{v}_{sh}(t+dt/2) \;-\; \vec{T}^{f}_{sh}(t)\,\big|\, D\vec{v}_{sh}(t+dt/2)\big| \;\doteq\; 0\,. \tag{168}$$

Inserting eq. (162) into eq. (168) yields

$$\Big[S(t) \;+\; \big|\;\vec{T}^{ct}_{sh}(t) \;-\; \vec{T}^{f}_{sh}(t)\;\big|\;\Big]\vec{T}^{f}_{sh}(t) \;\doteq\; S(t)\,\vec{T}^{ct}_{sh}(t)\,. \tag{169}$$

Eq. (169) means that $\vec{T}^{f}_{sh}(t)$ has the same direction as $\vec{T}^{ct}(t)$. Then condition (167) is replaced by

$$\text{If}\;\; \big|\vec{T}^{ct}_{sh}(t)\big| \;>\; S(t)\;\; \text{then}\;\; \vec{T}^{c}_{sh}(t) \;=\; S(t)\,\vec{T}^{ct}_{sh}(t)\big/\big|\vec{T}^{ct}_{sh}(t)\big|\;,\;\; \vec{T}^{c}_{n}(t) \;=\; \vec{T}^{ct}_{n}(t). \tag{170}$$

The modified approach behaves always well.

An assumption of the small displacements is necessary for the TSN method. The assumption means that the accumulating slip does not change the configuration of the partial nodes adjacent to each other. This means that $h \gg \big|D\vec{u}_{sh}\big|$, where h is a spatial

grid spacing. Also, a necessary condition is that the time-stepping algorithm is explicit and a force at a node accelerates only that node.

Accuracy of the TSN implementation heavily depends on the accuracy of calculation of the body forces $\vec{F}^{\pm}$ due to deformations in the halfspaces. Formally, at each time the surfaces of the halfspaces are the free surfaces. In fact, both Andrews (1973, 1976, 1999) and Day (1982) used an FD formulation on the partly-staggered grids in which the spatial differencing is equivalent to the finite-element method.

Stress Glut (SG) Method

Andrews (1999) describes the SG method that he used in his 1976 paper (Andrews, 1976). Instead of a surface with an explicit displacement discontinuity in the TSN method, an inelastic zone of a finite thickness is used in the SG method to represent the fault surface. The method can be implemented in the partly-staggered or staggered grid. Consider for simplicity a horizontal zone (perpendicular to the *z*-axis oriented positive downward) centered at a grid plane with grid positions of the stress tensor and bounded in the vertical direction by grid planes with grid positions of the displacement and particle-velocity vectors. The thickness of the fault zone is thus equal to one grid spacing *h*. Assume the velocity-stress formulation. At each time level stresses are updated as if there were no fault zone. Denote shear stress-tensor components located at the central horizontal grid plane as trial values (superscript *t*) and evaluate a magnitude of the shear trial traction vector $\left|\vec{T}_{sh}^{t}\right| = \left[\left(\tau_{zx}^{t}\right)^2 + \left(\tau_{zy}^{t}\right)^2\right]^{1/2}$. If, at a grid point, $\left|\vec{T}_{sh}^{t}\right| \le S$, S being the frictional strength of the fault, then $\tau_{zi} = \tau_{zi}^{t}\ ;\ i \in \{x, y\}$ at that grid point. If $\left|\vec{T}_{sh}^{t}\right| > S$, then, due to the colinearity, $\tau_{zi} = \left(S \Big/ \left|\vec{T}_{sh}^{t}\right|\right)\tau_{zi}^{t}\ ;\ i \in \{x, y\}$. The latter means an inelastic stress adjustment. Assuming that the corresponding inelastic strain is distributed over the fault thickness, the offset in stress, i.e., stress glut, is related to the increment of the seismic moment tensor in the volume of the grid cell:

$$\Delta M_{zi} = \left(\tau_{zi}^{t} - \tau_{zi}\right) \cdot h^3\ ;\ i \in \{x, y\}. \tag{171}$$

At the same time, the increment in the seismic moment tensor can be interpreted under the assumption of a shear slip along the central grid plane of the fault zone. Assuming a a normal vector $\vec{n}(0,0,1)$ and slip rate at a given grid position on the central grid plane $Dv_i = v_i^{+}\left(z^{+}\right) - v_i^{-}\left(z^{-}\right)$,

$$\Delta M_{zi} = \mu\, Dv_i\, h^2\, \Delta t\ ;\ i \in \{x, y\}. \tag{172}$$

Equating eqs. (171) and (172) we obtain for the slip rate

$$Dv_i = \frac{h}{\Delta t}\frac{\tau_{zi}^{t} - \tau_{zi}}{\mu}\ ;\ i \in \{x, y\}. \tag{173}$$

Andrews (1999) discusses computational details as well as the more complicated implementation of the method on the staggered grid.

Thick-Fault-Zone (TFZ) Method

Madariaga et al. (1998) described a velocity-stress staggered-grid method to study dynamic faulting. As in the SG method, no surface with explicit displacement and particle-velocity discontinuity is considered. Instead, an alternative fault zone of the finite thickness is centered at the grid plane with grid positions of the normal stress-tensor components. Considering again, e.g., a horizontal fault zone, frictional boundary conditions are applied on the two nearest grid planes with grid positions of the shear stress-tensor components, i.e., on the grid planes half grid spacing below and above the central grid plane. Because the horizontal displacement components are located on the central grid plane, the slip rate is evaluated as the difference between particle-velocity values at grid planes one grid spacing above and one grid spacing below the central grid plane, that is, over a thickness of two grid spacings. Such a configuration preserves symmetry of stresses and particle velocities about the fault plane. Madariaga et al. (1998) apply standard 4^{th}-order FD formulae to calculate spatial derivatives at all grid positions.

Comparison of the TSN, SG and TFZ Methods

Dalguer and Day (2004, 2006) performed an extensive numerical comparison of the three methods. Calculations were performed with the 2^{nd}-order TSN and 4^{th}-order staggered-grid SG and TFZ formulations using the same grid spacing h and uniform grid. The rupture propagation velocity in the fault-zone model is lower than that in the split model – likely due to the blunting of the stress concentration on the rupture front in the fault-zone models. The TSN solution converges substantially better than the SG solution, and far better than the TFZ solution. The SG method reaches convergence with a grid spacing $h/2$, while grid spacing smaller than $h/4$ is necessary for the TFZ method. Dalguer and Day therefore tested modified grid configurations for the SG and TFZ methods. With the fault thickness reduced to $0.75h$ in the SG and $0.5h$ in the TFZ modeling, the rupture velocities approach that in the TSN modeling. At the same time, the behaviors of both fault zones depend on the ratio between h and the fault thickness which has to be adjusted ad hoc. In any case, the theoretical efficiency of the 4^{th}-order fault-zone formulations is lost if sufficiently accurate results are to be obtained.

Alternative Approaches

An interesting approach was presented by Ionescu and Campillo (1999) who studied the 2D problem of slip instability under slip-dependent friction. They used a combination of two space-time FD grids. An interior (or body) grid is used to solve the equation of motion away from the fault. The other grid is used to implement frictional boundary conditions on the fault. The first-order hyperbolic system (velocity-stress formulation) is reduced on the fault to a first-order system in one space variable (orthogonal to the fault) for the shear velocity and shear stress-tensor components. Using the integration on the characteristic lines and frictional boundary conditions a nonlinear unstable ordinary differential equation for slip is obtained. The equation depends on the computed values of the stresses and particle velocities away from the fault. A small

local time step is used to solve the equation during the larger time step applied in the body grid.

Nielsen modified a standard application of the 4th-order staggered-grid FD scheme to investigate rupture propagation (e.g., Nielsen et al. 2000, Nielsen and Carlsson 2000). In order to satisfy the frictional boundary conditions with a slip rate and tractions evaluated at the same time, he approximates a field variable at a given time using a 2nd-order interpolation between their values at consecutive time levels. Thus he reformulates the velocity-stress formulation of the equation of motion and Hooke's law with the same time-derivative operator applied to the particle-velocity and stress-tensor components. In addition to this, Nielsen avoids application of the spatial-derivative operator across the fault if the operator should apply to a discontinuous field. He achieves this by reducing the spatial-derivative operator down to the 2nd-order in evaluating shear stress-tensor components at a grid point on the grid planes one grid spacing above and one grid spacing below the fault, if the grid point one grid spacing away is slipping.

Modeling of Non-planar Faults Using Partly-staggered Grids

Cruz-Atienza and Virieux (2004) developed a new FD approach to model the dynamic rupture propagation on non-planar faults. They used a 2D velocity-stress formulation on a partly staggered grid. Their formulation is based on a new application of the fault boundary conditions. No split nodes are considered, that is, there is no explicit discontinuity at any grid point. A finite source, rupturing fault, is represented by a set of neighboring numerical cells placed alongside a fault without sharing any stress grid point. Because this is the first FD approach enabling both medium heterogeneity and non-planar fault geometry, we describe its essential features in some detail.

Consider a Cartesian coordinate system and a corresponding spatial rectangular grid. A square $h \times h$ FD grid cell has particle-velocity vector positions at four corners and stress-tensor position at the center. Then one *n*-point square numerical cell is a set of $\sqrt{n} \times \sqrt{n}$ neighboring square FD cells. This means that one *n*-point square numerical cell has *n* stress-tensor grid positions (points). Considering a fixed spatial support *S* (square area), the scaling relation for a numerical cell is $S = n \cdot h_n^2$, where *n* is the number of FD square $h_n \times h_n$ grid cells making one *n*-point numerical cell. The greater *n* the smoother the fault-geometry discretization is.

Boundary conditions on the fault are applied locally in each numerical cell. The application means the following. A planar fault tangential to the discretized fault geometry is considered inside the cell. Let ϑ be an angle between the *x*-axis and the fault plane. The Cartesian stress-tensor components at a stress grid point are rotated into shear and normal stresses with respect to the fault plane. The same boundary condition, following a considered friction law, is applied at each stress grid point within the numerical cell. After imposing the boundary condition, the stresses are rotated back to the original coordinate system connected with the grid.

The fault plane always passes through the center of the numerical cell. Velocity grid points in a numerical cell belong to either positive or negative fault block. At a velocity grid point *I*, displacement u_I parallel to the fault plane is obtained from the projected particle velocity by simple time integration. Because no split nodes are considered, displacement u_I depends on a distance between the point and the fault. For any time *t*,

u_I will be at its maximum, if the point lies on a line passing through the center of the cell and perpendicular to the fault. It will be zero, if the grid point lies on the fault. For a given ϑ, it may happen that no velocity grid point lies on a line passing through the center of the cell and perpendicular to the fault. A weight function $H_I(\vartheta)$ for a grid point *I* is defined as a ratio between the maximum displacement and displacement, that is, $H_I(\vartheta) = \max_{\vartheta}\{u_I(t,\vartheta)\}/u_I(t,\vartheta)$. $H_I(\vartheta)$ does not depend on time and has to be determined for all grid points in a given type of a numerical cell. Then the weighted displacements $\tilde{u}_I(t) = u_I(t,\vartheta)\cdot H_I(\vartheta)$ do not depend on the fault orientation in the spatial grid. The relative displacement of the, for example, positive fault block, D^+ is then determined as $D^+ = \left(\sum_{I=1}^{p}\tilde{u}_I^2(t)\right)^{1/2} \Big/ p$, where *p* is the number of the velocity grid points. Points within an angular vicinity γ around the fault (two opposed sectors of a circle centered at the cell's center) are not considered because their displacements are too small. The angle is determined as $\gamma = \arctan\left(\sqrt{n}-1\right)$.

Cruz-Atienza and Virieux (2004) found that the zigzag discrete shape of the fault associated with a low number *n* of grid points leads to unwanted destructive dynamic interaction of cells. At the same time, as the grid spacing is smaller, the dynamic interaction is stronger. As a consequence, in order to increase numerical resolution, it is necessary both to reduce grid spacing and enlarge *n*. To guarantee the low-frequency equivalence between different discretizations of a fault length *L*, the scaling relationship $L \geq 30h_n\sqrt{n}$ has to be followed.

Nonreflecting Boundaries

Absorbing Boundary Conditions

For computational reasons it is almost always necessary to limit the computational domain to the part of the Earth in the vicinity of the seismic source and receivers as well as the Earth structure contributing to form the seismic response. This is achieved by applying so-called non-reflecting boundaries or absorbing boundary conditions (ABC) around the tractable truncated computational domain such that no energy is transmitted or reflected from the boundary of the computational domain back into its interior. Thus from the perspective of an observer located inside the computational domain the signals appear to have been perfectly absorbed by the boundary.

A significant proportion of the literature on time-domain FD modeling is devoted to the design of efficient ABC but most published approaches can be divided into two groups. The first group, including the popular Clayton-Engquist (1977), Higdon (1991), Lindman (1975) and Liao et al. (1984), attempt to extrapolate the wavefield beyond the edge of the computational domain and then use this extrapolated value in the spatial discretization operator used to update locations inside the computational domain. An interesting approach was suggested by Peng and Toksöz (1994, 1995).

Collino (1993) and later other authors attempted to apply so-called high-order ABCs which, in general, is an infinite sequence of ABCs with increasing accuracy. An advantage of the high-order ABCs is that they are implementable for an arbitrary high order (Givoli, 2004).

The second group, including the approach of Kosloff and Kosloff (1986) and Perfectly Match Layers (PML; Bérenger, 1994), gradually attenuate the amplitude of the wavefield within a "sponge" layer within the boundary.

For completeness, we should also mention work on complementary boundary conditions and operators (Smith, 1974; Schneider and Ramahi, 1998), which does not fit within either of the two groups. Dirichlet and Neumann boundary conditions are complementary as they have opposite reflection coefficients. By adding the response from two simulations with different complementary boundary conditions, the first-order boundary reflections will destructively interfere. Unfortunately, higher-order interactions will not necessarily cancel and the methods have therefore not found widespread application.

Each ABC approach has it own characteristics, advantages and disadvantages. In the first group mentioned above, for example, the Clayton-Engquist and Higdon methods have the advantage of requiring relatively little memory but only work well within a limited range of angles of incidence. Lindman's approach works well over a wide range of angles but only works when the material along the boundary is homogeneous. Liao's ABC works well over most angles and for some types of heterogeneity adjacent to the boundary but requires double precision implementation to maintain stability. It also requires more computer memory than the other methods listed above.

In the second group of ABCs, Kosloff's method (Kosloff and Kosloff, 1986) amounts to applying an exponential damping function of the wavefield within a “sponge” region surrounding the computational domain. Kosloff's method is effective at normal incidence and is very easy to implement but requires a relatively large amount of memory and can generate significant reflection artifacts away from normal incidence. A related method known as perfectly matched layers (PML) was first introduced for electromagnetic wave propagation by Bérenger (1994), and later

generalized for elastic wave propagation by Chew and Liu (1996), Collino and Tsogka (1998, 2001), Komatitsch and Tromp (2003), Marcinkovich and Olsen (2003), Festa and Nielsen (2003), and for viscoelastic anisotropic media by Chen et al. (2000). PML's have now become established as the most efficient absorbing boundary condition available, offering simplicity of implementation, stability, good absorption over a wide range of incident angles and frequencies and less memory requirements than Kosloff 's ABC. In this section we will therefore focus on PML's, review the theory and discuss issues related to their implementation.

The Perfectly Matched Layer (PML)

Following Chen et al. (2000), we define the split particle velocities $v_i^{(\gamma)}$ such that the equation of motion in a general heterogeneous anisotropic elastic medium is decomposed into three equations

$$\rho \dot{v}_i^{(\gamma)} = \sigma_{i\gamma,\gamma} \tag{174}$$

with

$$v_i = \sum_{\gamma=1}^{3} v_i^{(\gamma)} \tag{175}$$

where the Einstein summation convention is not assumed for the Greek letter γ. Similarly, the constitutive equation for the split stiffness tensors may be written as

$$\dot{\sigma}_{ij}^{(\gamma)} = c_{ij\gamma q} v_{q,\gamma} \tag{176}$$

with

$$\sigma_{ij} = \sum_{\gamma=1}^{3} \sigma_{ij}^{(\gamma)} . \tag{177}$$

Following Chew and Liu (1996), we introduce a modified spatial differencing operator

$$\tilde{\partial}_\gamma = \frac{1}{e_\gamma} \partial_\gamma , \tag{178}$$

where the denominator e_γ has been interpreted as a coordinate stretching variable. Outside the PML layers, vector $\vec{e} = (1,1,1)$. Inside the PML layers, a complex e_γ is needed in order to attenuate the split $\left(v^{(\gamma)}, \sigma^{(\gamma)}\right)$ in the γ direction. Assuming a time dependence of $e^{-i\omega t}$ we choose

$$e_\gamma = a_\gamma + \frac{i\Omega_\gamma}{\omega} \tag{179}$$

where a_γ and Ω_γ are the so-called PML medium profiles. In the time domain, this leads to the following equations for the partial variables:

$$\rho\left(a_\gamma \partial_t + \Omega_\gamma\right) v_i^{(\gamma)} = \partial_\gamma \sigma_{i\gamma} \tag{180}$$

and

$$\left(a_\gamma \partial_t + \Omega_\gamma\right) \sigma_{ij}^{(\gamma)} = c_{ij\gamma q}\, \partial_\gamma v_q \ . \tag{181}$$

The selection of the PML material profile a_γ and Ω_γ is key to the effective implementation of the PML ABC. Theoretically, these parameters can be arbitrary in the continuum space and the PML layers would perfectly absorb any incident wave. This is, however, not true in the discretized model. The discretization error is proportional to the product of the spatial discretization size and the contrast of these parameters (Chew and Weedon, 1994; Chew and Liu, 1996). A PML sponge of width $N = 10$ with the following profile at each layer $i = 1, 2, ..., N$ has been found to result in excellent absorption for many seismic applications for a wide range of frequencies, Courant numbers and wave types (Chen et al., 2000):

$$a_\gamma(i) = 1 + \frac{1}{2} a_{\max}\left(1 + \sin\left(\frac{N/2 - i + 1}{N}\pi\right)\right)^{2.8} \tag{182}$$

and

$$\Omega_\gamma(i) = \frac{1}{2}\Omega_{\max}\left(1 + \sin\left(\frac{N/2 - i + 1}{N}\pi\right)\right)^{2.8} \tag{183}$$

with $a_{\max} = 0.075$ and $\Omega_{\max} = 0.91/\Delta t$.

We note that the PML ABC differs fundamentally from the traditional material sponge ABCs such as the method by Kosloff and Kosloff (1986) as a result of the split wavefield formulation. For each set of split wavefields, only the propagation vector component normal to the boundary is complex. The propagation vector components parallel to the boundary remain the same across the boundary layers. As a result, a perfect match can be obtained while the wavefields are attenuated by the perfectly matched layers, at least in theory in the non-discretized model.

Finally, the extension of PML's to viscoelastic media is straightforward (Chen et al., 2000). The memory variables governing the viscoleastic behavior of the medium due to propagating waves are updated from the change in stress and record the history of the stress. The memory variables in the PML region are therefore split in exactly the same way as the stresses. The equation for updating the split stress fields becomes, see eq. (111),

$$\left(a_\gamma \partial_t + \Omega_\gamma\right) \sigma_{ij}^{(\gamma)} = c_{ij\gamma q}\, \tilde{\partial}_\gamma v_q + \sum_{l=1}^{n} r_l^{ij(\gamma)} \tag{184}$$

and the equation for updating the split memory variable fields is, see eq. (113),

$$\dot{r}_l^{\,ij(\gamma)}(t) + \frac{1}{\tau_{\sigma l}} r_l^{\,ij(\gamma)}(t) = \frac{1}{\tau_{\sigma l}}\left(1-\frac{\tau_{\varepsilon l}}{\tau_{\sigma l}}\right)\left[c_{ij\gamma q}\right]_R \tilde{\partial}_\gamma v_q \quad , \quad l=1,...,n \ , \quad (185)$$

where $\left[c_{ij\gamma q}\right]_R$ means relaxed moduli. The equations for updating the particle velocities in split form remain the same, eq. (180).

PML Reflection Coefficients

In Fig. 15 we show reflection and conversion coefficients for incident P- and S-waves. The curves were obtained from 2D simulations in a homogeneous isotropic elastic medium with a P-velocity of 2500 m/s, an S-velocity of 1500 m/s and a density of 1100 kg/m^3 where a point source was positioned close to the PML boundary (Chen et al., 2000). For incident P-waves the source was explosive, for S-waves the source was a force oriented normal to the PML boundary. In each case the source was a 50 Hz Ricker wavelet. The reflections were corrected for propagation distance and radiation pattern to obtain reflection and conversion coefficients.

Simulations were carried out for PML boundary thicknesses of 10, 20, 30, 40 and 50 cells, and compared to a 40 cell thick Kosloff ABC (shown in the dashed lines). First, the results show that the choice of a 10 grid-point wide PML boundary is roughly as efficient as the 40 grid-point wide boundary (justifying the values we used for cost comparisons in the previous section). However, the poor performance at low grazing angles may not be acceptable for many applications. Increasing the thickness of the PML boundaries drastically improves the effectiveness so that we are close to single-precision machine accuracy for the 50 grid-point wide boundaries. The PS-plot (top right of Fig. 15) reveals very little P-to-S conversion. Machine precision is achieved with a 20 cell thick PML.

The SS-reflection coefficient (bottom left in Fig. 15) shows a behavior similar to the PP-results. The SP-plot (bottom right in Fig. 15) does not show the same remarkable performance as the PS-converted wave reflection although the performance is still satisfactory. It is possible that the SS-and SP-results could be degraded by P-wave energy generated by the source used.

Fig. 16 shows the corresponding results for an anisotropic model with the same density and vertical velocities as the isotropic model but with a vertical to horizontal P-velocity ratio of 1.12 and an anellipticity of 0.16 as defined by Carrio et al. (1992). The results do not differ significantly from the ones shown in Fig. 15 for the isotropic case.

PML Implementation Issues and Computational Cost

In general eq. (180) is a system of nine equations: three partial, or split, velocities for each velocity component. The split elastic constitutive relation (181) is in general a system of eighteen equations: three partial stresses for each of six independent elements in the stress tensor. For the viscoelastic case, eq. (181) translates into eqs. (184) and (185) which, in general, are systems of eighteen equations. If all of these variables were required on the complete 3D FD grid, the resulting memory requirements would make this approach unattractive. However, because updating split field variables require only derivative of the full velocities and stresses, the domain in which the split field

variables are defined (and stored) is restricted to a relatively narrow region around the boundaries.

The PML formulation presented here requires almost the same number of calculations per grid point as the interior of the computational domain since most of the calculation required for updating each split field is nothing but a constituent of the conventional time-domain FD calculation which must be evaluated in any case (e.g., the spatial derivatives). However, because of the splitting of variables, there is a significant price to pay in storage per grid point (approximately a factor three depending on dimension, model properties, and other factors). Nevertheless, with a 10 grid-points wide PML sponge the PML conditions are still computationally significantly more efficient both in terms of CPU and memory compared to other ABC (Chen et al., 2000).

Recently Wang and Tang (2003) proposed an alternative PML implementation which avoids splitting the wavefields. The storage requirements per grid point are therefore equivalent to those in the interior of the grid. However, the CPU requirements increase to solve for a new set of differential equations with similar characteristics to the viscoelastic equations presented above.

We note that it is straightforward to interface PML boundary conditions with a free-surface condition.

As we have seen, despite what the name might suggest, PML's are still far from perfect. Because of inaccuracy related to discrete numerical implementations of PML's, a finite sponge width is required to avoid artificial reflections. The cost in terms of memory is therefore not insignificant, particularly for hybrid-modeling scenarios or grids that are narrow in one direction (e.g., cross-line), when the size of the absorbing boundary regions actually may be comparable to the size of the computational domain of interest. Moreover, if energy is incident under very low grazing angles, the PML's will cause significant reflections. The search for a truly perfect absorbing boundary condition is therefore likely to continue as demands for absorbing boundary conditions that are effective in small (deformed) time-domain FD grids and extreme low angles of incidence is increasing with the interest in 3D applications and hybrid modeling scenarios on the rise. One could then imagine solving the wave equation in 3D on grids that were only one or a few grid-points wide in the cross-line direction, at a cost that would be comparable to that of a 2D simulation. This would enable synthesizing seismic data with true 3D amplitudes such that multiples, surface waves, guided waves and body waves all had the correct relative phases and amplitudes.

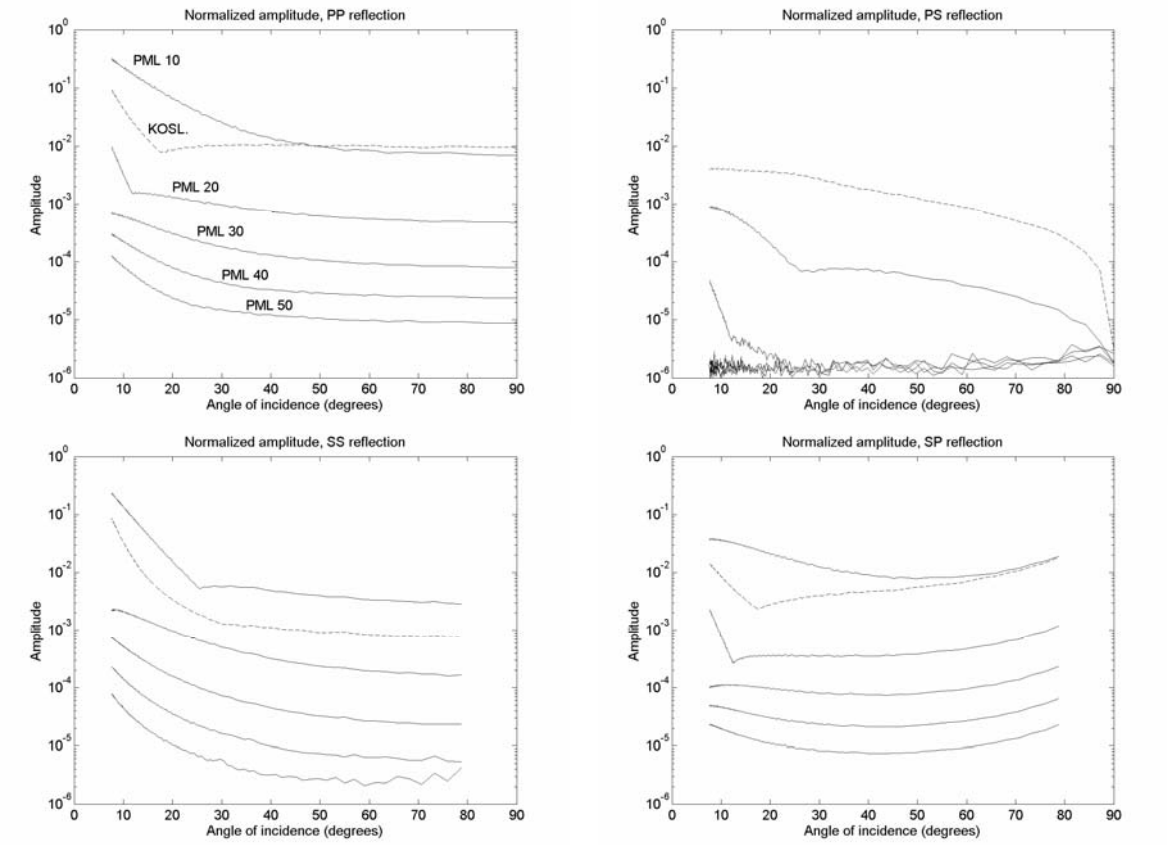

Figure 15: Amplitude reflection coefficient as a function of incidence angle for PML boundaries of width 10, 20, 30, 40 and 50 grid-points (solid) as well as for a 40 grid-points wide Kosloff sponge (dashed). Isotropic model. Top left: Normalized PP reflection. Top right: Normalized PS reflection. Bottom left: Normalized SS reflection. Bottom right: Normalized SP reflection. Reproduced from Chen et al. (2000).

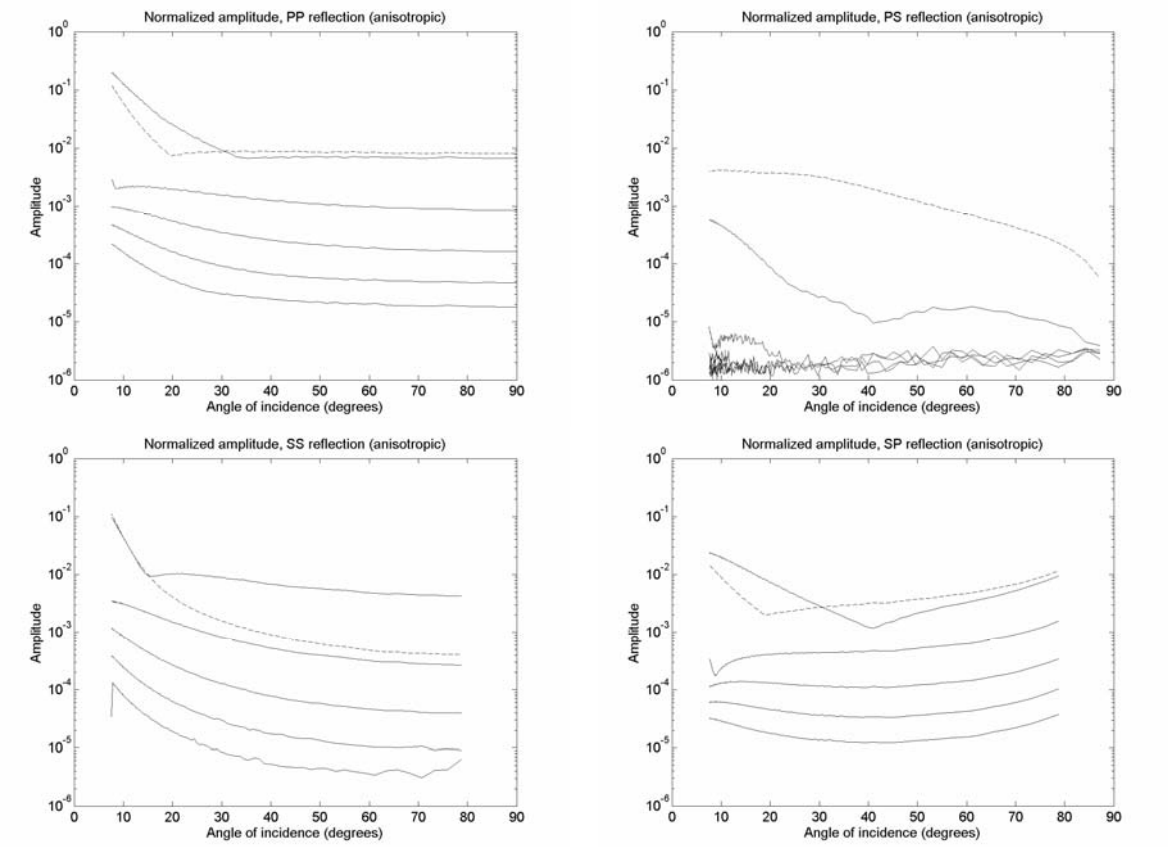

Figure 16: Same as Figure 15 but for an anisotropic model. Reproduced from Chen et al. (2000).

Memory Optimization and Parallelization

Memory Optimization

Memory Requirements in the Staggered-grid Schemes

Many examples of FD modeling of earthquake motion in large sedimentary basins or seismic wave propagation in complex models in seismic exploration require very large computer memory and CPU. In order to solve the most challenging problems of seismology, it is necessary to reduce both memory and CPU requirements. Thus, memory optimization, sophisticated programming and parallelization are practically necessary. Here we briefly review several possibilities to reduce memory requirements and the number of operations. We also briefly mention parallelization.

Consider staggered-grid FD schemes. Assume that the material parameters of the medium can vary between any two grid positions. Such heterogeneity can be referred to as the point-to-point heterogeneity. Though it is sometimes an improper simplification, a homogeneous medium inside a grid cell is assumed by some modellers. Such material parameterization can be referred to as homogeneous material cells.

Denote the displacement and particle-velocity components at time level m as U^m, V^m, W^m, and $\dot{U}^m$, $\dot{V}^m$, $\dot{W}^m$, respectively. In the case of the point-to-point heterogeneity, each grid position of the displacement or particle-velocity components is assigned its value of density, that is, there are ρ^U, ρ^V and ρ^W assigned to a grid cell. Similarly, the elastic (unrelaxed) moduli μ^{xy}, μ^{yz} and μ^{zx} are assigned to grid positions of the shear stress-tensor components, while κ and μ are assigned to the joint grid position of the normal stress-tensor components. Corresponding to the elastic moduli, the anelastic coefficients Y_l^{κ}, Y_l^{μ}, $Y_l^{\mu xy}$, $Y_l^{\mu yz}$ and $Y_l^{\mu zx}$; $l=1,...,n$, are assigned to the grid positions of the stress-tensor components.

An assumption of homogeneous material cells reduces the material parameters in a grid cell to $\rho, \kappa, \mu, Y_l^{\kappa}$ and Y_l^{μ}; $l=1,...,n$. Consider displacement-stress (DS), displacement-velocity-stress (DVS) and velocity-stress (VS) staggered-grid FD schemes (for the equations and simplified schemes see, e.g., Moczo et al., 2001) which are 2nd-order accurate in time. The three schemes require the following variables to be stored in primary memory for a grid cell:

$$\text{DS:}\quad U^m, V^m, W^m, U^{m-1}, V^{m-1}, W^{m-1} \tag{186}$$

$$\text{DVS:}\quad U^m, V^m, W^m, \dot{U}^{m-1/2}, \dot{V}^{m-1/2}, \dot{W}^{m-1/2} \tag{187}$$

$$\text{VS:}\quad \dot{U}^{m-1/2}, \dot{V}^{m-1/2}, \dot{W}^{m-1/2}, T_{xx}^{m-1}, T_{yy}^{m-1}, T_{zz}^{m-1}, T_{xy}^{m-1}, T_{yz}^{m-1}, T_{zx}^{m-1} \tag{188}$$

As discussed in the section on incorporation of the realistic attenuation, the coarse spatial sampling of the anelastic functions (memory variables) can be considered. In the spatial distribution used by Kristek and Moczo (2003), $n=4$ and each grid cell accommodates all six anelastic functions for just one of the relaxation frequencies, that is $\xi_l^{xx}, \xi_l^{yy}, \xi_l^{zz}, \xi_l^{xy}, \xi_l^{yz}$ and ξ_l^{zx}; $l \in \{1,2,3,4\}$.

Consider a computational region with dimensions *XL*, *YL* and *ZL*. Let $\beta_{\min}$ and $\alpha_{\max}$ be the minimum S-wave and maximum P-wave velocity, respectively. Let f_{ac} be the frequency up to which the FD computation should be sufficiently accurate. The maximum spatial grid spacing is the $h = (\beta_{\min} / f_{ac}) \cdot s$. Here, *s* is the spatial sampling ratio $s = h/\lambda_{\min}$ which has to be chosen based on the grid dispersion in the considered FD scheme and the wave propagation distance. The time step is $\Delta t = q \cdot p \cdot (h/\alpha)_{\min}$; $0 < p \le 1$, where *p* is the stability ratio and *q* depends on the FD scheme. For example, for the 2nd-order in time, 4th-order in space staggered-grid, $q = 6/(7\sqrt{3})$; see, e.g. Moczo et al. (2000).

Assuming a uniform grid with the grid spacing *h* in the three Cartesian directions, the numbers of the grid cells in the three directions are $MX = (XL/h)+1,\ MY = (YL/h)+1,\ MZ = (ZL/h)+1$.

In summary, the number of material parameters and field variables in the staggered-grid FD schemes are:

$$\text{DS, DVS:} \quad MX \cdot MY \cdot MZ \cdot [(3+5+5\cdot 4)+(6+6)] = MX \cdot MY \cdot MZ \cdot 40 \qquad (189)$$

and

$$\text{VS:} \quad MX \cdot MY \cdot MZ \cdot [(3+5+5\cdot 4)+(9+6)] = MX \cdot MY \cdot MZ \cdot 43 \qquad (190)$$

Here, $(3+5+5\cdot 4)$ stands for 3 densities, 5 unrelaxed moduli and $5\cdot 4$ anelastic coefficients, while $(6+6)$ for 6 displacement/particle-velocity components and 6 anelastic functions in one grid cell. In the VS scheme, $(9+6)$ stand 3 for particle-velocity components, 6 stress-tensor components and 6 anelastic functions. If the anelastic coefficients are spatially distributed in the same manner as the anelastic functions, $5\cdot 4$ is replaced by 5 in formulae (189) and (190). In the case of the homogeneous grid cells, $3+5+5\cdot 4$ is replaced by $1+2+2\cdot 4$.

Clearly, depending on the total number of the grid cells, $MX \cdot MY \cdot MZ$, the memory requirements can be very large.

The total number of the grid cells and thus the memory requirements can be reduced by using a higher-order approximation in space (for example, Dablain 1986), grid with varying size of the grid spacing or discontinuous grid. The 4th-order staggered-grid schemes were introduced by Bayliss et al. (1986) and Levander (1988). In recent FD modeling, the 4th-order accuracy in space is almost necessary. Yomogida and Etgen (1993) and Rodrigues (1993) used the 8th-order displacement-stress schemes. The rectangular grid with a varying size of the grid spacings was first used by Boore (1970) in the 1D problem. Mikumo and Miyatake (1987) applied the varying size of the grid spacing in the 3D case in a homogeneous medium. Moczo (1989) applied the grid with the varying size of the grid spacing to the 2D SH problem in the laterally heterogeneous medium, Pitarka (1999) presented the 3D velocity-stress scheme. Jastram and Behle (1992), Jastram and Tessmer (1994), Falk et al. (1996), Moczo et al. (1996), Kristek et al. (1999), Aoi and Fujiwara (1999), Hayashi et al. (2001), and Wang et al. (2001) introduced discontinuous grids.

Given some spatial grid, the core memory can be reduced using core memory optimization. While simple variants were used before, Graves (1996) described an

optimized procedure. Moczo et al. (1999) presented a combined memory optimization which naturally combines core and disk memory optimizations. One other possibility to reduce the core memory is the use of the material cell types (e.g., Moczo et al., 2001). Here we briefly characterize the corresponding reductions.

Material Cell Types

In most models it is possible to efficiently describe heterogeneity of the medium by a spatial distribution of integer numbers (a look-up table). In this fashion each grid cell is assigned an integer number which represents a type of a material grid cell, that is, a set of material parameters characterizing the medium inside the grid cell. Such a description is efficient if there are sub-volumes of the computational model that can be covered by many grid cells of the same material type. Let K be the total number of different material types necessary to characterize heterogeneity of the whole model. Then the number of the material parameters and variables needed by the schemes is reduced to

$$\text{DS, DVS:} \quad MX \cdot MY \cdot MZ \cdot (6+6+1) \; + \; (3+5+5 \cdot 4) \cdot K \tag{191}$$

and

$$\text{VS:} \quad MX \cdot MY \cdot MZ \cdot (9+6+1) \; + \; (3+5+5 \cdot 4) \cdot K \tag{192}$$

assuming that $K < MX \cdot MY \cdot MZ$ which is the case even in relatively complex models. The number one added to the numbers of the field variables represents the distribution of the integers corresponding to the material cell types. In the case of the coarsely distributed anelastic coefficients or homogeneous material grid cells, the same reductions as in formulae (189) and (190) apply.

Core Memory Optimization

In core memory optimization method (Graves, 1996) such that only limited number of grid planes are kept in core memory all possible time updates for these planes are carried out. The subset of planes, say, *NP* planes, repeatedly moves throughout the whole model space, and the displacement or particle-velocity components, stress-tensor components and anelastic functions are successively (plane by plane) and periodically overwritten in disk. The key aspect in that all possible time updates are performed for the planes in the core memory means that the procedure is split into three parts – roll-in, cascade, and roll-out. Consider, for example, that the subset is made of horizontal grid planes. Then in the formulae (191) and (192) *MZ* is replaced by *NP*. The smaller the *NP*, the larger the reduction is.

Combined Memory Optimization

It is obvious that whereas the requirement for core memory can be significantly reduced, the needed amount of disk space can become very large. Although available disk space becomes larger and access to disk memory becomes faster, still, in principle it is possible to reduce also the disk memory needed in the core-memory-optimization

procedure. In the disk memory optimization (Moczo et al., 1999), the wavelet transform is applied first to 2D array of each displacement or particle-velocity component and each anelastic function. The transform decreases the information entropy. Then the sets of the wavelet coefficients are compressed by a standard compression procedure. Thus, for example, instead of the $MX \cdot MY$ displacement-component values in one grid plane only a relatively short stream of zeros and ones has to be written in disk. The total number of the material parameters and field variables stored in disk is then

$$\text{DS, DVS:} \quad MX \cdot MY \cdot MZ \cdot \left[(6+6)/CR + 1\right] + (3+5+5\cdot 4)\cdot K \tag{193}$$

and

$$\text{VS:} \quad MX \cdot MY \cdot MZ \cdot \left[(9+6)/CR + 1\right] + (3+5+5\cdot 4)\cdot K \tag{194}$$

where *CR* is the compression ratio. A reasonable value is about 10. Moczo et al. (1999) found that the increase of the CPU time due to one passage of the subset of planes with compression was always smaller than 0.75% of the time for one passage without compression. This is because the increase due to compression itself is partly compensated by the smaller number of the I/O operations.

Spatial Discontinuous Grid

In many models the S and P wave velocities are lower near the Earth's surface. In such a case it is advantageous to cover the lower part with a coarser spatial grid. Due to the structure of the staggered grid, the most natural combined (discontinuous) grid is the one whose upper part is the $h \times h \times h$ grid and the lower part the $3h \times 3h \times 3h$ grid (Aoi and Fujiwara, 1999; Kristek et al., 1999, Robertsson and Holliger, 1997). Let *MZH* be the number of the grid cells in the *z*-direction in the upper grid. Let *MZ3H* be the number of the grid cells in the *z*-direction in the lower grid. Assuming only the material cell types, the number of material parameters and variables needed by the schemes is

DS, DVS:

$$\left[MX \cdot MY \cdot MZH + \left(\frac{MX-1}{3}+1\right)\cdot\left(\frac{MY-1}{3}+1\right)\cdot MZ3H\right] \cdot\left[6+6+1 + (3+5+5\cdot 4)\cdot K\right] \tag{195}$$

and

VS:

$$\left[MX \cdot MY \cdot MZH + \left(\frac{MX-1}{3}+1\right)\cdot\left(\frac{MY-1}{3}+1\right)\cdot MZ3H\right] \cdot\left[9+6+1 + (3+5+5\cdot 4)\cdot K\right] \tag{196}$$

Formulae (195) and (196) are easy to modify if the core or combined memory optimization are applied.

A combination of the material cell types, combined memory optimization and discontinuous grid typically can reduce the memory requirements by more than one order of magnitude. An example is given by Moczo et al. (2001) for the modeling of the 1995 Kobe, Japan earthquake.

Spatially Varying Time Step

Falk et al. (1998) and Tessmer (2000) introduced a combined grid in which a smaller time step is applied to the upper part of the grid while a larger time step is applied to the lower part. Their techniques considerably reduce CPU cost.

Discontinuous Space-Time Grids

Kang and Baag (2004a, b) developed efficient techniques for 2D and 3D 4^{th}-order staggered-grid modeling. They combined discontinuous grid in space with a discontinuous time step. While time integration in a finer grid with grid spacing h is performed with time step Δt, time integration in a coarser grid with grid spacing $3h$ is performed with time step $3\Delta t$. The finer grid covers 2D or 3D rectangular subregion which may have a planar free surface. This enables efficient modeling of localized surface sedimentary structures. Proportionality of the time step to the grid spacing is due to the fact that the two spatial grids have to overlap in the medium with a higher speed. The technique considerably reduces both the number of grid points and the number of operations.

Parallelization

Because the FD operators are local, the FD algorithms are suitable for parallelization. Over the past decade, several distinct approaches have been applied to parallelize FD codes.

Message Passing Libraries

Message-passing libraries, such as the Message Passing Interface (MPI, Gropp et al. 1994), represent an approach suitable for shared or distributed memory architectures. The MPI typically requires the involvement of the sender-receiver communication: the source process makes a call to send data and the destination process makes a call to receive it. While the scaling of the MPI parallelized codes can be very good, the preparation of the code can require considerable time and effort. The resulting MPI parallelized code often differs substantially from the original source code.

Parallelizing Compilers

Some compilers are capable of producing a parallel code that is portable to shared and distributed memory machines. The compiler analyzes the inside-code dependences and can produce a parallelized code with or without additional user's directives and/or language extensions. The High-performance Fortran language (HPF, Koelbel et al.,

1994) is one of the best known examples. In some cases the resulting parallel code is quite efficient (e.g., Caserta et al., 2002) but deficiencies of the approach are also known. In an automatic parallelization regime, compilers often make conservative assumptions on data dependence, which usually yields lower efficiency.

Interactive Parallelization Tools

There are parallelization tools which provide a user with the possibility of combining the automatic parallelization analysis with user's knowledge of the code. Whereas such interactive tools usually lead to quick parallelization, the efficiency can be limited due to non-optimized nesting, multiple decompositions and Fortran 90 constructs. Often additional manual modifications of the source code are necessary to obtain good performance.

High-level Library-based Tools

Library-based tools exist which are designed to help the user with the application of the lower-level libraries, such as MPI. Particularly, a user does not need to handle all details of the MPI parallelization. Some tools enable the use of additional optimizations specific for the machine architecture. The preparation of the parallel code may still be very time consuming and invasive.

Directive-based Parallelization

Some computer manufacturers, for example Cray and SGI, introduced the possibility to manually supplement parallelization directives in the source code. In the beginning, the directives were mainly used to support loop-level shared memory parallelization. Recently SGI's OpenMP has become the best known and standard tool for relatively efficient and quick parallelization. One problem is that the OpenMP is most efficient only with shared-memory architectures.

Acknowledgments

The authors would like to thank Y. H. Chen, L. A. Dalguer, S. M. Day, R. T. Coates, M. Gális, R. J. Geller, I. Ionescu, J. Kristek, V. Maupin, S. Nielsen, and J. Virieux for useful discussions and comments on selected topics. Thanks go also to D. Lafleur and W. Kimman for misprint corrections. The work was supported in part also by the Geophysical Institute, Slovak Academy of Sciences.

References

Aki, K. and P. G. Richards, 1980. Quantitative Seismology. Theory and Methods, Vol. I and II. *W. H. Freeman & Co.*, *San Francisco*.

Alekseev, A. S. and B. G. Mikhailenko, 1980. The solution of dynamic problems of elastic wave propagation in inhomogeneous media by a combination of partial separation of variables and finite-difference methods. *J. Geophys.* 48, 161-172.

Alterman, Z. and F. C. Karal, 1968. Propagation of elastic waves in layered media by finite-difference methods. *Bull. Seism. Soc. Am.* 58, 367-398.

Anderson, D. A., J. C. Tannehill, and R. H. Pletcher, 1984. Computational fluid mechanics and heat transfer. *Hemisphere Publishing Corporation*.

Andrews, D. J., 1973. A numerical study of tectonic stress release by underground explosions. *Bull. Seism. Soc. Am.* 63, 1375 – 1391.

Andrews, D. J., 1976. Rupture propagation with finite stress in antiplane strain. *J. Geophys. Res.* 81, 3575-3582.

Andrews, D. J., 1999. Test of two methods for faulting in finite-difference calculations. *Bull. Seism. Soc. Am.* 89, 931 – 937.

Aochi, H. and E. Fukuyama, 2002. Three-dimensional nonplanar simulation of the 1992 Landers earthquake. *J. Geophys. Res.* 107, doi 10.1029/2000JB000061.

Aoi, S. and H. Fujiwara, 1999. 3D finite-difference method using discontinuous grids. *Bull. Seism. Soc. Am.* 89, 918-930.

Backus, G. E., 1962. Long-wave elastic anisotropy produced by horizontal layering, *J. Geophys. Res.* 67, 4427-4440.

Bayliss, A., K. E. Jordan, B. J. LeMesurier, and E. Turkel, 1986. A fourth-order accurate finite-difference scheme for the computation of elastic waves. *Bull. Seism. Soc. Am.* 76, 1115-1132.

Bérenger, J.-P., 1994. A perfectly matched layer for the absorption of electromagnetic waves. *J. Comp. Phys.* 114, 185-200.

Blanch, J. O. and J. O. A. Robertsson, 1997. A modified Lax-Wendroff correction for wave propagation in media described by Zener elements. *Geophys. J. Int.* 131, 381-386.

Blanch, J. O., J. O. A. Robertsson, and W. W. Symes, 1995. Modeling of a constant Q: Methodology and algorithm for an efficient and optimally inexpensive viscoelastic technique. *Geophysics* 60, 176-184.

Boore, D. M., 1970. Love waves in nonuniform waveguides: finite difference calculations. *J. Geophys. Res.* 75, 1512-1527.

Boore, D., 1972. Finite-difference methods for seismic wave propagation in heterogeneous materials. *Methods in Computational Physics*, Vol. 11, B. A. Bolt, ed., *Academic Press*, New York.

Bouchon, M., 1981. A simple method to calculate Green's functions for elastic layered media. *Bull. Seism. Soc. Am.* 71, 959-971.

Carcione, J. M., 1994. The wave equation in generalized coordinates. *Geophysics* 59, 1911-1919.

Carcione, J. M., 2001. Wave fields in real media: wave propagation in anisotropic, anelastic and porous media. *Pergamon*.

Carcione, J. M. and F. Cavallini, 1994. A rheological model for anelastic anisotropic media with applications to seismic wave propagation. *Geophys. J. Int.* 119, 338-348.

Carcione, J. M., G. C. Herman, and A. P. E. ten Kroode, 2002. Seismic modeling. *Geophysics* 67, 1304-1325.

Carcione, J. M., D. Kosloff, and R. Kosloff, 1988a. Wave propagation simulation in a linear viscoacoustic medium. *Geophys. J.* 93, 393-407.

Carcione, J. M., D. Kosloff, and R. Kosloff, 1988b. Wave propagation simulation in a linear viscoelastic medium. *Geophys. J.* 95, 597-611.

Carcione J. M. and J. P. Wang, 1993. A Chebyshev collocation method for the elastodynamic eqiuation in generalized coordinates. *Comp. Fluid Dyn. J.* 2, 269-290.

Carrio, P., J. Costa, J. E. Ferrer-Pinheiro, and M. Schoenberg, 1992. Cross-borehole tomography in anisotropic media. *Geophysics* 57, 1194-1198.

Caserta, A., V. Ruggiero, and P. Lanucara, 2002. Numerical modelling of dynamical interaction between seismic radiation and near-surface geological structures: a parallel approach. *Computers & Geosciences* 28, 1069-1077.

Chaljub, E., Komatitsch, D., Vilotte, J. P., Capdeville, Y., and Festa, G., 2006 Spectral Element Analysis in Seismology. Accepted for publication in *Advances in Wave Propagation in Heterogeneous Earth*, Ru-Shan Wu and Valerie Maupin, Eds., in the series *'Advances in Geophysics'*, R. Dmowska, ed., *Elsevier Academic Press*.

Chen, Y. H., R. T. Coates, and J. O. A. Robertsson, 2000. Extension of PML ABC to Elastic Wave Problems in General Anisotropic and Viscoelastic Media: *Schlumberger OFSR research note*.

Chew, W. C. and Q. H. Liu, 1996. Perfectly matched layers for elastodynamics: a new absorbing boundary condition. *J. Comp. Acoustics* 4, 341-359.

Chew, W. C. and W. H. Weedon, 1994. A 3D perfectly matched medium from modified Maxwell's equations with stretched coordinates. *Microwave Opt. Tech. Lett.* 7, 599-604.

Clayton, R. and B. Engquist, 1977. Absorbing boundary conditions for acoustic and elastic wave equations. *Bull. Seism. Soc. Am.* 67, 1529-1540.

Cohen, G. C., 2002. Higher-order numerical methods for transient wave equations. *Springer*.

Collino, F., 1993. High order absorbing boundary conditions for wave propagation models. Straight line boundary and corner cases. In *Kleinman, R. et al., Eds., Proc. of the Second International Conference on Mathematical and Numerical Aspects of Wave Propagation. SIAM, Delaware, 161-171.*

Collino, F. and C. Tsogka, 1998. Application of the PML absorbing layer model to the linear elastodynamic problem in anisotropic heterogeneous media. *INRIA*, *Rapport de recherche, n. 3471*.

Collino F. and C. Tsogka, 2001. Applications of the PML absorbing layer model to the linear elastodynamic problem in anisotropic heterogeneous media. *Geophysics* 66, 294-305.

Coutant, O., 1989. Program of numerical simulation AXITRA. Res. Rep. LGIT (in French), *Université Joseph Fourier*, Grenoble.

Coutant, O., J. Virieux, and A. Zollo, 1995. Numerical source implementation in a 2D finite difference scheme for wave propagation. *Bull. Seism. Soc. Am.* 85, 1507-1512.

Crampin, S., and S. Chastin, 2003. A review of shear wave splitting in the crack-critical crust. *Geophys. J. Int.* 155, 221-240.

Crase, E., 1990. High-order (space and time) finite-difference modeling of the elastic wave equation. *60th Ann. Intl. Meeting, Soc. Expl. Geophys., Expanded Abstracts*, 987-991.

Crase, E., Ch. Wideman, M. Noble, and A. Tarantola, 1992. Nonlinear elastic waveform inversion of land seismic reflection data, *J. Geophys. Res.* 97, 4685-4703.

Cruz-Atienza, V. M. and J. Virieux, 2004. Dynamic rupture simulation of non-planar faults with a finite-difference approach. *Geophys. J. Int.* 158, 939-954.

Dablain, M. A., 1986. The application of high-order differencing to the scalar wave equation. *Geophysics* 51, 54-66.

Dalguer, L. A. and S. M. Day, 2004. Split nodes and fault zone models for dynamic rupture simulation. *EoS Trans. AGU, 85(47), Fall Meet. Suppl.*, Abstract S41A-0944.

Dalguer, L. A. and S. M. Day, 2006. Comparison of fault representation methods in finite difference simulations of dynamic rupture. *Bull. Seism. Soc. Am.*, in press.

Day, S. M., 1977. Finite element analysis of seismic scattering problems. PhD. Dissertation, *University of California, San Diego*.

Day, S. M., 1982. Three-dimensional simulation of spontaneous rupture: the effect of nonuniform prestress. *Bull. Seism. Soc. Am.* 72, 1881-1902.

Day, S. M., 1998. Efficient simulation of constant Q using coarse-grained memory variables. *Bull. Seism. Soc. Am.* 88, 1051-1062.

Day, S. M., 2005. Personal communication.

Day, S. M. and C. R. Bradley, 2001. Memory-efficient simulation of anelastic wave propagation. *Bull. Seism. Soc. Am.* 91, 520-531.

Day, S. M., L. A. Dalguer, N. Lapusta, and Y. Liu, 2005. Comparison of finite difference and boundary integral solutions to three-dimensional spontaneous rupture. *J. Geophys. Res.* **110**, B12307, doi: 10.1029/2005JB003813.

Day, S. M. and J. B. Minster, 1984. Numerical simulation of wavefields using a Padé approximant method. *Geophys. J. Roy. astr. Soc.* 78, 105-118.

Durran, D. R., 1999. Numerical methods for wave equations in geophysical fluid dynamics. *Springer*.

Eisner, L. and R. Clayton, 2002. Equivalent medium parameters for numerical modeling in media with near-surface low velocities. *Bull. Seism. Soc. Am.* 92, 711-722.

Emerman, S. H., W. Schmidt, and R. A. Stephen, 1982. An implicit finite-difference formulation of the elastic wave equation. *Geophysics* 47, 1521-1526.

Emmerich, H., 1989. 2-D wave propagation by a hybrid method. *Geophys. J. Int.* 99, 307-319.

Emmerich, H., 1992. PSV-wave propagation in a medium with local heterogeneities: a hybrid formulation and its application. *Geophys. J. Int.* 109, 54-64.

Emmerich, H. and M. Korn, 1987. Incorporation of attenuation into time-domain computations of seismic wave fields. *Geophysics* 52, 1252-1264.

Falk, J., E. Tessmer, and D. Gajewski, 1996. Tube wave modelling by the finite-differences method with varying grid spacing. *PAGEOPH*, 148, 77-93.

Falk, J., E. Tessmer, and D. Gajewski, 1998. Efficient finite-difference modelling of seismic waves using locally adjustable time steps. *Geophys. Prosp.*, 46, 603-616.

Fäh, D., 1992. A hybrid technique for the estimation of strong ground motion in sedimentary basins. Diss. ETH Nr. 9767, *Swiss Federal Institute of Technology*, Zurich.

Festa, G. and S. Nielsen, 2003. PML absorbing boundaries. *Bull. Seism. Soc. Am.*, 93, 891-903.

Fink, M. 1997. Time reversed acoustics. *Physics Today*, 34-40.

Fornberg, B., 1988. Generation of finite difference formulas on arbitrary spaced grids. *Math. Computation* 51, 699-706.

Forsythe, G. E. and W. R. Wasow, 1960. Finite Difference Methods for Partial Differential Equations. *J. Wiley & Sons, New York*.

Frankel, A., 1993. Three-dimensional simulations of ground motions in the San Bernardino Valley, California, for hypothetical earthquakes on the San Andreas fault. *Bull. Seism. Soc. Am.* 83, 1020-1041.

Frankel, A. and W. Leith, 1992. Evaluation of topographic effects on P- and S-waves of explosions at the Northern Novaya Zemlya test site using 3-D numerical simulations. *Geophys. Res. Lett.* 19, 1887-1890.

Geller, R. J. and T. Ohminato, 1994. Computation of synthetic seismograms and their partial derivatives for heterogeneous media with arbitrary natural boundary conditions using the Direct Solution Method. *Geophys. J. Int.* 116, 421-446.

Geller, R. J. and N. Takeuchi, 1995. A new method for computing highly accurate DSM synthetic seismograms. *Geophys. J. Int.* 123, 449-470.

Geller, R. J. and N. Takeuchi, 1998. Optimally accurate second-order time-domain finite difference scheme for the elastic equation of motion: one-dimensional case. *Geophys. J. Int.* 135, 48-62.

Givoli, D., 2004. High-order local non-reflecting boundary conditions: a review. *Wave Motion* 39, 319-326.

Graves, R. W., 1996. Simulating seismic wave propagation in 3D elastic media using staggered-grid finite differences. *Bull. Seism. Soc. Am.* 86, 1091-1106.

Graves, R. W. and S. M. Day, 2003. Stability and accuracy analysis of coarse-grain viscoelastic simulations. *Bull. Seism. Soc. Am.* 93, 283-300.

Gropp, W., E. Lusk, and A. Skjellum, 1994. Using MPI, Portable Parallel Programming with the Message Passing Interface. *MIT Press*.

Hayashi, K., D. R. Burns, and M. N. Toksöz, 2001. Discontinuous-grid finite-difference seismic modeling including surface topography. *Bull. Seism. Soc. Am.* 91, 1750-1764.

Helbig, K., 1984. Anisotropy and dispersion in periodically layered media. *Geophysics* 49, 364-373.

Hestholm, S., 1999. Three-dimensional finite difference viscoelastic wave modelling including surface topography. *Geophys. J. Int.* 139, 852-878.

Hestholm, S. and B. O. Ruud, 1994. 2-D finite difference elastic wave modeling including surface topography. *Geophys. Prospect.* 42, 371-390.

Hestholm, S. and B. O. Ruud, 2002. 3D free-boundary conditions for coordinate-transform finite-difference seismic modeling. *Geophys. Prosp.* 50, 463-474.

Higdon, R. L., 1991. Absorbing boundary conditions for elastic waves. *Geophysics* 56, 231-241.

Holberg, O., 1987. Computational aspects of the choice of operator and sampling interval for numerical differentiation in large-scale simulation of wave phenomena. *Geophys. Prosp.* 35, 629-655.

Holliger, K. and J. O. A. Robertsson, 1998. Effects of the shallow subsurface on the upper crustal seismic reflection images. *Tectonophysics* 286, 161-169.

Igel, H., P. Mora, and B. Riollet, 1995. Anisotropic wave propagation through finite-difference grids. *Geophysics* 60, 1203-1216.

Ilan, A., 1977. Finite-difference modeling for P-pulse propagation in elastic media with arbitrary polygonal surface. *J. Geophys.* 43, 41-58.

Ilan, A. and D. Loewenthal, 1976. Instability of finite-difference schemes due to boundary conditions in elastic media. *Geophys. Prosp.* 24, 431-453.

Ilan, A., A. Ungar, and Z. S. Alterman, 1975. An improved representation of boundary conditions in finite difference schemes for seismological problems. *Geophys. J. R. Astr. Soc.* 43, 727-745.

Ionescu, I. R. and M. Campillo, 1999. Influence of the shape of the friction law and fault finiteness on the duration of initiation. *J. Geophys. Res.* 104, 3013-3024.

Isaacson, E. and H. B. Keller, 1966. Analysis of Numerical Methods. *J. Wiley & Sons, New York.*

Jastram, C. and A. Behle, 1992. Acoustic modeling on a grid of vertically varying spacing. *Geophys. Prosp.* 40, 157-169.

Jastram, C. and E. Tessmer, 1994. Elastic modelling on a grid with vertically varying spacing. *Geophys. Prosp.* 42, 357-370.

Jih, R.-S., K. L. McLaughlin, and Z. A. Der, 1988. Free-boundary conditions of arbitrary polygonal topography in a two-dimensional explicit elastic finite-difference scheme. *Geophysics* 53, 1045-1055.

Kang, T.-S. and Ch.-E. Baag, 2004a. Finite-difference seismic simulation combining discontinuous grids with locally variable timesteps. *Bull. Seism. Soc. Am.*, 94, 207-219.

Kang, T.-S. and Ch.-E. Baag, 2004b. An efficient finite-difference method for simulating 3D seismic response of localized basin structures. *Bull. Seism. Soc. Am.*, 94, 1690-1705.

Kay, I. and E. S. Krebes, 1999. Applying finite element analysis to the memory variable formulation of wave propagation in anelastic media. *Geophysics* 64, 300-307.

Kelly, K. R., R. W. Ward, S. Treitel, and R. M. Alford, 1976. Synthetic seismograms: a finite-difference approach. *Geophysics* 41, 2-27.

Klimeš, L., 1996. Accuracy of elastic finite differences in smooth media. *PAGEOPH*, 148, 39-76.

Koelbel, C., D. Loverman, R. Shreiber, G. Steele Jr., and M. Zosel, 1994. The High-performance Fortran Handbook. *MIT Press*.

Komatitsch, D., F. Coutel, and P. Mora, 1996. Tensorial formulation of the wave equation for modeling curved interfaces. *Geophys. J. Int.* 127, 156-168.

Komatitsch, D. and J. Tromp, 2003. A Perfectly Matched Layer (PML) absorbing condition for the second-order elastic wave equation. *Geophys. J. Int.* 154, 146-153.

Kosloff, R. and D. Kosloff, 1986. Absorbing boundaries for wave propagation problems. *J. Comp. Phys.* 63, 363-376.

Kristek, J. and P. Moczo, 2003. Seismic wave propagation in viscoelastic media with material discontinuities – a 3D 4^{th}-order staggered-grid finite-difference modeling. *Bull. Seism. Soc. Am.* 93, 2273-2280.

Kristek, J., P. Moczo, and R. J. Archuleta, 2002. Efficient methods to simulate planar free surface in the 3D 4th-order staggered-grid finite-difference schemes. *Studia Geophys. Geod.* 46, 355-381.

Kristek, J., P. Moczo, I. Irikura, T. Iwata, and H. Sekiguchi, 1999. The 1995 Kobe mainshock simulated by the 3D finite differences. *The Effects of Surface Geology on Seismic Motion, Vol. 3, K. Irikura, K. Kudo, H. Okada, and T. Sasatani, eds., 1361-1368, Balkema, Rotterdam.*

Kummer, B. and A. Behle, 1982. Second-order finite-difference modeling of SH-wave propagation in laterally inhomogeneous media. *Bull. Seism. Soc. Am.* 72, 793-808.

Kummer, B., A. Behle, and F. Dorau, 1987. Hybrid modelling of elastic-wave propagation in two-dimensional laterally inhomogeneous media. *Geophysics* 52, 765-771.

Laws, R. and E. Kragh, 2002. Rough seas and time-lapse seismic. *Geophys. Prosp.* 50, 195-208.

Lax, P. D. and B. Wendroff, 1964. Difference schemes for hyperbolic equations with high order accuracy. *Comm. Pure appl. Math.* 27.

Lecomte, I., H. Gjøystdal, F. Maaø, R. Bakke, Å. Drottning, and T.-A. Johansen, 2004. Efficient and flexible seismic modelling of reservoirs: the HybriSeis concept. *The Leading Edge* 23,432-437.

Levander, A. R., 1988. Fourth-order finite-difference P-SV seismograms. *Geophysics* 53, 1425-1436.

Levander, A. R., 1989. Finite-difference forward modeling in seismology, In: *James, D. E., Ed., The encyclopedia of solid Earth geophysics. Van Nostrand Reinhold*, 410-431.

Liao, Z., H. L. Wong, Y. Baipo, and Y. Yifan, 1984. A transmitting boundary for transient wave analysis. *Scientia Sinica* A27, 1063-1076.

Lindman, E. L., 1975. Free space boundary conditions for the time dependent wave equation. *J. Comp. Phys.* 18, 66-78.

Liu, H.-P., D. L. Anderson, and H. Kanamori, 1976. Velocity dispersion due to anelasticity; implications for seismology and mantle composition. *Geophys. J. R. astr. Soc.* 47, 41-58.

Luo, Y. and G. Schuster, 1990. Parsimonious staggered grid finite-differencing of the wave equation. *Geophys. Res. Let.* 17, 155-158.

Madariaga, R., 1976. Dynamics of an expanding circular fault. *Bull. Seism. Soc. Am.* 67, 163-182.

Madariaga, R., K. Olsen, R. Archuleta, 1998. Modeling dynamics rupture in a 3D earthquake fault model. *Bull. Seism. Soc. Am.* 88, 1182-1197.

Magnier, S-A., P. Mora and A. Tarantola, 1994. Finite differences on minimal grids. *Geophysics* 59, 1435-1443.

Marchuk, G. I., 1982. Methods of numerical mathematics. *Springer Verlag*.

Marcinkovich, C. and K. Olsen. On the implementation of perfectly matched layers in a three-dimensional fourth-order velocity-stress finite difference scheme. *J. Geophys. Res.* 108 (B5), 2276, doi: 10.1029/2002JB002235.

Marfurt, K. J., 1984. Accuracy of finite-difference and finite-element modeling of the scalar and elastic wave equations. *Geophysics* 49, 533-549.

McDonal, F. J., F. A. Angona, L. R. Mills, R. L. Sengbush, R. G. van Nostrand, and J. E. White, 1958. Attenuation of shear and compressional waves in Pierre shale. *Geophysics* 23, 421-439.

Mikumo, T. and T. Miyatake, 1987. Numerical modeling of realistic fault rupture processes. In: *Seismic Strong Motion Synthetics, B.A. Bolt, ed., Academic Press*, 91-151.

Mitchell, A. R., 1969. Computational Methods in Partial Differential Equations. *J. Wiley & Sons*, *London*.

Mitchell, A. R. and D. F. Griffiths, 1994. The Finite Difference Method in Partial Differential Equations. *J. Wiley & Sons*, *New York*.

Mittet, R., 2002. Free-surface boundary conditions for elastic staggered-grid modeling schemes. *Geophysics* 67, 1616-1623.

Mizutani, H., R. J. Geller, and N. Takeuchi, 2000. Comparison of accuracy and efficiency of time-domain schemes for calculating synthetic seismograms. *Phys. Earth Planet. Int.* 119, 75-97.

Moczo, P., 1989. Finite-difference technique for SH-waves in 2-D media using irregular grids - application to the seismic response problem. *Geophys. J. Int.* 99, 321-329.

Moczo, P., 1998. Introduction to Modeling Seismic Wave Propagation by the Finite-Difference Method. Lecture Notes. *Kyoto University*. Available in pdf format at ftp://ftp.nuquake.sk/pub/Papers

Moczo, P. and P.-Y. Bard, 1993. Wave diffraction, amplification and differential motion near strong lateral discontinuities. *Bull. Seism. Soc. Am.* 83, 85-106.

Moczo, P., E. Bystrický, J. Kristek, J. M. Carcione, and M. Bouchon, 1997. Hybrid modeling of P-SV seismic motion at inhomogeneous viscoelastic topographic structures. *Bull. Seism. Soc. Am.* 87, 1305-1323.

Moczo, P. and J. Kristek, 2005. On the rheological models used for time-domain methods of seismic wave propagation. *Geophys. Res. Lett.* 32, L01306, doi: 10.1029/2004GL021598.

Moczo, P., J. Kristek, and E. Bystrický, 2001. Efficiency and optimization of the 3D finite-difference modeling of seismic ground motion. *J. Comp. Acoustics* 9, 593-609.

Moczo, P., J. Kristek, and M. Gális, M., 2004a. Simulation of planar free surface with near-surface lateral discontinuities in the finite-difference modeling of seismic motion. *Bull. Seism. Soc. Am.* 94, 760-768.

Moczo, P., J. Kristek, and L. Halada, 2000. 3D 4^{th}-order staggered-grid finite-difference schemes: stability and grid dispersion. *Bull. Seism. Soc. Am.* 90, 587-603.

Moczo, P., J. Kristek, and L. Halada, 2004b. The Finite-Difference Method for Seismologists. An Introduction. *Comenius University*, *Bratislava*. Available in pdf format at ftp://ftp.nuquake.sk/pub/Papers

Moczo, P., J. Kristek, V. Vavryčuk, R. J. Archuleta, and L. Halada, 2002. 3D heterogeneous staggered-grid finite-difference modeling of seismic motion with volume harmonic and arithmetic averaging of elastic moduli and densities. *Bull. Seism. Soc. Am.* 92, 3042-3066.

Moczo, P., P. Labák, J. Kristek, and F. Hron, 1996. Amplification and differential motion due to an antiplane 2D resonance in the sediment valleys embedded in a layer over the halfspace. *Bull. Seism. Soc. Am.* 86, 1434-1446.

Moczo, P., M. Lucká, J. Kristek, and M. Kristeková, 1999. 3D displacement finite differences and a combined memory optimization. *Bull. Seism. Soc. Am.* 89, 69-79.

Morton, K. W. and D. F. Mayers, 1994. Numerical Solution of Partial Differential Equations. *Cambridge University Press*.

Mufti, I. R., 1985. Seismic modeling in the implicit mode. *Geophys. Prosp.* **33**, 619-656.

Muir, F., J. Dellinger, J. Etgen, and D. Nichols, 1992. Modeling elastic fields across irregular boundaries. *Geophysics* 57, 1189-1193.

Murphy, W. F. III, 1982. Effects of partial saturation on attenuation in Massilon sandstone and Vycor porous glass. *J. Acoust. Soc. Am.* 71, 1458-1468.

Nielsen S. and J. M. Carlson, 2000. Rupture Pulse Characterization: Self-Healing, Self-Similar, Expanding Solutions in a Continuum Model of Fault Dynamics. *Bull. Seism. Soc. Am*. 90, 1480-1497.

Nielsen S., J. M. Carlson, K. Olsen, 2000. Influence of friction and fault geometry on earthquake rupture. *J. Geophys. Res.* 105B, 6069-6088,

Nielsen, P., F. If, , P. Berg, and O. Skovgaard, 1994. Using the pseudospectral technique on a curved grid for 3D acoustic forward modeling. *Geophys. Prospect.*, 42, 321-341.

O'Brien, G., M. Hyman, and S. Kaplan, 1951. A study of the numerical solution of partial differential equations. *J. Math. Phys.* **29**, 233-251.

Ohminato, T. and B. A. Chouet, 1997. A free-surface boundary condition for including 3D topography in the finite-difference method. *Bull. Seism. Soc. Am*. 87, 494-515.

Ottosen, N. S. and H. Petersson, 1992. Introduction to the finite element method. *Prentice Hall*.

Peng, C. and M. N. Toksöz, 1994. An optimal absorbing boundary condition for finite difference modeling of acoustic and elastic wave propagation. *J. Acoust. Soc. Am.* 95, 733-745.

Peng, C. and M. N. Toksöz, 1995. An optimal absorbing boundary condition for elastic wave modeling. *Geophysics* 60, 296-301.

Pierson W. J. and L. Moskowitz, 1964. A proposed spectral form for fully developed wind seas based on the similarity theory of S. A. Kitaigorodskii. *J. Geophys. Res.* 69, 5181-5190.

Pitarka, A., 1999. 3D elastic finite-difference modeling of seismic motion using staggered grids with nonuniform spacing. *Bull. Seism. Soc. Am.* 89, 54-68.

Pitarka, A. and K. Irikura, 1996. Modeling 3D surface topography by finite-difference method: Kobe-JMA station site, Japan, case study. *Geophys. Res. Lett.* 23, 2729-2732.

Pratt, R. G., 1990. Inverse Theory Applied to Multi-Source cross-hole Tomography. Part 2: Elastic Wave-Equation Method. *Geophys. Prosp.* 38, 311-329.

Pratt, R. G., C. Shin, and G. J. Hicks, 1998. Gauss-Newton and full Newton methods in frequency-space seismic waveform inversion, *Geophys. J. Int.* 133, 341-362.

Richtmyer, R. D. and K. W. Morton, 1967. Difference Methods for Initial Value Problems. *J. Wiley & Sons*, New York; (reprinted by Kreiger, New York, 1994).

Robertsson, J. O. A., 1996. A numerical free-surface condition for elastic/viscoelastic finite-difference modeling in the presence of topography. *Geophysics* 61, 1921-1934.

Robertsson, J. O. A., J. O. Blanch, and W. W. Symes, 1994. Viscoelastic finite-difference modeling. *Geophysics* 59, 1444-1456.

Robertsson, J. O. A. and C. H. Chapman, 2000. An efficient method for calculating finite-difference seismograms after model alterations. *Geophysics* 65, 907-918.

Robertsson, J. O. A., and R. T. Coates, 1997. Finite-difference modeling of Q for qP- and qS-waves in anisotropic media. *67th Ann. Internat. Mtg., Soc. Expl. Geophys., Expanded Abstracts*, 1846-1849.

Robertsson, J. O. A. and K. Holliger, 1997. Modeling of seismic wave propagation near the Earth's surface. *Phys. Earth Planet. Int.* 104, 193-211.

Robertsson, J. O. A., Laws, R.,. C. H. Chapman, J.-P. Vilotte, and E. Delavaud, 2005. Modelling of scattering of seismic waves from a corrugated rough sea surface: a comparison of three methods. *Geophys. J. Int.*, in press.

Robertsson, J. O. A., A. Levander, and K. Holliger, 1996. A hybrid wave propagation simulation technique or ocean acoustic problems. *J. Geophys. Res.* 101, 11225-11241.

Robertsson, J. O. A., S. Ryan-Grigor, C. Sayers, and C. H. Chapman, 2000. A finite-difference injection approach to modeling of seismic fluid flow monitoring. *Geophysics* 65, 896 – 906.

Rodrigues, D., 1993. Large scale modelling of seismic wave propagation. PhD. Thesis, *Ecole Centrale Paris*.

Rodrigues, D. and P. Mora, 1993. An efficient implementation of the free-surface boundary condition in 2-D and 3-D elastic cases. *63th Ann. Intl. Meeting, Soc. Expl. Geophys., Expanded Abstracts*, 215-217.

Saenger, E. H., N. Gold, and S. A. Shapiro, 2000. Modeling the propagation of elastic waves using a modified finite-difference grid. *Wave Motion* 31, 77-92.

Saenger, E. H. and T. Bohlen, 2004. Finite-difference modeling of viscoelastic and anisotropic wave propagation using the rotated staggered grid. *Geophysics* 69, 583-591.

Schneider, J. B. and O. M. Ramahi, 1998. The complementary operators method applied to acoustic finite-difference time-domain simulations. *J. Acoust. Soc. Am.* 104, 686-693.

Schoenberg, M. and F. Muir, 1989. A calculus for finely layered anisotropic media. *Geophysics* 54, 581-589.

Shtivelman, V., 1984. A hybrid method for wave field computation. *Geophys. Prospect.* 32, 236-257.

Shtivelman, V., 1985. Two-dimensional acoustic modelling by a hybrid method, *Geophysics* 50, 1273-1284.

Slawinski, R. A. and E. S. Krebes, 2002. The homogeneous finite-difference formulation of the P-SV-wave equation of motion. *Studia Geoph. Geod.* 46, 731-751.

Sochacki, J. S., J. H. George, R. E. Ewing, and S. B. Smithson, 1991. Interface conditions for acoustic and elastic wave propagation. *Geophysics* 56, 168-181.

Smith, W. D., 1974. A nonreflecting plane boundary for wave propagation problems. *J. Comp. Phys.* 15, 492-503.

Spencer, J. W. Jr., 1981. Stress relaxation at low frequencies in fluid-saturated rocks. *J. Geophys. Res.* 86, 1803-1812.

Stead, R.J. and D. V. Helmberger, 1988. Numerical-analytical interfacing in two dimensions with applications to modeling NTS seismograms. *In Scattering and Attenuation of Seismic Waves, A. Aki and R. S. Wu, Eds., pp. 157-193. Birkhauser, Basel, Switzerland.*

Strang, G. and G. J. Fix, 1973. An analysis of the finite element method. *Prentice-Hall, Englewood Cliffs, NJ.*

Taflove, A. and S. C. Hagness, 2005. Computational electrodynamics: The finite-difference time-domain method. *Artech House*.

Takenaka, H., T. Furumura, and H. Fujiwara, 1998. Recent developments in numerical methods for ground motion simulation. *The Effects of Surface Geology on Seismic Motion, Vol. 2, K. Irikura, K. Kudo, H. Okada, and T. Sasatani, eds., 91-101, Balkema, Rotterdam*.

Takeuchi, N. and R. J. Geller, 2000. Optimally accurate second order time-domain finite difference scheme for computing synthetic seismograms in 2-D and 3-D media. *Phys. Earth Planet. Int.* 119, 99-131.

Takeuchi, N. and R. J. Geller, 2003. Accurate numerical methods for solving the elastic equation of motion for arbitrary source locations. *Geophys. J. Int.* 154, 852-866.

Tal-Ezer, H., J. M. Carcione, and D. Kosloff, 1990. An accurate and efficient scheme for wave propagation in linear viscoelastic media. *Geophysics* 55, 1366-1379.

Tessmer, E., 2000. Seismic finite-difference modeling with spatially varying time steps. *Geophysics* 65,1290-1293.

Tessmer, E. and D. Kosloff, 1994. 3-D elastic modeling with surface topography by a Chebyshev spectral method. *Geophysics* 59, 464-473.

Tessmer, E., D. Kosloff, and A. Behle, 1992. Elastic wave propagation simulation in the presence of surface topography. *Geophys. J. Int.* 108, 621-632.

Thomson, W. (Lord Kelvin), 1856. Elements of a mathematical theory of elasticity. *Phil. Trans. R. Soc.* 166, 481-498.

van Manen, D. J., J. O. A. Robertsson, and Curtis, 2005. Modeling of wave propagation in inhomogeneous media. *Phys. Rev. Lett.* 94, 164301-164304.

Virieux, J., 1984. SH-wave propagation in heterogeneous media: velocity-stress finite-difference method. *Geophysics* 49, 1933-1957.

Virieux, J., 1986. P-SV wave propagation in heterogeneous media: velocity-stress finite-difference method. *Geophysics* 51, 889-901.

Wang, Y., J. Xu, and G. T. Schuster, 2001. Viscoelastic wave simulation in basins by a variable-grid finite-difference method. *Bull. Seism. Soc. Am.* 91, 1741-1749.

Wang, T. and Tang, X., 2003. Finite-difference modeling of elastic wave propagation: A nonsplitting perfectly matched layer approach. *Geophysics* 68, 1749-1755.

Xu, T. and G. A. McMechan, 1995. Composite memory variables for viscoelastic synthetic seismograms. *Geophys. J. Int.* 121, 634-639.

Xu, T. and G. A. McMechan, 1998. Efficient 3-D viscoelastic modeling with application to near-surface land seismic data. *Geophysics* 63, 601-612.

Yomogida, K. and J. T. Etgen, 1993. 3-D wave propagation in the Los Angeles basin for the Whittier-Narrows earthquake. *Bull. Seism. Soc. Am.* 83, 1325-1344.

Zahradník, J., 1995. Comment on 'A hybrid method for estimation of ground motion in sedimentary basins: Quantitative modeling for Mexico City' by D. Fäh, P. Suhadolc, St. Mueller and G.F. Panza. *Bull. Seism. Soc. Am.* 85, 1268-1270.

Zahradník, J., and F. Hron, 1992. Robust finite-difference scheme for elastic waves on coarse grids. *Studia Geophys. Geodaet.* 36, 1-19.

Zahradník, J., P. Moczo, and F. Hron, 1993. Testing four elastic finite-difference schemes for behaviour at discontinuities. *Bull. Seism. Soc. Am.* 83, 107-129.

Zahradník, J. and P. Moczo, 1996. Hybrid seismic modeling based on discrete-wavenumber and finite-difference methods. *PAGEOPH*, 148, 21-38.

Zahradník, J. and E. Priolo, 1995. Heterogeneous formulations of elastodynamic equations and finite-difference schemes. *Geophys. J. Int.*, 120, 663-676.

Zeng, X., 1996. Finite difference modeling of viscoelastic wave propagation in a generally heterogeneous medium in the time domain, and a dissection method in the frequency domain. Ph.D. Thesis, *University of Toronto*.

Zhang, J., 1997. Quadrangle-grid velocity-stress finite-difference method for elastic-wave-propagation simulation. *Geophys. J. Int.* 131, 127-134.

Zhang, Ch. And W. W. Symes, 1998. Fourth order, full-stencil immersed interface method for elastic waves with discontinuous coefficients. *1998 SEG Expanded Abstracts*.

Zienkiewicz, O. C. and R. L. Taylor, 1989. The finite element method. 4th edition, vol. 1, *McGraw-Hill*.